MODELING AND DESIGN OF SPECIALTY OPTICAL FIBERS AND WAVEGUIDES FOR SUPERCONTINUUM GENERATION

A Thesis Submitted
in Partial Fulfilment of the
Requirements for the Degree of

DOCTOR OF PHILOSOPHY

in

PHYSICS

by

DRISHTI SINGH TOMER
(2K19/PHDAP/501)

Under the Supervision of

Dr. AJEET KUMAR
Associate Professor
Department of Applied Physics
Delhi Technological University

Department of Applied Physics

DELHI TECHNOLOGICAL UNIVERSITY
(Formerly Delhi College of Engineering)
Shahbad Daulatpur, Main Bawana Road, Delhi-110 042, India

March 2026

DEDICATED

TO

MY BELOVED FAMILY!!!

ACKNOWLEDGMENTS

I am very pleased to pay my gratitude to many wonderful people who have helped me throughout the Ph.D. journey.

First and foremost, I would like to express my deepest gratitude to my supervisor, ***Dr. Ajeet Kumar***, for his exceptional guidance and support throughout my research journey. His insightful advice, constructive criticism, and constant encouragement have been invaluable. I am especially thankful for the peaceful and research-oriented environment he fostered, which greatly contributed to my work. The knowledge and experiences gained under his mentorship will undoubtedly benefit my future research endeavors.

I express respect towards ***Prof. Prateek Sharma*** (Honorable Vice-Chancellor, Delhi Technological University), ***Prof. Vinod Kumar*** (Head & DRC chairperson of the Department of Applied Physics) and ***Delhi Technological University*** for providing me worthy infrastructure for carrying my research work. I am further thankful to the ***SRC*** and ***DRC*** members for their valuable suggestions. Also, I would like to thank ***all other faculty and staff members*** of the Department for their help and cooperation.

My sincere thanks to ***Dr. Than Singh Saini*** (Assistant professor, NIT, Kurukshetra) whose suggestions and discussions helped me carrying out my research work. I am thankful for my research fellows who created positive, calm, helpful and assiduous environment in the laboratory. I am also thankful for all my friends who always motivates me.

I am deeply grateful to my beloved parents, ***Mr. Ranbir Singh Tomer*** and ***Mrs. Mamta Singh Tomer***, whose constant blessings and unwavering support have always guided me. I extend heartfelt thanks to my loving husband, ***Mr. Nitin Pratap Singh***, for his continuous encouragement, patience, and motivation throughout this journey. I also wish to acknowledge my caring sisters, ***Ms. Naina Tomer*** and ***Ms. Vanshika Singh***, who have always been ready to lend a helping hand. Their collective support has created a stress-free and nurturing environment that allowed me to focus wholeheartedly on my research. I remain truly indebted to my entire family for their steadfast moral support.

I acknowledge the initiatives and support from the establishment of ***TIFAC***-Centre of Relevance and Excellence in Fiber Optics and Optical Communication at Delhi Technological University (Formerly Delhi College of Engineering) Delhi, through the Mission REACH program of Technology Vision-2020 of the Government of India.

I am also thankful to the optical societies ***SPIE*** and ***OPTICA*** (formerly known as ***OSA***) who gave me chance to enhance my network of research.

Above all, I thank God for giving me the perseverance and strength to show up at my lab each day and work through the ups and downs of my Ph.D. journey.

Drishti Singh Tomer

(2K19/PHDAP/501)

DELHI TECHNOLOGICAL UNIVERSITY

(Formerly Delhi College of Engineering)

Shahbad Daulatpur, Main Bawana Road, Delhi-42

CANDIDATE'S DECLARATION

I, **Drishti Singh Tomer (2K19/PHDAP/501)** hereby certify that the work which is being presented in the thesis entitled **" Modeling and Design of Specialty Optical Fibers and Waveguides for Supercontinuum Generation"** in partial fulfillment of the requirements for the award of the Degree of Doctor of Philosophy, submitted in the Department of Applied Physics, Delhi Technological University is an authentic record of my own work carried out during the period from **January 2020** to **August 2025** under the supervision of **Dr. Ajeet Kumar, Department of Applied Physics, Delhi Technological University**.

The matter presented in the thesis has not been submitted by me for the award of any other degree of this or any other Institute.

Candidate's Signature

This is to certify that the student has incorporated all the corrections suggested by the examiners in the thesis and the statement made by the candidate is correct to the best of our knowledge.

06-03-2026

Signature of Supervisor

Signature of External Examiner

DELHI TECHNOLOGICAL UNIVERSITY

(Formerly Delhi College of Engineering)

Shahbad Daulatpur, Main Bawana Road, Delhi-42

CERTIFICATE BY THE SUPERVISOR

Certified that **Drishti Singh Tomer (2K19/PHDAP/501)** has carried out her research work presented in this thesis entitled **"Modeling and Design of Specialty Optical Fibers and Waveguides for Supercontinuum Generation"** for the award of **Doctor of Philosophy** from Department of Applied Physics, Delhi Technological University, Delhi, under my supervision. The thesis embodies results of original work, and studies are carried out by the student herself and the contents of the thesis do not form the basis for the award of any other degree to the candidate or to anybody else from this or any other University/Institution.

06-03-2026

Dr. Ajeet Kumar

(Supervisor)

Associate Professor Department of

Applied Physics

Delhi Technological University

Date:

ABSTRACT

This thesis focuses on the modeling and design of specialty optical fibers and waveguides for supercontinuum generation, targeting applications across diverse domains of nonlinear optics and photonic systems. By employing highly nonlinear materials such as silica, chalcogenides, and organic liquids, these designs aim to generate broad supercontinuum spectra spanning from the visible to the mid-infrared. The approach emphasizes short interaction lengths and low input peak powers, while maintaining high temporal coherence to maximize bandwidth and ensure spectral flatness. These specialty optical fibers and waveguides find applications in various fields like biomedical, military and sensing technologies.

Supercontinum generation is the process where amalgamation of various nonlinear phenomena including stimulated Raman scattering, self-phase modulation, cross-phase modulation, and four-wave mixing takes place. They work together on an intense pump beam, leading to a significant amount of spectral broadening compared to the original pump beam in an optical fiber. The generated supercontinuum sources can be used to discern chemicals, inspect food quality, detect explosives and hazardous gases, ulcer and cancer diagnosis, frequency comb generation, optical imaging, and optical coherence tomography.

In this thesis, we have numerically designed photonic crystal fibers and waveguides for supercontinuum generation across the visible to mid-infrared spectrum using the finite element method. By optimizing core and cladding geometries and adjusting core – cladding materials, we have minimized dispersion at the pump wavelength. The impact of input peak power, pulse width, fiber length and coherence on supercontinuum broadening has been numerically analyzed.

The proposed waveguide structure with a parabolic core, implemented in a chalcogenide glass results in the generation of a mid-IR supercontinuum spectrum when pumped in the normal dispersion region. This design is crucial as the fabricated rectangular waveguide does not remain rectangular after laser post processing but becomes similar to the proposed parabolic design. Another chalcogenide based graded-index hybrid cladding photonic crystal fiber is suitable for the generation of an ultra-broadband supercontinuum spectrum from 1 μm to 11 μm in MIR domain when pumped with the peak power of 0.75 kW at 5μm with 50 fs pulse width. We have also proposed liquid-infiltrated photonic crystal fibers to enhance the nonlinearity of silica fibers, enabling the generation of a highly coherent broadband supercontinuum. Ethanol based photonic crystal fiber results in a flat-top dispersion profile with a low peak power of 0.55kW at a pump wavelength of 1.55 μm. Another photonic crystal fiber design infiltrated with nitrobenzene results

in a spectrum ranging from 1.3 μm to 2.0 μm for the circular design (#C), from 0.9 μm to 2.3 μm for the elliptical *x*-polarised design (#EX) and from 1.0 μm to 2.4 μm for the elliptical *y*-polarised design (#EY). For dual infiltrated photonic crystal fibers we have a broadband supercontinuum spanning from 1.3 μm – 1.8 μm for design #A, 1.0 μm – 2.4 μm for design #B, 1.2 μm – 2.5 μm for design #C and 0.9 μm – 2.5 μm for design #D is obtained by using a fiber length of 4 mm to 8 mm with 50 fs secant laser pulse source and pump power of 600 W to 800 W. The suggested waveguide and photonic crystal fiber designs can be employed for various critical applications involving detection of explosives, various gases, cancers, ulcers and enhanced monitoring systems for food quality detection.

LIST OF PUBLICATIONS

PUBLICATIONS IN REFEREED JOURNALS (THESIS)

1. **D.S. Tomer** and A. Kumar, "Design and numerical modeling of chalcogenide parabolic-core waveguide for on-chip supercontinuum generation extending from near-IR region to mid-IR region", ***Microwave and Optical Technology Letters, 66(3), e34105 (2024). https://doi.org/10.1002/mop.34105***
2. **D.S. Tomer** and A. Kumar, "A Graded Index Hybrid Photonic Crystal Fiber for Supercontinuum Generation using $AsSe_2$-As_2S_5,"***Journal of Optics, 54, (3268-3277) (2025). https://doi.org/10.1007/s12596-024-01954-3***
3. **D.S. Tomer** and A. Kumar, "Ethanol-infiltrated circular photonic crystal fiber for low peak power supercontinuum generation from near-infrared to mid-infrared region", ***Journal of Optics 1-9 (2024). https://doi.org/10.1007/s12596-024-02152-x***
4. **D.S. Tomer** and A. Kumar, "Photonic crystal fibres infiltrated with nitrobenzene for low peak power supercontinuum generation in NIR to MIR region", ***Journal of Modern Optics, 72(4–6), 175–187 (2025). https://doi.org/10.1080/09500340.2025.2478641***
5. **D.S. Tomer** and A. Kumar, "A comparative study of photonic crystal fibers filled with organic liquids for low peak power supercontinuum generation", ***Journal of Nonlinear Optical Physics and Materials. https://doi.org/10.1142/S021886352550050X***

RESEARCH WORK PRESENTED/PUBLISHED IN REFEREED NATIONAL AND INTERNATIONAL CONFERENCES (THESIS)

1. **D.S. Tomer** and A. Kumar , "Photonic crystal fiber infiltrated with nitrobenzene for nonlinear applications", ***2nd International Conference on Recent trends in Applied Physics and Material Science* (*RAM 2024*)**, 15-16 Nov 2024, Bikaner Technological University (BTU), Bikaner, Rajasthan, India.
2. **D.S. Tomer** and A. Kumar, "A highly nonlinear photonic crystal fiber with two zero dispersion wavelengths for nonlinear applications", ***International Conference on Atomic, Molecular, Material, Nano, and Optical Physics with Applications* (*ICAMNOP 2023*)** ,

20-22 Dec 2023 , Department of Applied Physics, Delhi Technological University, Delhi, India.

3. **D.S. Tomer** and A. Kumar, "Nonlinear applications of photonic crystal fiber with organic solvent toluene using computational analysis", ***9th National Conference on Nanoscience and Instrumentation Technology* (*NCNIT-2021*),** 20-21 Nov 2021, Department of Physics, NIT, Kurukshetra, India.
4. **D.S. Tomer** and A. Kumar, "Computational analysis of toluene infiltrated photonic crystal fibers for nonlinear applications", ***44th Annual Symposium of the Optical Society of India: Frontiers in Optics and Photonics* (*FOP21*)**, 24-27 Sep 2021, IIT Delhi, India.

PUBLICATIONS IN REFEREED INTERNATIONAL CONFERENCES (OUTSIDE THESIS)

1. A. Khamaru, K. Sharma, **D.S. Tomer** & A. Kumar, "Mid-IR supercontinuum generation in dispersion flattened $As_{38}Se_{62}$ chalcogenide photonic crystal fiber", ***Journal of Physics: Conference Series, 2426*(*1*), *012002* (*2023*)**.

TABLE OF CONTENTS

LIST OF TABLES

LIST OF FIGURES

Figure 7.15 The coherence evolution using **(a)** pump power 800 W, 50 fs pulse width, 4 mm fiber length for (#A), **(b)** 800 W, 50 fs, 8 mm for (#B) , **(c)** 800W, 50 fs, 8 mm for (#C) and **(d)** 600W, 50 fs, 8 mm for (#D) at 1.55 micron.

LIST OF ABBREVIATIONS

PCF	Photonic Crystal Fiber
PML	Perfectly Matched Layer
FEM	Finite Element Method
NIR	Near Infrared Region
MIR	Mid Infrared Region
SPM	Self Phase Modulation
XPM	Cross Phase Modulation
FWM	Four Wave Mixing
SRS	Stimulated Raman Scattering
OCT	Optical Coherence Tomography
CVD	Chemical Vapour Deposition
TE	Transverse Electric
ZDW	Zero Dispersion Wavelength
RI	Refractive Index
OWB	Optical Wave Breaking
ANDi	All Normal Dispersion
MI	Modulation Instability
EMA	Effective Mode Area
WDM	Wavelength Division Multiplexing
SCG	Super Continuum Generation
MOF	Microstructured Fiber
EDFA	Erbium-Doped Fiber Amplifier
HF	Holey Fiber

CHAPTER 1: INTRODUCTION

1.1 Introduction

In the field of optics, the study centers on the behavior of light, particularly its interaction with matter. Equally critical is understanding the response of a medium to optical excitation and the resulting light–matter interactions. When light falls on a medium it polarises it. The strength of applied field determines nature of response. Weak field Intensity leads to linear material response whereas high intensity leads to nonlinear material response. Nonlinear media exhibit optical properties that do not respond linearly to an incident electric field. Laser light, with its high intensity and unique features such as monochromaticity, low divergence, and coherence, differs significantly from conventional light sources. These characteristics enable lasers to strongly influence the optical response of materials. In nonlinear optics, the principle of superposition, which holds in linear systems, no longer applies to pulse propagation.

The laser, invented by T. H. Maiman in 1960 using a ruby crystal, sparked major advances in optics [1]. After its invention optical world has revolutionized not only the field of communication but also offered its excellence in the fields of medical sciences, industry, defense, optical sensing, imaging and spectroscopy [2]. Javan et al. soon developed a continuous 15 mW He-Ne laser at 1.15 μm [3]. In 1962, McClung et al. used Q-switching to achieve pulses 100 times stronger than earlier ruby lasers [4]. The first mode-locked laser was demonstrated in 1963 by Hangrove et al., and later used by Mocker et al. to study mode dynamics in passive Q-switched lasers [5].

Geusic et al. first demonstrated the Q-switched Nd:YAG laser [6], while Mears et al. introduced the erbium-doped fiber amplifier (EDFA) at 1.55 μm in 1987 [7]. Although EDFAs became essential in long-distance fiber-optic communication, they were unsuitable for high-power fiber laser applications.Commercial solid and gas lasers can reach kilowatt outputs but face issues like size and heat management. Fiber lasers, first demonstrated by E. Snitzer in 1961 using Nd^{3+}-doped fibers, address these challenges with compact size, high gain, and up to 95% efficiency [8].

Laser technology has enabled high-power systems with ultra-short, controllable pulses. Key nonlinear optics milestones include second harmonic generation by Franken et al. (1962) [9], UV frequency mixing by Bass et al. (1962) [10], the Kerr effect in liquids by Maker et al. (1964) [11], and optical parametric oscillation by Giordmaine et al. (1965) [12].

These theoretical and experimental studies of optical phenomena emerged soon after the advent of laser technology. In future, electronic circuits would be replaced by photonic circuits due to low

loss, high speed computing and less energy consumption. Optical and photonic devices like waveguides and optical fibers have the ability to confine and modulate light in a useful manner at micro and nanoscales. In this thesis, special types of optical fibers and waveguides have been designed and their analysis have been done which can be used for various applications like diagnosis and sensing technologies.

Supercontinuum generation (SCG) is an optical process in which an intense ultrashort pulse gets broadened during interaction with a nonlinear medium. SCG term was first coined by Alfano and Shapiro in 1970 with double frequency generation experiment of photons in the presence of nonlinear medium [13-17] . SCG is led by optical linear and nonlinear effects i.e., group velocity dispersion, nonlinearity, self-phase modulation (SPM): The optical pulse induces changes in its own phase, broadening the spectrum, cross-phase modulation (XPM), stimulated Raman scattering (SRS): The energy from the pulse is transferred to lower-frequency modes through molecular vibrations, four-wave mixing (FWM): The interaction between different spectral components of the pulse generates new frequencies, Self-frequency shift: The pulse shifts to longer wavelengths as it propagates, contributing to the broadening and solitons generation [13,14].

During the 1990s, total internal reflection-based optical fibers were widely used for guiding light over long distances, making them ideal for studying nonlinear effects like SCG due to their ability to maintain high optical intensities. Specialty fibers, designed by altering glass composition and geometry, enable tailored optical properties. High nonlinear refractive indices and broad transparency windows (found in materials like silica, tellurite, fluoride, and chalcogenides) are critical for broadband SCG. Geometry further influences nonlinear behavior and dispersion control. Photonic crystal fibers (PCFs), with small core sizes and engineered dispersion, are especially effective for SCG studies. PCFs are characterized by a symmetric air-hole cladding structure, emerging as a promising alternative to conventional optical fibers for nonlinear applications. Typically made from materials such as fused silica, liquids, tellurite, fluoride, and chalcogenide glasses. They have been extensively studied both theoretically and experimentally for supercontinuum generation [18-30]. SCG in PCFs requires materials with high nonlinearity and transparency. Silica, with a transmission range of 0.3–2.5 μm, is commonly used for generating supercontinuum in visible and near-Infrared (NIR) regions due to its high purity, low cost, and simple synthesis process [31]. Price et al. achieved SCG from 0.3–1.6 μm in 15 cm pure silica fiber at 50 kW [32], while Labruyère et al. demonstrated 0.37–1.75 μm using 10 kW in 55 cm Ge-doped silica PCF [33]. Begum et al. numerically reported 0.96–1.89 μm SCG in 1 m silica PCF at 1.06, 1.31, and 1.55 μm pump wavelengths [34].Vindas et al. generated a 1200 nm SCG bandwidth in a

5 m silica-based fiber [35].

Literature shows that supercontinuum generation in silica-based fibers typically require long fiber length and high pump power. This limitation can be addressed by engineering PCFs with flattened dispersion or by infiltrating organic liquids to enhance nonlinearity, enabling broadband SCG in the visible to NIR region at lower power and shorter length. However, due to high absorption beyond 2.5 μm, silica is ineffective in the mid-infrared (MIR), where soft glasses offer a more suitable alternative for extending the SC spectrum. Tellurite and fluoride glasses offer higher nonlinearity and broader transparency than silica, enabling MIR SCG up to ~5–7 μm, though with higher losses [36]. Chalcogenide glasses have become extensively utilized and are recognized as superior candidates for mid-infrared SC generation due to their favourable nonlinear optical properties and broad transparency windows up to 20 μm. These materials are composed of chalcogen elements from group 16 of the periodic table, such as sulfur, selenium, and tellurium [37,38]. These reasons make such glasses an ideal choice for nonlinear photonic devices in the MIR region. Chalcogenide glasses like As-S, As-Se, Ge-As-S, and Ge-As-Se are commonly used for active and passive MIR material fabrication [39-42]. PCFs based on Chalcogenides are increasingly employed for broadband supercontinuum generation in MIR spectral region, owing to their high nonlinearity, excellent film-forming capability, and thermal/optical stability. These fibers enable ultra-broadband SCG over a few millimetres of length at low peak pump powers. However, many reported SC sources still rely on extended fiber lengths to achieve broad spectral widths.

This study presents a numerical investigation of PCF designs based on highly nonlinear chalcogenide materials and organic liquids, optimized to support ultra-broadband SCG across the visible, NIR and MIR regimes using short fiber length and low input power. Reducing fiber length minimizes propagation and bending losses, enhancing efficiency and compactness. Chalcogenide materials are selected for their strong nonlinearity, compatibility with fiber fabrication techniques, and reasonable thermal stability for solid-state devices, while organic liquids are chosen for their high tunability and ease of infiltration into microstructured geometries. The final material choice depends on the intended application, required nonlinear performance, fabrication constraints and thermal operating conditions [43,44].

The proposed designs approach addresses the growing demand for compact, broadband light sources in applications such as spectroscopy, gas sensing, biomedical imaging, optical coherence tomography (OCT), wavelength-division multiplexing (WDM), and free-space optical communications [45-47]. From the perspective of integrated photonics, SCG facilitates the development of chip-scale broadband light sources that can be incorporated into lab-on-chip

devices, optical communication systems, and on-chip signal processing platforms. The integration of dispersion-engineered microstructured fibers and highly nonlinear materials supports the realization of compact, robust, and energy-efficient photonic components suitable for large-scale industrial deployment. Consequently, continued advancements in SCG research directly contribute to the development of scalable broadband light sources and multifunctional photonic systems that meet the growing demands of modern industrial, biomedical, and telecommunication technologies.

1.2 Objectives of the thesis

The primary focus of this study is to achieve the following objectives:

1. To explore the potential of parabolic-core waveguide designs in chalcogenide materials for on-chip integration and broadband SCG in the NIR to MIR range.
2. To develop and model a graded-index hybrid photonic crystal fiber using chalcogenide glasses (e.g., $AsSe_2$–As_2S_5) aimed at enhancing spectral broadening and nonlinear interactions across a broad wavelength range.
3. To investigate the impact of various infiltrating materials on the nonlinear optical properties and SCG performance of circular and hybrid photonic crystal fibers.
4. To conduct numerical simulations to optimize dispersion engineering and nonlinear coefficient tailoring in novel PCF structures for improved spectral flatness and efficiency in low-power SCG applications.
5. To design and analyze photonic crystal fiber structures infiltrated with nonlinear materials such as nitrobenzene and ethanol for efficient low peak power supercontinuum generation spanning from the near-infrared to mid-infrared region.

1.3 Overview of the thesis

The present thesis comprises eight chapters and a brief summary of each chapter is presented as follows:

Chapter 1 presents an introduction to the advancements in nonlinear optics, accompanied by a comprehensive overview of specialty optical fibers and the principles of supercontinuum generation.

Chapter 2 represents the numerical methods used for modal analysis of proposed designs and

generating supercontinuum in fibers. A well-established numerical technique Finite-Element Method (FEM) based COMSOL Multiphysics Software is employed for performing mode analysis of the proposed PCFs and waveguide which involves fragmentation of the design into finite elements and these are further solved numerically. To analyse the modes and for performing further calculations & graphing, MATLAB programming software is used.

Chapter 3 presents the design and computational examination of a waveguide structure with a parabolic core, implemented in $AsSe_2$ chalcogenide glass. This structure aims to generate a mid-Infrared supercontinuum spectrum, covering the wavelength range of 1.4 to 7.6 μm. It includes molecular fingerprint region as well as earth's atmospheric transparent window. A pulsed laser providing pulses of peak power of 250 W and pulse width of 200 fs at 2 μm was considered as the pump. The results illustrate that the broadband supercontinuum spectrum can be achieved in a short (~8 mm) waveguide pumped with commercially available fiber laser at 2 μm. The novelty of this work lies in the generation of a mid-Infrared supercontinuum spectrum using a parabolic-core waveguide pumped in the normal dispersion region, which has not been investigated earlier. This design is crucial as the fabricated rectangular waveguide does not remain rectangular after laser post processing but becomes similar to the proposed parabolic design. The proposed design of the waveguide may substantially broaden the range of functions available in future for integrated photonics.

Chapter 4 shows the design and simulate an especially engineered photonic crystal structure. $AsSe_2$ is used in the solid core and As_2S_5 in graded-index hybrid cladding. Hybrid cladding region with inner cladding as a graded helical structure and outer cladding is a hexagonal structure. We have tailored the structural parameters to obtain nearly zero flat-top dispersion profile with all normal dispersion profile. The dispersion at 5μm is -53.13 ps/nm-km with effective mode area of the fundamental mode as 4.18 μm^2. Proposed PCF is suitable for the generation of an ultra-broadband supercontinuum spectrum from 1 μm to 11 μm in MIR domain when pumped with the peak power of 0.75 KW at 5μm with 50 fs pulse width. Proposed PCF design holds potentiality for applications like early cancer diagnostics, gas sensing and food quality check.

Chapter 5 depicts the computational modeling of a silica based Photonic Crystal Fiber infiltrated with ethanol for NIR to MIR supercontinuum generation. Full vectorial finite element method has been used to analyse the impact of infiltration. A flat-top dispersion profile has been obtained with a low peak power of 0.55 kW at a pump wavelength of 1.55 μm. A dispersion value of +30.231 ps/nm-km is obtained in the anomalous region. For the proposed structure nonlinear coefficient is as high as 281.4 $W^{-1}km^{-1}$ with effective mode area of 4.16 μm^2 at 1.55 μm. A broadband

supercontinuum spanning from 1.25 μm to 3.0 μm is achieved by using a fiber length of 20 cm with 60 fs secant laser pulse source. The suggested PCF design assure several critical applications such as biomedical diagnostics and sensing applications.

Chapter 6 showcases a comparative study of two silica-based PCFs that have been infiltrated with nitrobenzene for the purpose of generating supercontinuum light with low peak power in near-infrared to mid-infrared ranges. The analysis of the infiltration's impact was conducted using a full vectorial finite element method. For the symmetrical circular design (#C), we obtained a dispersion value of approximately +30.211 ps/nm/km, an effective mode area of 4.13 μm² and a nonlinear coefficient of 1962.0 $W^{-1}km^{-1}$ at a wavelength of 1.55 μm. In contrast, the asymmetrical designs—elliptical *x*-polarised (#EX) and elliptical *y*-polarised (#EY)—exhibited dispersions of approximately -10.852 ps/nm-km and -8.356 ps/nm-km respectively along with effective mode areas of 4.55 μm² and 4.60 μm² and nonlinear coefficients of 1780.9 $W^{-1}km^{-1}$ and 1761.5 $W^{-1}km^{-1}$. By utilizing a fiber length of 10 mm, a 50 fs secant laser pulse source, and a pump power of 650 W, we achieved a broad supercontinuum spectrum ranging from 1.3 μm to 2.0 μm for the circular design (#C), from 0.9 μm to 2.3 μm for the elliptical *x*-polarised design (#EX) and from 1.0 μm to 2.4 μm for the elliptical *y*-polarised design (#EY). The proposed PCF designs are promising for various applications, including enhanced gas sensing capabilities and improved food quality monitoring systems.

Chapter 7 presents a comparative study of PCFs infiltrated with nonlinear organic liquids nitrobenzene and ethanol for NIR to MIR SCG. To analyze the impact of infiltration a full vectorial FEM has been employed. For Silica based PCF (#A), dispersion around +52.25 ps/nm-km, effective mode area as 6.57 μm^2 and nonlinear coefficient as 1234.18 $W^{-1}km^{-1}$ is obtained at 1.55 μm. For other infiltrated designs (#B), (#C) & (#D) at 1.55μm dispersion around +20.81 ps/nm/km, -20.84 ps/nm/km, + 3.74 ps/nm/km, effective mode area as 1.45 μm^2 and nonlinear coefficient as 5596.22 $W^{-1}km^{-1}$, 5569.71 $W^{-1}Km^{-1}$ and 5584.28 $W^{-1}Km^{-1}$ is obtained respectively. A broadband supercontinuum spanning from 1.3 μm – 1.8 μm for design #A, 1.0 μm – 2.4 μm for design #B, 1.2 μm – 2.5 μm for design #C and 0.9 μm – 2.5 μm for design #D is obtained by using a fiber length of 4 mm to 8 mm with 50 fs secant laser pulse source and pump power of 600 W to 800 W. The suggested PCF design can be employed for detection of explosives, various gases, cancers, ulcers and food quality.

Chapter 8 offers a comprehensive summary of the research conducted for this thesis, highlighting the key conclusions and results. It also explores the potential future scope and social impact of the present study.

REFERENCES

[1] T H Maiman, “Stimulated optical radiation in ruby”, Nature, 187, 493-494 (1960).

[2] National Research Council, “ Harnessing Light: Optical Science and Engineering for the 21st Century”. The National Academies Press, Washington, DC (1998).

[3] A Javan, W R Bennett Jr, and D R Herriott, "Population inversion and continuous optical maser oscillation in a gas discharge containing a He-Ne mixture", Physical Review Letters, 6(3), 106 (1961).

[4] F J McClung, and R W Hellwarth, "Giant optical pulsations from ruby", Journal of Applied Physics, 33(3), 828-829 (1962).

[5] L E Hargrove, R L Fork, and M A Pollack, "Locking of He–Ne laser modes induced by synchronous intracavity modulation", Applied Physics Letters, 5(1), 4-5 (1964).

[6] H W Mocker, and R J Collins, "Mode competition and self-locking effects in a Q-switched ruby laser", Applied Physics Letters, 7(10), 270-273 (1965).

[7] A J DeMaria, C M Ferrar and G E Danielson Jr, "Mode locking of a Nd^{3+}- doped glass laser", Applied Physics Letters, 8(1), 22-24 (1966).

[8] J E Geusic, H M Marcos and Le Grand Van Uitert, "Laser oscillations in Nd-doped yttrium aluminum, yttrium gallium and gadolinium garnets", Applied Physics Letters ,4(10),182-184 (1964).

[9] E Snitzer, "Proposed fiber cavities for optical masers", Journal of Applied Physics, 32(1), 36-39 (1961).

[10] R J Mears, L Reekie, I M Juancey and D N Payne, “Low-noise erbium-doped fiber amplifier operating at 1.54 μm,” Electronics Letters, 23, 1026-1028 (1987).

[11] M Bass, P A Franken, A E Hill, C W Peters and G. Wein reich, "Optical mixing", Physical Review Letters, 8(1), 18 (1962).

[12] J A Giordmaine, and Robert C Miller, "Tunable coherent parametric oscillation in $LiNbO_3$ at optical frequencies", Physical Review Letters, 14(24), 973 (1965).

[13] R R Alfano and S L Shapiro, “Observation of self-phase modulation and picosecond pulse generation in a nonlinear optical fiber”, Physical Review Letters, 24 (11), 584–587 (1970).

[14] T S Saini, A Kumar and R K Sinha, “Broadband mid-infrared supercontinuum spectra spanning 2-15 μm using As_2Se_3 chalcogenide glass triangular-core graded-index photonic crystal fiber”, Journal of Lightwave Technology, 33(18), 3914-3920 (2015).

[15] G P Agrawal, “Nonlinear Fiber Optics”, 5th ed., Elsevier Academic Press, (2013).

[16] P Russell, “Photonic crystal fibers”, Science, 299, 358–362 (2003).

[17] J M Dudley, G Genty and S Coen, “Supercontinuum generation in photonic crystal fiber”, Reviews of Modern Physics, 78, 1135–1184 (2006).

[18] J K Ranka, R S Windeler, and A J Stentz, “Visible continuum generation in air-silica microstructure optical fibers with anomalous dispersion at 800 nm”, Optics Letters, 25, 25-27 (2000).

[19] T S Saini, A Kumar, and R K Sinha, “Broadband mid-IR supercontinuum generation in As_2Se_3 based chalcogenide photonic crystal fiber: A new design and analysis”, Optics Communications, 347, 13 – 19 (2015).

[20] T S Saini, A Bailli, A Kumar, R Cherif, M Zghal and R K Sinha, “Design and analysis of equiangular spiral photonic crystal fiber for mid-infrared supercontinuum generation”, Journal of Modern Optics, 62(19), 1570 – 1576 (2015).

[21] J Swiderski and M Michalska, “Mid-infrared supercontinuum generation in a single-mode thulium-doped fiber amplifier”, Laser Physics Letters, 10(3), 035105 (2013).

[22] C Xia, M Kumar, M Y Cheng, O P Kulkarni, M N Islam, A Galvanauskas, F L Terry, M J Freeman, D A Nolan and W A Wood, “Supercontinuum Generation in Silica Fibers by Amplified Nanosecond Laser Diode Pulses”, IEEE Journal of Selected Topics in Quantum Electronics, 13(3), 789-787 (2007).

[23] D Ghosh, S Roy, Mrinmay Pal, A Pal, S K Bhadra, J McCarthy, H Bookey and A Kar, “Generation of supercontinuum and its theoretical study in three-ring silica microstructured optical fibers”, Applied Optics, 48 (2009).

[24] T Taru, M Hirano, T Sasaki and Knight, “Supercontinuum generation in pure silica core cut-off shifted single-mode fibers”, Conference on Quantum electronics and Laser Science Conference, IEEE, 1-2 (2009).

[25] K M Hilligsøe, T V Andersen, H N Paulsen, C K Nielsen and K Mølmer, “Supercontinuum generation in a photonic crystal fiber with two zero dispersion wavelengths”, Optics Express, 12, 1045-1054 (2004).

[26] A Agrawal, M Tiwari, Y O Azabi, V Janyani, B M A Rahman, and K T V Grattan, "Ultrabroad supercontinuum generation in tellurite equiangular spiral photonic crystal fiber", Journal of modern Optics, 60(12), 956-962 (2013).

[27] B Wanjun, X L Juanjuan, X Liangming and L Meisong, “Mid-infrared SCG in silica photonic crystal fibers”, Applied Optics, 55, 6355-6362 (2016).

[28] M R Karim, B M A Rahman, Y O Azabi, A Agrawal and G P Agrawal, "Ultra broadband mid-infrared supercontinuum generation through dispersion engineering of chalcogenide microstructured fibers", Journal of the Optical Society of America B, 32(11), 2343-2351(2015).

[29] I Kubat, C S Agger, U Moller, A B Seddon, Z Tang, S Sujecki, T M Benson, D Furniss, S Lamrini, K Scholle, P Fuhrberg, B Napier, M Farries, J Ward, P M Moselund, and O Bang, “Mid-infrared supercontinuum generation to 12.5 μm in large NA chalcogenide step-index fibers pumped at 4.5 μm”, Optics Express, 22, 19169–19182 (2014).

[30] A Agrawal, N Kejalakshmy, B M A Rahman, and K T V.Grattan, "Soft glass equiangular spiral photonic crystal fiber for supercontinuum generation", IEEE Photonics Technology Letters, 21(22), 1722-1724 (2009).

[31] J M Dudley and J R Taylor, eds. “Supercontinuum generation in optical fibers”, Cambridge University Press (2010).

[32] J H V Price, T M Monro, K Furusawa, W Belardi, J C Baggett, S Coyle, C Netti, J J Baumnerg, R Paschotta and D J Richardson, “UV generation in a pure-silica holey fiber”, Applied Physics B, 77(2-3), 291-298 (2003).

[33] A Labruyère, P Leproux, V Couderc, V Tombelaine, J Kobelke, K Schuster, H Bartelt, S Hilaire, G Huss, and G Mélin, “Structured-Core GeO_2-Doped Photonic-Crystal Fibers for Parametric and Supercontinuum Generation”, IEEE Photonics Technology Letters, 22(16), 1259-1261 (2010).

[34] F Begum, and P E Abas, “Near-infrared supercontinuum generation in silica-based photonic crystal fiber”, Progress in Electromagnetics Research, 89, 149-159 (2019).

[35] J C Vindas, S T Piero, A Diez and M V Andres, “Supercontinuum generation in highly Ge-doped core Y-shaped microstructured optical fiber”, Appied Physics B, 98, 371-376, (2010).

[36] V A G Rivera and D Manzani “Technological Advances in Tellurite Glasses”, Springer International Publishing (2017).

[37] N Granzow, S P Stark, M A Schmidt, A S Tverjanovich, L Wondraczek and J Russell, "Supercontinuum generation in chalcogenide-silica step-index fibers", Optics Express, 19(21), 21003-21010 (2011).

[38] J Sanghera and D Gibson, "Optical properties of chalcogenide glasses and fibers", In Chalcogenide Glasses, Woodhead Publishing, 113-138 (2014).

[39] M R Karim, B M A Rahman and G P Agrawal, “Dispersion Engineered $Ge_{11.5}As_{24}Se_{64.5}$ nanowire for supercontinuum generation: a parametric study”, Optics Express, 22, 31029- 31040 (2014).

[40] T S Saini, A Kumar and R K Sinha, “Broadband mid-IR supercontinuum generation in As_2Se_3 based chalcogenide photonic crystal fiber: A new design and analysis”, Optics Communications, 347, 13 – 19 (2015).

[41] T S Saini, A Bailli, A Kumar, R Cherif, M Zghal, and R K Sinha, “Design and analysis of equiangular spiral photonic crystal fiber for mid-infrared supercontinuum generation”, Journal of Modern Optics, 62(19), 1570 – 1576 (2015).

[42] A G N Chaitanya, T S Saini, A Kumar and R K Sinha, “Ultra-broadband mid-IR supercontinuum generation in $Ge_{11.5}As_{24}Se_{64.5}$ based chalcogenide graded-index photonic crystal fiber: design and analysis”, Applied Optics, 55(36), 10138 – 10145 (2016).

[43] T S Saini and R K Sinha, "Mid-infrared supercontinuum generation in soft-glass specialty optical fibers: a review", Progress in Quantum Electronics, 78, 100342 (2021).

[44] S Liu, W Gao, H Li, Y Dong, H Zhang, “Liquid-filled simplified hollow-core photonic crystal fiber”, Optics & Laser Technology, 64, 140-144 (2014).

[45] I Hartl, X D Li, C Chudoba, R K Ghanta, T H Ko, J G Fujimoto, J K Ranka and R S Windeler, “Ultrahigh-resolution optical coherence tomography using continuum generation in an air-silica microstructure optical fiber”, Optics Letters, 26, 608–610 (2001).

[46] P Hsiung, Y Chen, T H Ko, J G Fujimoto, C J S De Matos, S V Popov, J R Taylor and V P Gapontsev, “Optical coherence tomography using a continuous-wave, high-power, Raman continuum light source”, Optics Express, 12, 5287–5295 (2004).

[47] H Takara, T Ohara, T Yamamoto, H Masuda, M Abe, H Takahashi, and T Morioka, “Field demonstration of over 1000-channel DWDM transmission with supercontinuum multi-carrier source”, Electronics Letters, 41, 270–271 (2005).

CHAPTER 2: NUMERICAL METHODOLOGY

When an electromagnetic pulse propagates through a medium, it experiences various phenomena such as attenuation (or loss) and dispersion. These effects arise due to the interaction between the electromagnetic wave and the atomic or molecular structure of the medium. In particular, dispersion leads to the temporal spreading of the pulse as different frequency components travel at different velocities, while loss results in a gradual reduction of pulse energy. In a nonlinear optical medium especially under conditions of high optical field intensity, such as those found in optical waveguides and PCFs additional effects come into play that significantly influence pulse propagation. Two prominent nonlinear phenomena are the Kerr effect and the Raman effect. The Kerr effect refers to the intensity-dependent change in the refractive index of the medium. As the optical intensity changes, the refractive index of the medium also changes, leading to self-phase modulation and other nonlinear optical behaviors. This results in phenomena such as spectral broadening and soliton formation.

On the other hand, Raman effect arises from the inelastic scattering of photons, where incident light interacts with vibrational modes (phonons) of the medium. This effect enables energy transfer between the light field and the medium, leading to a frequency shift in the propagating light (known as the Stokes and anti-Stokes shifts), and plays a crucial role in processes such as Raman amplification and supercontinuum generation [1]. Together, these nonlinear effects (intensity-dependent refractive index modulation and photon-phonon interactions) govern the complex dynamics of high-intensity electromagnetic pulse propagation in nonlinear optical media like waveguides and PCFs.

Both time dependent and frequency dependent formulations can be employed for the effective computational study of the SCG process in waveguide and PCF designs. The frequency-dependent formulation is predominantly employed in practice due to its structural analogy with the nonlinear Schrödinger equation (NLSE). Moreover, it explicitly captures the frequency dependence of both linear and nonlinear effects, including attenuation, chromatic dispersion, Kerr nonlinearity, and the spatial distribution of the electric field through mode area variations [2].

In frequency domain, chromatic dispersion of arbitrary order is incorporated directly through the propagation constant without requiring high-order temporal derivatives, which improves numerical stability and reduces computational complexity. This approach is particularly advantageous when simulating ultrashort pulses with wide spectral broadening, where dispersion and spectral effects dominate.

A well-established numerical technique Finite-Element Method (FEM) based COMSOL Multiphysics Software is employed for performing mode analysis of the proposed waveguide and PCFs designs. This technique involves fragmentation of the design into finite elements and these are further solved numerically. The COMSOL Multiphysics software requires a minimum of 4 GB RAM for efficient operation. We have used 32 GB RAM for better run time. The computational time is highly dependent on the RAM size and mesh grid size. In the FEM simulations, three types of mesh sizes are available: coarse, normal and fine. Each mesh type involves a trade-off between computational time and numerical accuracy. It is important to note that the computational time increases with the structural complexity of the design, as more intricate geometries require a denser distribution of elements to accurately resolve field variations. The coarse mesh requires the shortest computational time but provides the lowest spatial resolution and precision. The normal mesh offers improved accuracy with moderate computational time, while the fine mesh provides the highest level of precision at the expense of significantly increased computational time. A convergence analysis was performed to evaluate the reliability of the numerical results. The results obtained using the normal and fine mesh settings were found to be very similar, indicating that the solution had effectively converged. Although the normal mesh already provided sufficiently accurate results, the fine mesh was ultimately selected to ensure maximum numerical precision and robustness in the reported data. To analyse the modes and for performing further calculations & graphing, MATLAB programming software is used.

2.1 Linear attributes

The wavelength dependent refractive index of the used materials were calculated by using the Sellmeier equation 2.1

$$n^2(\lambda) = 1 + \sum_{k=1}^{N} \frac{B_k \lambda^2}{\lambda^2 - b_k^2} \quad (2.1)$$

The sellmeier coefficients are different for each material in chapter 3, $AsSe_2$ (B_1 = 6.751, B_2 = 0, B_3 = 0.1768, b_1^2 = 0.1034 μm^2, b_2^2 = 153.7990 μm^2, b_3^2 = 10^{-32} μm^2) and MgF_2 (B_1 = 0.48755708, B_2 = 0.39875031, B_3 = 2.3120353, b_1^2 = 0.00188 μm^2, b_2^2 = 0.00895 μm^2, b_3^2 = 566.1355 μm^2) [1,3].

In chapter 4, we have $AsSe_2$ - As_2S_5 combination, where B_1 = 6.751, B_2 = 0, B_3= 0.1768, b_1^2 = 0.1034 μm^2 , b_2^2 = 153.7990 μm^2, b_3^2 = 10^{-32} μm^2 for $AsSe_2$ and B_1 = 2.1361, B_2 = 0.0693, B_3 = 1.7637, b_1^2 = 0.0954 μm^2, b_2^2 = 225.0001 μm^2, b_3^2= 2.1783 × 10^{-7} μm^2 for As_2S_5 [4-5].

In chapter 5, 6 and 7, B_1 = 0.83189, B_2 = −0.15582, b_1^2 = 0.0093 μm^2, b_2^2 = −49.452 μm^2 for ethanol and for silica glass are B_1 = 0.69616630, B_2 = 0.40794260, B_3 = 0.89747940, b_1^2 = 0.00467914μm^2, b_2^2=0.01351206μm^2, b_3^2 = 97.93400253μm^2 [6].

In chapter 6 and 7, B_1 = 1.30628, B_2 =0.00502, b_1^2 = 0.02268 μm^2, b_2^2 = 0.18487 μm^2 for nitrobenzene [7].

To calculate the dispersion characteristics of the proposed PCF structures in the units of (ps/nm-km) the following correlation has been employed as shown in equation below

$$D(\lambda) = -\frac{\lambda}{c}\frac{\partial^2 Re(n_{eff})}{\partial \lambda^2} \tag{2.2}$$

In this context, the real part of the effective mode index is indicated as Re(n_{eff}), which describes the portion of the mode index that corresponds to the actual propagation characteristics of the mode within the medium. Additionally, *c* represents the speed of light in free space, or vacuum, which is a fundamental constant used in calculating the propagation properties of light in the absence of any material medium. Using Equation (2.3), the effective mode area (A_{eff}) of the propagating mode having units of μm^2 has been calculated, where the amplitude of the electric field of the light is represented by *E*.

$$A_{eff} = \frac{\left(\iint_{-\infty}^{\infty}|E|^2 dx\, dy\right)^2}{\left(\iint_{-\infty}^{\infty}|E|^4 dx\, dy\right)} \tag{2.3}$$

2.2 Nonlinear attributes

In the simulations, the initial input laser pulse deliberated is a hyperbolic secant, as depicted in the equation below

$$\mathrm{A(0,T)} = \sqrt{\mathrm{P_0}}\ \mathrm{sech}\frac{\mathrm{T}}{\mathrm{T_0}} \tag{2.4}$$

The equation introduces various components: The pulse envelope *A* (0, T), characterizes the shape of the pulse. P_0, the peak power of the input pulse. T_0 is full- width-at-half-maxima (FWHM) divided by 1.7627, specifically tailored for hyperbolic secant pulses. *T* is the concurrent frame associated with the group velocity of the pulse envelope.

The time domain-dependent generalized nonlinear Schrödinger equation (GNLSE) can be expressed as

$$\frac{\partial A}{\partial z} + \frac{\alpha}{2}A - \left(\sum_{n\geq 2}\frac{i^{n+1}}{n!}\beta_n\frac{\partial^n}{\partial T^n}\right) = i\gamma\left(1 + \frac{i}{\omega_0}\frac{\partial}{\partial T}\right)\left(A(z,t)\int_{-\infty}^{\infty}R(T)\times|A(z,T-T)|^2 dT + i\Gamma_R(z,T)\right) \tag{2.5}$$

We have implemented the frequency domain-dependent GNLSE to study the pulse propagation and SC generation in the proposed waveguide and PCF. The following GNLSE is solved using Split-

Step Fourier method to obtain the widening of the spectral range observed in the generated SC as

$$\frac{\partial \tilde{A}'}{\partial z} = i\bar{\gamma}(\omega)\exp\left(-\hat{L}(\omega)z\right)\mathcal{F}\left\{\bar{A}(z,T)\int_{-\infty}^{\infty}R(T')|\bar{A}(z,T-T')|^2dT'\right\} \quad (2.6)$$

Where, $\tilde{A}'$ is envelope or the covering of the output pulse which represents its modulation amplitude or shape, $\bar{A}(z,T)$ the envelope at distance *z* at time *t*. $\bar{A}(z,\omega)$, the Fourier transform of $\bar{A}(z,T)$. The frequency-dependent nonlinear coefficient $\bar{\gamma}(\omega)$ is obtained by taking into account its dependency on the frequency

$$\bar{\gamma}(\omega) = \frac{n_2 n_0 \omega}{c n_{eff}(\omega) A_{eff}^{\frac{1}{4}}(\omega)} \quad (2.7)$$

n_2 corresponds to the nonlinear refractive index, which is specifically 2.3×10^{-17} m^2/W for $AsSe_2$ chalcogenide glass used in chapters 3 and 4 [8], 2.89×10^{-20} m^2/W for silica at 1.55 μm used in chapters 5 and 6 [2] & 2.0×10^{-18} m^2/W for nitrobenzene used in chapter 7 [9].

The symbol n_0 represents the glass refractive index at the wavelength needed to calculate n_2 and *c* being the speed of light in free space (vacuum). The expression for the altered variables are stated as

$$\tilde{A}'(z,\omega) = \tilde{A}(z,\omega)\exp(-\hat{L}(\omega)z) \quad (2.8)$$

The following equation shows the linear operator $\hat{L}(\omega)$ as

$$\hat{L}(w) = i(\beta(\omega) - \beta(\omega_0) - \beta_1(\omega_0)[\omega - \omega_0]) - \frac{\alpha(\omega)}{2} \quad (2.9)$$

Where, β: propagation constant, β_1: the inverse of the group velocity of pulse envelope, α: the total loss and ω_0: the reference frequency.

The organic liquids have a negligible material loss as a consequence of low absorption coefficients. We have considered the material loss of silica in the simulations due to smaller fiber propagating length [10].

The Raman response function R (t) is defined as

$$R(t) = (1-f_R)\delta(T) + f_R\frac{\tau_1^2+\tau_2^2}{\tau_1\tau_2^2}\exp\left(-\frac{T}{\tau_2}\right)\sin\left(\frac{T}{\tau_1}\right)\mathrm{H(T)} \quad (2.10)$$

This is relation has been used in chapter 3, 4 and 5 where core material is solid. Here, H(T) being the Heaviside step function depends on *T*. For the $AsSe_2$ glass, Raman parameters: Fractional Raman response (f_R), Raman period (τ_1), damping time (τ_2), are 0.148, 15.34 fs and 106.1 fs respectively [11]. For silica glass $f_R = 0.245$, $\tau_1 = 12.25$ fs and $\tau_2 = 32$ fs [12].

In chapter 6 and 7, where core material is a liquid we have few more contributing terms in the Raman response function which are given below

$$R(t) = (1 - f_R)\delta(T) + f_R\, h_m(t)\mathrm{H(T)} \tag{2.11}$$

$$h_m(t) = A_1 e^{(-t/t_{diff})}\left(1 - e^{(-t/t_{rise,1})}\right) + A_2 e^{(-t/t_{int})}\left(1 - e^{(-t/t_{rise,1})}\right) + A_3\, e^{(-t^2/2t_{fast}^2)}\sin(t/t_{rise,2}\,) \tag{2.12}$$

where, A_1 (1/s) = 0.0288, A_2 (1/s) = 0.0930, A_3 (1/s) = 1.475, t_{diff} (ps) = 31.8, $t_{rise,1}$ (ps) = 0.15, t_{int} (ps) = 0.51, t_{fast} (ps) = 0.08, $t_{rise,2}$ (ps) = 0.10. For nitrobenzene, the Raman parameters f_R is around 0.87.

2.3 Coherence

A LASER light is highly coherent but when we perform SCG this coherence nature is effected due to pulse broadening. To find out the exact nature of the pulse, coherence is evaluated. We have employed one photon per mode noise model which can help in investigating the coherent property of SCG. The relation to find out coherence has been shown in equation 2.13

$$|g_{12}(\lambda(t_1 - t_2)| = \frac{|<E_1^*(\lambda,t_1)E_2(\lambda,t_2)>|}{(<|E_1(\lambda,t_1)^2|><|E_2(\lambda,t_2)^2|>)^{1/2}} \tag{2.13}$$

In this study, the modulus of complex degree of first-order coherence g_{12} is used to calculate the degree of coherence which varies from 0 to 1. Value one signifies a perfectly coherent spectrum and value zero means no coherence. A value in between 0 to 1 shows moderate coherence behaviour [13]. The electric fields of individual SCG pairs are represented as $E_1(\lambda, t_1)$ and $E_2(\lambda, t_2)$, where λ represents the wavelength, and t_1 and t_2 are time variables associated with consecutive SCG spectra. These electric fields correspond to sequential spectra produced by the SCG process, allowing us to examine subtle variations in spectral coherence over time. Angular brackets are used to indicate an average taken across the entire ensemble of pulses, providing a comprehensive measure of the spectral properties. To specifically analyze how coherence depends on wavelength alone, we set the time difference between pulses, $\Delta t = t_1 - t_2$ to zero, effectively isolating wavelength as the primary variable in our coherence assessment.

REFERENCES

[1] G P Agrawal, “Nonlinear fiber optics”, In Nonlinear Science at the Dawn of the 21st Century, Springer, Berlin Heidelberg ,195-211 (2000). https://doi.org/10.1016/B978-0-12-817040-3.00007-9

[2] J M Dudley, G Genty and S Coen, “Supercontinuum generation in photonic crystal fiber”, Reviews of Modern Physics, 78, 1135–1184 (2006).

[3] J Yuan, Z Kang, F Li et al., “Mid-infrared octave-spanning supercontinuum and frequency comb generation in a suspended germanium-membrane ridge waveguide”, Journal of Light Technology, 35, 2994-3002 (2017).

[4] M Diouf, A Wague and M Zghal, “Numerical investigation of anultra-broadband coherent mid-infrared supercontinuum in a chalcogenide $AsSe_2$-As_2S_5 multimaterial photonic crystal fiber”, Journal of Optical Society of America B, 36(2), 8–14 (2019).

[5] T Cheng, Y Kanou, D Deng, X Xue, M Matsumoto, T Misumi, T Suzuki and Y Ohishi, “Fabrication and characterization of a hybrid fiber with a large refractive index difference”, Optical Express, 22, 13322–13329 (2014).

[6] H V Le, V L Cao, H T Nguyen, A M Nguyen, R Buczyński and R Kasztelanic, “Application of ethanol infiltration for ultra flattened normal dispersion in fused silica photonic crystal fibers”, Laser Physics, 28(11), art. 115106 (2018).

[7] Chu Van L, Nguyen Thi T, Hoang Trong D, et al., “Comparison of supercontinuum spectrum generating by hol ow core PCFs filled with nitrobenzene with different lattice types”, Optical Quantum Electronics, 54(5), 300 (2022).

[8] T S Saini and V R Supradeepa, “Tellurium-oxide coated silicon nitride hybrid waveguide for near-to-mid-IR supercontinuum generation: design and analysis”, Journal of Modern Optics, 68, 29-36 (2021).

[9] S Kedenburg, A Steinmann, R Hegenbarth et al., “Nonlinear refractive indices of nonlinear liquids: wavelength dependence and influence of retarded response”, Applied Physics B, 117, 803–816 (2014).

[10] V Devika, M S Mani Rajan, H Thenmozhi et al., “Flower core photonic crystal fibres for supercontinuum generation with low birefringent structure for biomedical imaging”, Journal of Optics, 52, 539–547(2023).

[11] M Diouf, A Wague and M Zghal, “Numerical investigation of an ultra-broadband coherent mid-infrared supercontinuum in a chalcogenide $AsSe_2$-As_2S_5 multimaterial photonic crystal fiber”, Journal of Optical Society of America B, 36(2), 8–14 (2019).

[12] H V Le, V L Cao, H T Nguyen, A M Nguyen, R Buczyński and R Kasztelanic, “Application of ethanol infiltration for ultra- flattened normal dispersion in fused silica photonic crystal fibers”, Laser Physics, 28(11), art. 115106 (2018).

[13] Z Guo, J Yuan, C Yu et al., “Highly coherent supercontinuum generation in the normal dispersion liquid-core photonic crystal fiber”, Progress In Electromagnetics Research, 48, 67–76 (2016).

CHAPTER 3: CHALCOGENIDE PARABOLIC-CORE WAVEGUIDE FOR ON-CHIP SUPERCONTINUUM GENERATION EXTENDING FROM NEAR-IR REGION TO MID-IR REGION *

3.1 Introduction

Mid-infrared supercontinuum generation using integrated waveguides has been a stimulating and active research topic for the last two decades [1,2]. Mid-IR region offers two optical windows (i.e., 3−5 μm and 8−13 μm) which are optically transparent to the earth's atmosphere. Various sorts of Mid-IR light sources have been developed which are finding potential applications in diverse fields including optical communications, optical coherence tomography, medical endoscopy and gas sensing [3–6]. Ultrafast photonics plays a crucial role in SCG, as it involves the use of femtosecond or picosecond laser pulses [7–11]. SC spectrum is generated when the large number of nonlinear effects such as stimulated Raman scattering, self-phase modulation, cross-phase modulation and four-wave mixing act all together on an intense pump beam to root the large spectral broadening of the original pump beam [12]. Microstructured fibers, Photonic crystal fibers and waveguides have recently attracted significant research interest due to its high designing freedom [13].

Different materials like silica, tellurite and chalcogenide glasses have been used in waveguides, PCF and various step index fibers for employing SCG in mid-IR [14–19]. Silica based optical waveguides can be used to realize the strong modal confinement and dispersion profile. At the same time, silica needs a very high power pumping source to generate SC spectrum as it holds a feeble optical nonlinearity. The inherent opacity of silica in the mid- IR region (beyond 2.5 μm) impedes efficient SCG. Pumping air cladded silicon-germanium waveguides at 4.0 μm with an average power >10 W can be employed for achieving the broadband mid-IR SCG with higher power [10]. However, to obtain mid-IR SCG such air cladded silicon-germanium rooted waveguides possess a limitation of the necessity of using an unfamiliar pump source operating at a wavelength >4 μm.

Recently, a new photonic platform based on Si_3N_4 and Hydex material has been introduced for various nonlinear applications such as on-chip optical frequency comb generation and short optical pulse generation [20]. Ahmad et al. documented a waveguide configuration that provides a SC spectrum

** D.S. Tomer and A. Kumar, "Design and numerical modeling of chalcogenide parabolic-core waveguide for on-chip supercontinuum generation extending from near-IR region to mid-IR region. Microwave and Optical Technology Letters, 66(3), e34105 (2024).https://doi.org/10.1002/mop.34105.*

with an all-normal dispersion profile, spanning from 950 to 2100 nm [21]. Soliton fission process along with the emission of the dispersive waves is responsible for the broadening in the SC spectrum if pumped in the anomalous dispersion region. The SCG by the process of soliton fission is vulnerable to the laser shot noise which makes SC unstable. By considering 10 kW as peak power at 2 micron a SC spectrum spanning (~0.95−5.50 μm) has been reported for a new design of hybrid TeO_2-coated-Si_3N_4 waveguide deposited on sapphire substrate [22]. Psaila et al. were the first to report the initial observation of the self—phase modulation phenomenon in a chalcogenide waveguide when pumped with an ultrafast laser [23]. The numerical modeling of an As_2Se_3 based waveguide has been reported for broadband mid- IR SCG [16]. The mid-IR SC spectrum has been investigated using the dispersion-designed channel waveguide in $Ge_{11.5}As_{24}Se_{64.5}$ based chalcogenide glass with MgF_2 as a substrate [24]. Very recently, the rib waveguide structures generating broadband mid-IR SC have been reported for the application of on-chip photonic devices [1,16]. The chalcogenide materials are preferred for broadband SCG because of the lower peak power requirement and high nonlinearity.

In this work, we report a mid-IR SC spectrum extending from 1.4 to 7.6 μm using an 8 mm long parabolic-core chalcogenide waveguide pumped with 250 W, 200 fs laser pulses at 2 μm. In comparison to recently reported result [1, 25] we obtained similar broader coherent mid-IR SC spectrum with lower peak power of input laser pulse. The produced SC source can be used to discern chemicals, inspect food quality, detect explosives and hazardous gases, ulcer and cancer diagnosis, frequency comb generation, optical imaging, and OCT. Considering five segments of this work, 1st segment provides the brief introduction and overview of the work, 2nd segment includes the parabolic-core waveguide designing and its importance. In the 3rd and 4th section, the extensive illustration of the analytical methodology used and results and discussion, respectively. In the last section, entire work has been concluded followed by references.

3.2 Design parameters of the proposed parabolic-core $AsSe_2$ waveguide

The illustration of the transverse cross-sectional view of the designed parabolic-core waveguide structure is provided in Figure 3.1(a). Waveguide structure comprises of a parabolic-core of the $AsSe_2$ chalcogenide glass on MgF_2 substrate. Here, MgF_2 is considered as an upper cladding of the waveguide as well. As can be seen in Figure 3.1(a), "a" and "h_0"

represents the core width, and the height, respectively. The trench depth has been denoted by "t." From the fabrication perspective, the film of $AsSe_2$ can be deposited by the plasma etching chemical vapour deposition (CVD) technique. The optimal thickness of the $AsSe_2$ layer, set at 1.25 μm, is designed to get normal dispersion during operation at 2 μm. Significantly, the suggested parabolic waveguide accommodates few modes in its core, and their effective mode indices meet the criterion

for suppressing mode coupling ($\Delta n > 0.5 \times 10^{-3}$), and therefore, effectively minimize inter-mode coupling. Here, Δn is the difference between the effective indices of any two modes [17]. Between the two modes, the fundamental transverse electric mode (TE-mode) has been chosen as the propagating mode for the simulations. Figure 3.1(b) demonstrates the normalized electric field patterns of the propagating TE-mode in the core of the parabolic waveguide at 2.0 μm. The structural parameters of the proposed waveguide structure (a = 1 μm; h_0 = 1.25 μm; t = 0.6 μm).

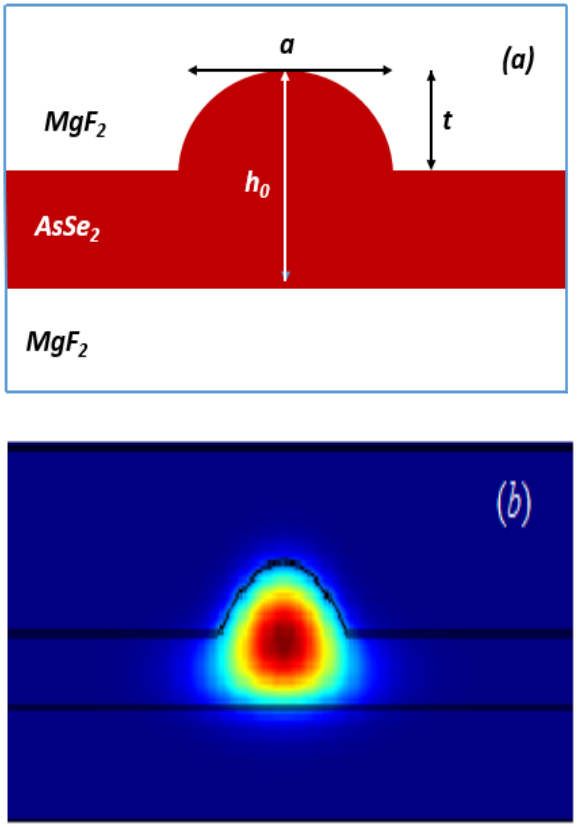

Figure 3.1

Figure 3.1 (*a*) The transverse cross-sectional view of the proposed parabolic-core waveguide and **(*b*)** electric field distribution of fundamental TE mode at 2 μm.

The core shape is designed as stated in the following power law expression and q = 0.5 for parabolic core profile $h = [(h_0^2 (1 - (t/h_0) (x^4/a)^q))^{0.5}]$; $-a/2 \leq x \leq a/2$ [1]. Here, h_0 is the maximum height of the core and x represents transverse distance from the centre of the core. A Perfectly Matched Layer (PML) has been employed at the outer boundary to prevent artificial reflections from the edges of the computational domain. We have used rectangular PML of width 1 μm.

3.3 Formulations and method of analysis

The parabolic-core waveguide structure is designed and thereafter the effective mode index (n_{eff}) of the fundamental TE-mode is determined using COMSOL software which uses full-vectorial finite

element method. The linear and nonlinear characteristics has been explained with great depth in chapter 2. The wavelength dependent refractive index of $AsSe_2$ chalcogenide glass and MgF_2 materials was calculated by using the Sellmeier equation, mentioned in equation 2.1 and other parameters required simulation has been discussed in chapter 2.

3.4 Results and discussions

For a waveguide structure the broadening in the supercontinuum spectrum primarily depends upon the nonlinearity of material and the dispersion characteristics [24]. The dispersion profile has been evaluated after optimizing core width for a (1.0 μm, 1.5 μm, 2.0 μm) and core height values for h_0 (1.25 μm, 1.50 μm, 1.75 μm, 2.0 μm), the same has been illustrated in Figs. 3.2 & 3.3 respectively.

As depicted in Fig. 3.2, the dispersion curve corresponding to a =1 μm is showing minimum dispersion at 2 μm. In Fig. 3.3, varying h_0 parameter does not impact the dispersion profile significantly as the net effective mode index remains almost same which is obvious. The dispersion curve exhibit two zero dispersion wavelengths (ZDWs) for the given waveguide design. The n_{eff} of fundamental TE mode is found to be 2.59494 at 2 μm. The two ZDWs are falling around ~2.32 μm and ~3.77 μm. This design offers anomalous dispersion in the wavelength range between ~2.32 μm and ~3.77 μm.

The expansion of the supercontinuum spectrum primarily relies on the dispersion profile of the waveguide structure and the characteristics of the input pulse. In normal dispersion profile SPM is the main cause of broadening. There is no soliton formation, as in the case of anomalous regime where soliton fission and SRS are responsible. In case of normal dispersion, dispersion and nonlinearity do not cancel each other. Instead, they work in the same general direction where nonlinearity broadens the spectrum, while dispersion spreads the pulse in time. As a result, the pulse gradually stretches and evolves smoothly. The behavior is stable and predictable and solitons do not form.

In the anomalous dispersion regime, dispersion can balance the nonlinear effect of the medium. This balance allows the pulse to maintain its shape, forming what is known as a soliton. However, this regime is more sensitive to disturbances. Small fluctuations can grow, leading to effects such as modulation instability and soliton breakup, which produce very strong spectral broadening.

If all normal dispersion is introduced in the nonlinear process the spectrum is relatively flat and a single pulse is maintained at the time domain. Consequently, SC with high coherence can be achieved which is vital in practical applications. To generate SC in the normal dispersion regime, one approach is to pump the fiber well below the zero dispersion wavelength, preventing the generated spectrum

from extending into the anomalous dispersion region. If the pumping is chosen in between these wavelengths (i.e., anomalous dispersion region), then the broadband spectrum will be obtained but the coherency will be compromised. To obtain the coherent and smooth SC spectrum, the pumping should be done in normal dispersion region i.e. at the wavelength < 2.3 μm and > 3.77 μm [27,28].

For the proposed waveguide structure, we have two possible wavelength regions to be chosen as pump wavelength, one with wavelength < 2.3 μm and the other with wavelength > 4.7 μm. To approximate the performance of the proposed parabolic-core $AsSe_2$ waveguide structure, we have considered commercially available Tm-doped fiber laser source at 2.0 μm as a pump source. So, the pump wavelength of 2 μm have been considered in all the simulations. The value of dispersion, D = -101.2 ps/nm-km and the propagation loss of the fiber is 1.17×10^{-2} dB/m at 2 μm.

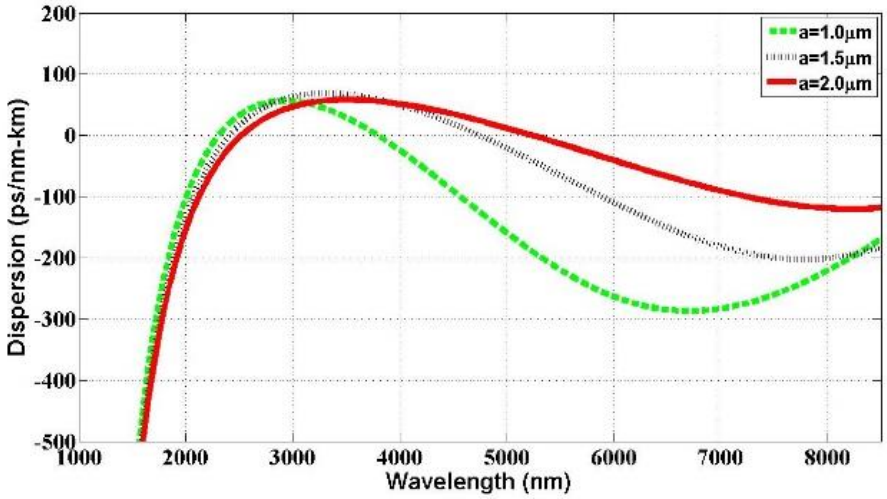

Figure 3.2 Effect of Core Width "a" on dispersion characteristic of the parabolic-core $AsSe_2$ chalcogenide rib waveguide for h_0 =1.25 μm.

Figure 3.4 illustrates the graph depicting the effective mode area and non-linearity as functions of wavelength. In Fig. 3.4, effective mode area for the fundamental mode is recorded as 1.51 μm² and nonlinearity coefficient as 47.85 W^{-1} m^{-1} at 2 μm. To deal with the fabrication imperfecions, a tolerance study was done. The design parameters were changed by +3%, the change in effective mode area and non-linearity were around +6%. When they were changed by -3%, change in area and nonlinearity was about -2%. The average change is around 4%.

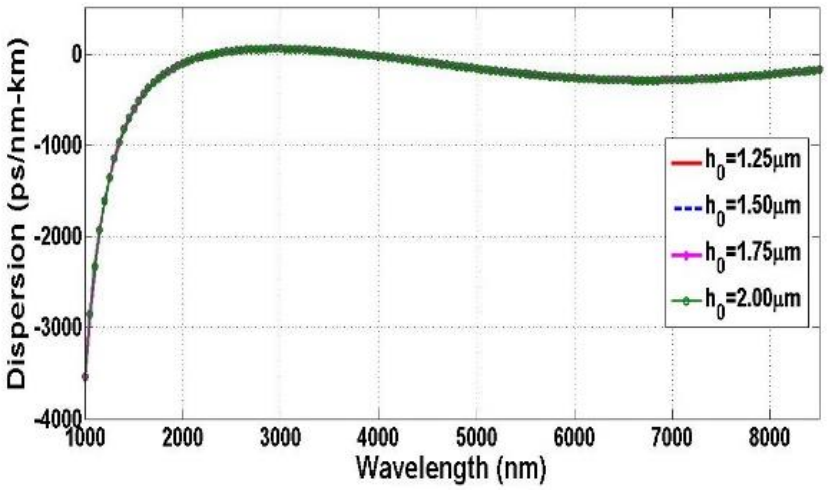

Figure 3.3 Effect of Core height "h_0" on the dispersion characteristic of the parabolic-core $AsSe_2$ chalcogenide rib waveguide for a = 1 μm.

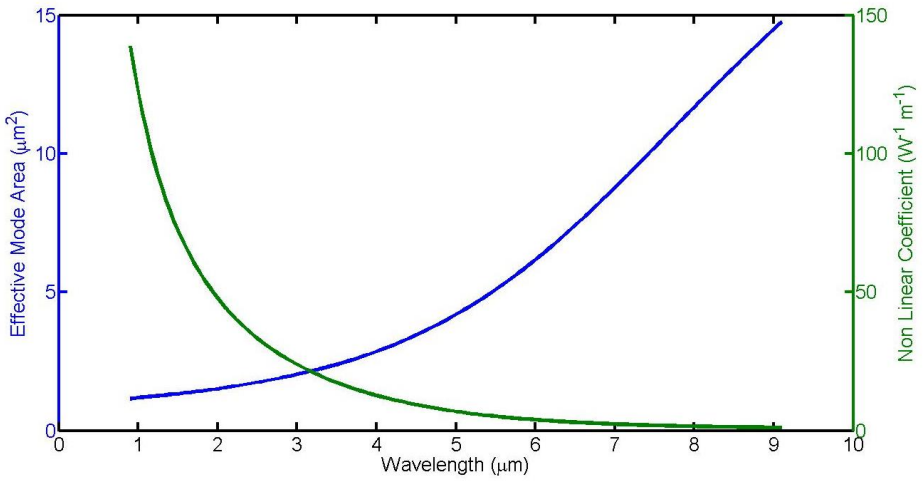

Figure 3.4 The spectral changes in the effective mode area and nonlinear coefficient with respect to wavelength.

The SC broadening results were influenced by using variable fiber length and input pump peak power. Figures 3.5 & 3.6 depict the progression of broadening in SC spectrum along the variable length of the waveguide and variable input power respectively. As observed in Fig. 3.5, the fiber length is varied from 2 mm to 8 mm at 2.0 μm wavelength using 250 W pump power. Below 8 mm fiber length broadening is less. A broadband SC spectrum extending from 1.4 – 7.6 μm can be generated with 8 mm long parabolic-core waveguide pumped with 200 fs laser pulses. Beyond 8 mm noise increases, maximum broadening is observed for 8 mm.

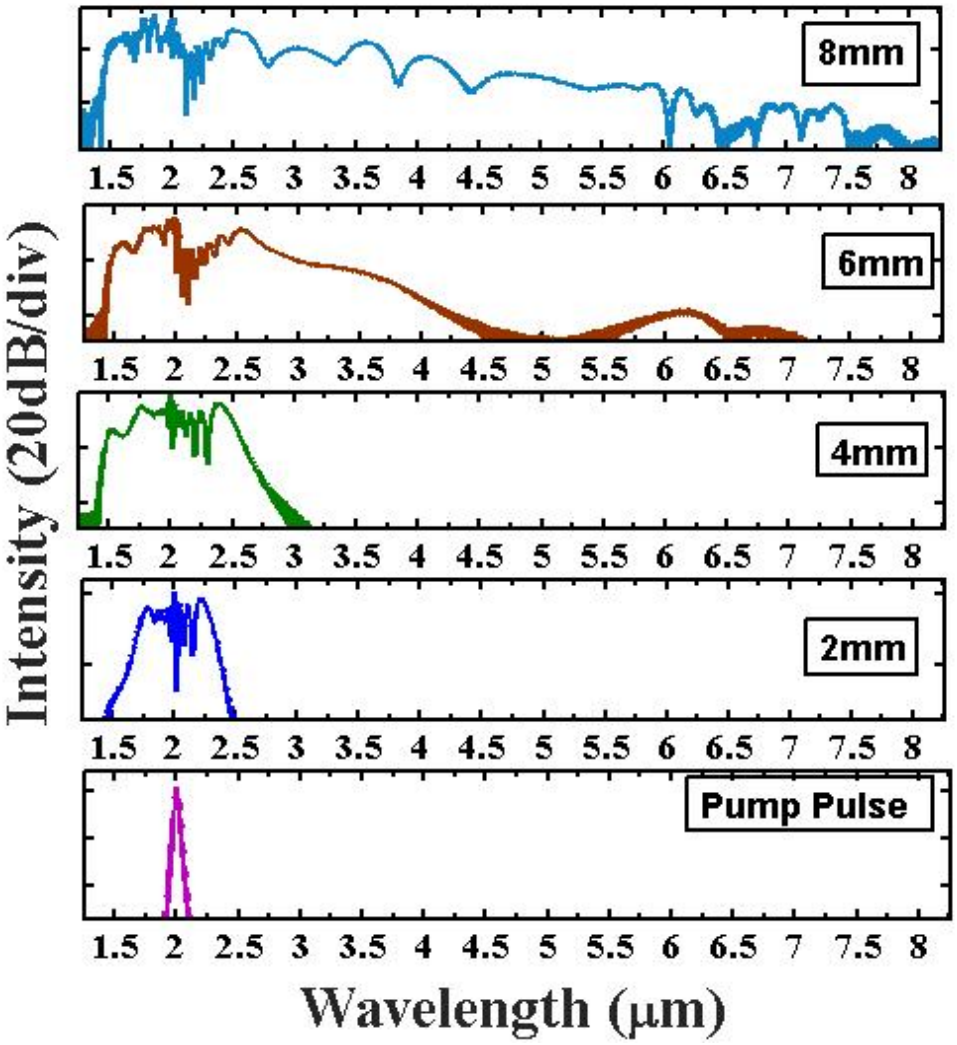

Figure 3.5 The variation in the SC intensity at 2.0 μm in response to the length, induced by 200 fs laser pulses with 250 W pump power.

Similarly, as depicted in fig.3.6 the influence of changing pump power is examined across a range of values: 100 W, 150 W, 200 W, 250 W, 300 W, 400 W, and 500 W. The most significant broadening is observed at a pump power of 250 W. On increasing the peak power the spectral broadening increases and reaches at maximum broadening. Further increase in input peak power add undesirable fluctuations in the supercontinuum spectrum.

For the proposed design various parameters have been evaluated, nonlinear length $L_{NL}= 1/\gamma P_0$ as 8.3×10^{-5}m (P_0 = input peak power); β_2 as 2.15×10^{-25} s^2/m; dispersion length $L_D = (T_0^2/\beta_2)$ as 1.06×10^{-1}m; T_{FWHM} as 200 fs; T_0 as $T_{FWHM}/1.763$; soliton number N = sqrt (L_D/L_{NL}) as 35.5 respectively [3,4].

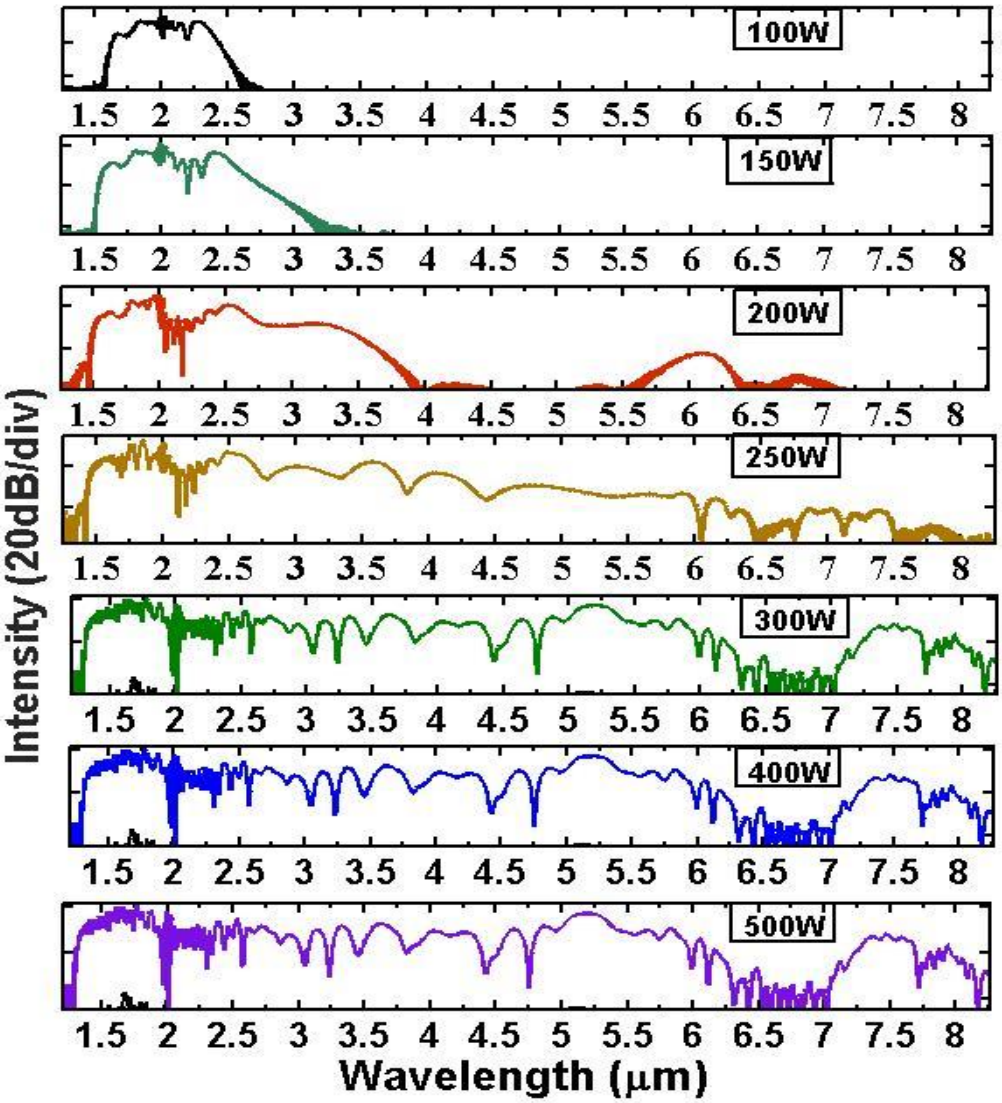

Figure 3.6 The variation in SC intensity with the input pulse peak power with 8 mm fiber length with 200 fs laser pulses at 2.0 μm.

Near-to-mid-IR supercontinuum pulses that are repeatable from shot to shot are crucial for enhancing image penetration depth and regaining a 10 dB signal-to-noise ratio [28, 29].In this paper, we concentrate on the extensive range of SC spectra achieved with minimal pump power within a short length of the suggested waveguide.

3.5 Conclusion

In summary, the reported parabolic-core waveguide structure offers normal dispersion at pump wavelength of 2 μm. The novelty of this work lies in the generation of mid-IR SC spectrum using parabolic-core waveguide design, which has not been investigated earlier. To improve the crystallinity and reduce the transmission loss in the waveguide the laser post processing has to be performed after patterning the rectangular waveguide on chip. While doing laser post processing, the corners of the rectangular waveguide become round and hence the shape of the waveguide guide

is altered. Consequently, in practice, the shape of waveguide become parabolic. Hence, for precise spectral broadening of the SC spectrum, we examined the design of the parabolic-core waveguide. An efficient broadband coherent mid-IR SC spectrum extending from 1.4 to 7.6 μm is reported in an 8 mm long parabolic-core chalcogenide waveguide when subjected to 250 W & 200 fs laser pulse at a wavelength of 2 μm. From an application standpoint, the utilization of such waveguide-based broadband coherent NIR to MIR SC light holds great significance in various critical domains, including early cancer diagnostics, food quality control, security, sensing, and the recognition of a sustained optical frequency comb for enabling high- precision spectroscopy and OCT. Additionally, the reported waveguide, which generates NIR to MIR SC light, has the potential to significantly expand the range of functionalities achievable in future photonic integrated circuits.

REFERENCES

[1] J K Ranka, R S Windeler and A J Stentz, "Visible continuum generation in air-silica microstructure optical fibers with anomalous dispersion at 800 nm", Optics Letters, 25, 25 (2000). doi:10. 1364/OL.25.000025

[2] M El-Amraoui, G Gadret, J C Jules et al., "Microstructured chalcogenide optical fibers from As_2S_3 glass: towards new IR broadband sources", Optics Express, 18, 26655 (2010). doi:10.1364/ OE.18.026655

[3] T S Saini, U K Tiwari and R K Sinha, "Design and analysis of dispersion engineered rib waveguides for on-chip mid-infrared supercontinuum", Journal of Lightwave Technology, 36, 1993-1999 (2018). doi:10.1109/ JLT.2018.2800282

[4] T S Saini and R K Sinha, "Mid-infrared supercontinuum generation in soft-glass specialty optical fibers: a review", Progress in Quantum Electronics, 78, 100342 (2021). doi:10.1016/j.pquantelec.2021.100342

[5] W Chen, S Qiao, Z Zhao,S Gao, Y Wang and Y Ma, "Sensitive carbon monoxide detection based on laser absorption spectroscopy with hollow-core antiresonant fiber", Microwave Optical Technology Letters, 66, e33780 (2024). doi:10.1002/mop.33780

[6] Z Lang, S Qiao and Y Ma, "Fabry—Perot-based phase demodulation of heterodyne light-induced thermoelastic spectroscopy", Light: Advanced Manufacturing, 4(3), 233-242 (2023). doi: 10.37188/lam.2023.023

[7] M Guan, D Chen, S Hu, H Zhao and P You, "Review article theoretical insights into ultrafast dynamics in quantum materials", Ultrafast Science, 2022, art. 9767251 (2022). doi:10.34133/2022/9767251

[8] Z Hui, X Bu, Y Wang et al., "Bi_2O_2Te Nanosheets saturable absorber-based passive mode-locked fiber laser: from soliton molecules to harmonic soliton", Advance Optical Materials, 10, 2201812 (2022). doi:10.1002/adom.202201812

[9] Z Zhang, J Zhang, Y Chen et al., "Bessel terahertz pulses from superluminal laser plasma filaments ", Ultrafast Science, 2022(1), (2022). doi:10.34133/2022/9870325

[10] X Li, W Xu, Y Wang et al., "Optical-intensity modulators with PbTe thermoelectric nanopowders for ultrafast photonics", Applied Materials Today, 28, 101546 (2022). doi:10.1016/j.apmt.2022.101546

[11] X Li, X Huang, Y Han et al. , "High-performance γ-MnO_2 dual core, pair-hole fiber for ultrafast photonics", Ultrafast Science, 3, 0006 (2023). doi:10.34133/ultrafastscience.0006

[12] R R Alfano, S L Shapiro, "Emission in the region 4000 to 7000 Å via four-photon coupling in glass", Physical Review Letters, 24, 584-587 (1970). doi:10.1103/PhysRevLett.24.584

[13] M Sharma, S Mishra, B Ung et al., "Annular core photonic crystal fiber for propagation of optical vortices", In: Conference on Lasers and Electro-Optics, OSA Technical Digest, Optica Publishing Group, paper STu3R.2 (2020). doi:10.1117/12.2528233

[14] T S Saini, A Kumar and R K Sinha, "Broadband mid-infrared supercontinuum spectra spanning 2–15 μm Using As_2Se_3 chalcogenide glass triangular-core graded-index photonic crystal fiber", Journal of Light Technology, 33, 3914-3920 (2015). doi:10.1109/ JLT.2015.2418993

[15] W Yuan, "2–10 μm mid-infrared supercontinuum generation in As_2Se_3 photonic crystal fiber", Laser Physics Letter, 10, 095107 (2013). doi:10.1088/1612-2011/10/9/095107

[16] T S Saini, A Kumar and R K Sinha, "Design and modelling of dispersion-engineered rib waveguide for ultra broadband mid infrared supercontinuum generation", Journal of Modern Optics, 64, 143-149 (2017). doi:10.1080/09500340.2016.1216190

[17] R Cherif, A B Salem, T S Saini, A Kumar, R K Sinha and M Zghal, "Design of small core tellurite photonic crystal fiber for slow light-based application using stimulated Brillouin scattering", Optical Engineering, 54, 075101 (2015). doi:10.1117/1.OE.54.7.075101

[18] J Yuan, Z Kang, F Li et al., "Mid-infrared octave-spanning supercontinuum and frequency comb generation in a suspended germanium-membrane ridge waveguide", Journal of Light Technology, 35, 2994-3002 (2017). doi:10.1109/JLT.2017.2703644

[19] Z Hui, L Zhang and W Zhang, "CMOS compatible on-chip telecom-band to mid-infrared supercontinuum generation in dispersion-engineered reverse strip/slot hybrid Si_3N_4 waveguide", Journal of

Modern Optics, 65, 53-63 (2018). doi:10.1080/09500340.2017. 1376718

[20] D J Moss, R Morandotti, A L Gaeta and M Lipson, "New CMOS compatible platforms based on silicon nitride and Hydex for nonlinear optics", Nature Photonics, 7, 597-607 (2013). doi:10.1038/ nphoton.2013.183

[21] H Ahmad, M R Karim and B M A Rahman, "Dispersion-engineere dsilicon nitride waveguides for mid-infrared supercontinuum generation covering the wavelength range 0.8–6.5 μm", Laser Physics, 29, 025301 (2019). doi:10.1088/1555-6611/aaf63d

[22] T S Saini and V R Supradeepa, "Tellurium-oxide coated silicon nitride hybrid waveguide for near-to-mid-IR supercontinuum generation: design and analysis", Journal of Modern Optics, 68, 29-36 (2021). doi:10.1080/09500340.2021.1874556

[23] N D Psaila, R R Thomson, H T Bookey et al., "Supercontinuum generation in an ultrafast laser inscribed chalcogenide glass waveguide", Optics Express, 15, 15776 (2007). doi:10.1364/OE.15. 015776

[24] M R Karim, B M A Rahman and G P Agrawal, "Mid-infrared super continuum generation using dispersion-engineered $Ge_{11.5}As_{24}Se_{64.5}$ chalcogenide channel waveguide", Optics Express, 23, 6903 (2015). doi:10.1364/OE.23.006903

[25] G P Agrawal, "Nonlinear fiber optics", In Nonlinear Science at the Dawn of the 21st Century. Springer, Berlin Heidelberg, 195-211 (2000). https://doi.org/10.1016/B978-0-12-817040-3.00007-9

[26] T S Saini, N P Trung Hoa, K Nagasaka et al., "Coherent midinfrared supercontinuum generation using a rib waveguide pumped with 200 fs laser pulses at 2.8 μm", Applied Optics, 57, 1689 (2018). doi:10.1364/AO.57.001689

[27] M Bigot-Astruc, D Boivin and P Sillard, "Design and fabrication of weakly-coupled few-modes fibers", Photonics Society Summer Topical Meeting Series, Seattle, WA, USA, IEEE, 189-190 (2012). doi:10.1109/PHOSST.2012.6280766

[28] K Nagasaka, L Liu, T H Tuan et al., "Numerical investigation of highly coherent mid-infrared supercontinuum generation in chalcogenide double-clad fiber", Optical Fiber Technology, 36, 82-91 (2017). doi:10.1016/j.yofte.2017.03.002

[29] H Kawagoe, S Ishida, M Aramaki et al., "Development of a high power supercontinuum source in the 17 μm wavelength region for highly penetrative ultrahigh-resolution optical coherence tomography", Biomedical Optics Express, 5, 932 (2014). doi:10.1364/BOE.5.000932

CHAPTER 4: A GRADED INDEX HYBRID PHOTONIC CRYSTAL FIBER FOR SUPERCONTINUUM GENERATION USING $AsSe_2$- As_2S_5 *

4.1 Introduction

In the previous chapter, we have discussed about the importance of mid-IR domain in SCG for a waveguide [1-3]. In this chapter we will discuss about the SCG of a PCF in mid-IR domain. PCF being a special class of fibers also called holey fibres (HFs) or the microstructured fibers (MOFs) due to their exclusive linear and nonlinear properties they have been a good choice among researchers [4]. The reason for such fascination is their properties such as dispersion management, large mode area with endlessly single-mode operation, higher birefringence, SCG and high power delivery. When compared to traditional optical fibers, PCF requires lesser initial peak power of the input laser pulses. It results in a huge spectral broadening at a very mimimal peak power this fact can be utilized in applications like frequency metrology [5]. The fiber of choice has traditionally been the silica PCF because it can be made endlessly single-mode, its dispersion can be tailored and its ZDW can move down into the visible region [6].

Chalcogenide glasses have wider transmission range and a greater nonlinear coefficient in a MIR waveband when compared to silica (non-transparent beyond 2.5 μm), sulfur, fluoride and telluride glasses (long wavelength spectrum is limited at 5 μm) [7]. The chalcogenide materials are preferred for broadband SCG because of the lower peak power requirement and high nonlinearity. Compared to single glass chalcogenide fibers, step-index fibers with hybrid-glasses offer several benefits. Firstly, they exhibit a higher refractive-index (RI) difference between the fiber core and cladding, enhancing the effectiveness of lightconfinement in the core and reducing loss. Secondly, the fiber's numerical aperture is increased due to the higher RI difference, facilitating the collection of light into the core during coupling. Lastly, effective controlling over the chromatic dispersion can be achieved by using multiple glasses. Consequently, a hybrid fiber composed of two types of chalcogenide glass

* ***D.S. Tomer*** *and A. Kumar, "A graded index hybrid photonic crystal fiber for supercontinuum generation using* $AsSe_2$-As_2S_5*,"Journal of Optics, 54, (3268-3277) (2025). https://doi.org/10.1007/s12596-024-01954-3*

proves to be well-suited for SC generation, especially in extending to the M-IR band [8].

Photonic crystals, waveguides, and photonic crystal fibers all leverage the control of light propagation through structural design and material choice. They share foundational principles such as the use of periodic structures and photonic bandgaps, while differing in their specific forms and applications [9–18]. Several theoretical and experimental studies have documented the exploration of silica, tellurite, fluoride, and chalcogenide glasses in the context of step-index fibers, PCFs and waveguides for SCG [1,19–29]. The experimental demonstration of the broadening in SC spectrum from 2.1 to 3.1 μm has been performed by Shaw et al. using a PCF in As_2Se_3 chalcogenide glass [19]. The bandwidth of SCG is maximized by Hu et al. using As_2Se_3 chalcogenide PCF for input pulse at the wavelength of 2.5 μm [20]. Petersen et al. reported a Mid-IR SC spectra, spanning 1.4–13.3 μm by using a chalcogenide step-index fiber [9]. To achieve high nonlinearity at 1.55 μm a composite PCF of As_2Se_3 glass and tellurite is modeled by Liao et al. [10]. Saini et al. presented a triangular core graded-index (GI) PCF for SCG [21]. The SCG of bandwidth 1–6 μm has been computationally analyzed by Seifouri et al. in a PCF made up of As_2Se_3-MgF_2 composition [22]. An equiangular spiral shaped PCF structure is theoretically presented by Saini et al. to generate the SC spectrum, spanning 1.2–15μm [23]. Salem et al. have done the numerical investigation of a tapered As_2S_3 PCF design using a pulse energy of 100 pJ pumping at 4.7μm for generation of ultra-broadband SC spectrum [24]. Numerical modeling of an As_2Se_3 rib waveguide is reported by Saini et al. for SCG [25]. In our previously published work, we have done numerical modelling of a parabolic core waveguide for SCG [2]. Using a Ge-Sb-S chalcogenide based waveguide, nonlinear characterization is carried out by Choi et al. for the demonstration of the SC spectrum [26]. A Ga-Sb-S based PCF has been studied for coherent SCG by injecting a laser pulse of 50 fs pulse width and 20 kW peak power in 1 cm fiber length at 4.5 μm [27]. The numerical simulations with an experimental extensive study has been performed by Xing et al to generate SCG spanning, 1.9–2.34 μm at −20 dB power level in a 2 cm long fiber [28]. A 150 mm long $Ge_{11.5}$ As_{24} $Se_{64.5}$ based PCF is numerically simulated for effective SC spanning, 1.4–10 μm using 85 fs input laser pulse at 3.1 μm with peak power of 5 kW [29]. Recently, the maximum SC range covering one octave in a chalcogenide step-index fiber with $AsSe_2$ core and As_2S_5 cladding from 1550 -3300 nm is obtained with 20 cm long fiber at 2000 nm pulses in normal dispersion region [1]. Among the well-known chalcogenides the transparency range of the $AsSe_2$ core glass extended from approximately 0.83 to 18.9 μm, surpassing that of the conventional materials like As_2Se_3 (0.8-10 μm) [30]. In this study, we have designed an innovative PCF structure by combining $AsSe_2$ and As_2S_5 materials, resulting in a significant difference in refractive indices.

The $AsSe_2$-As_2S_5 composition was carefully chosen for their admirable compatibility during the drawing process to prevent interface cracking. Also, the significant contrast between their refractive index facilities efficient control over chromatic dispersion [31].

In our reported design we are experiencing broader supercontinuum generation at a low input pump power. Also the trade-off between broadening and coherence has been efficiently addressed. The generated supercontinuum source can be used to discern chemicals, inspect food quality, detect explosives and hazardous gases, ulcer and cancer diagnosis, frequency comb generation, optical imaging, and optical coherence tomography. This chapter includes five segments in total. First segment provides the brief introduction and overview of the work. While, the second segment includes about the PCF designing and its importance. Third segment, provides the extensive illustration of the methodology used. Fourth segment comprises of results and its discussion. At the end, conclusion of the entire work has been provided in section five followed by references.

In this work, we report a mid-IR supercontinuum spectrum extending form 1 μm - 11 μm at 5 μm using a 4 mm long fiber pumped with 50 fs laser pulses of 750 W. In comparison to recently reported results we obtained broader coherent mid-IR supercontinuum spectrum with comparatively lower peak power of input laser pulse.

4.2 Design principle of PCF

Figure 4.1(a) shows the cross-sectional view of proposed PCF. The core is structured using $AsSe_2$ with diameter d_{core}. Cladding is hybrid with two regions, inner cladding and outer cladding. Inner cladding is a graded helical structure around a fixed core. Outer cladding is a hexagonal structure. As_2S_5 is used as a cladding material in combination with air holes. The cladding comprises of 6 layers of hexagonal structured air-holes, where the first 3 layers of air holes have been eliminated from the center to design inner graded helical structure. The inner cladding structure consists of 8 helical patterns and each pattern comprises 3 air holes as shown in Figs .4.1(c) & 4.1(d). For effective detention of light and its propagation through the core forked shift of air holes along with grading is presumed. First three layers of the proposed graded – index (GI) helical shape are arranged with diameter of 1st, 2nd and 3rd ring as $d_1 > d_2 > d_3$, The value of d_3 is constant as 0.50 μm but d_1 and d_2 has been changed. The distance from the center of the first ring is constant and represented as r_0, which is 2.0 μm. The pitch (Λ= spacing between two air holes) in other rings is optimized by changing Λ from 1.8 μm to 2.2 μm with a period of 0.2 μm.

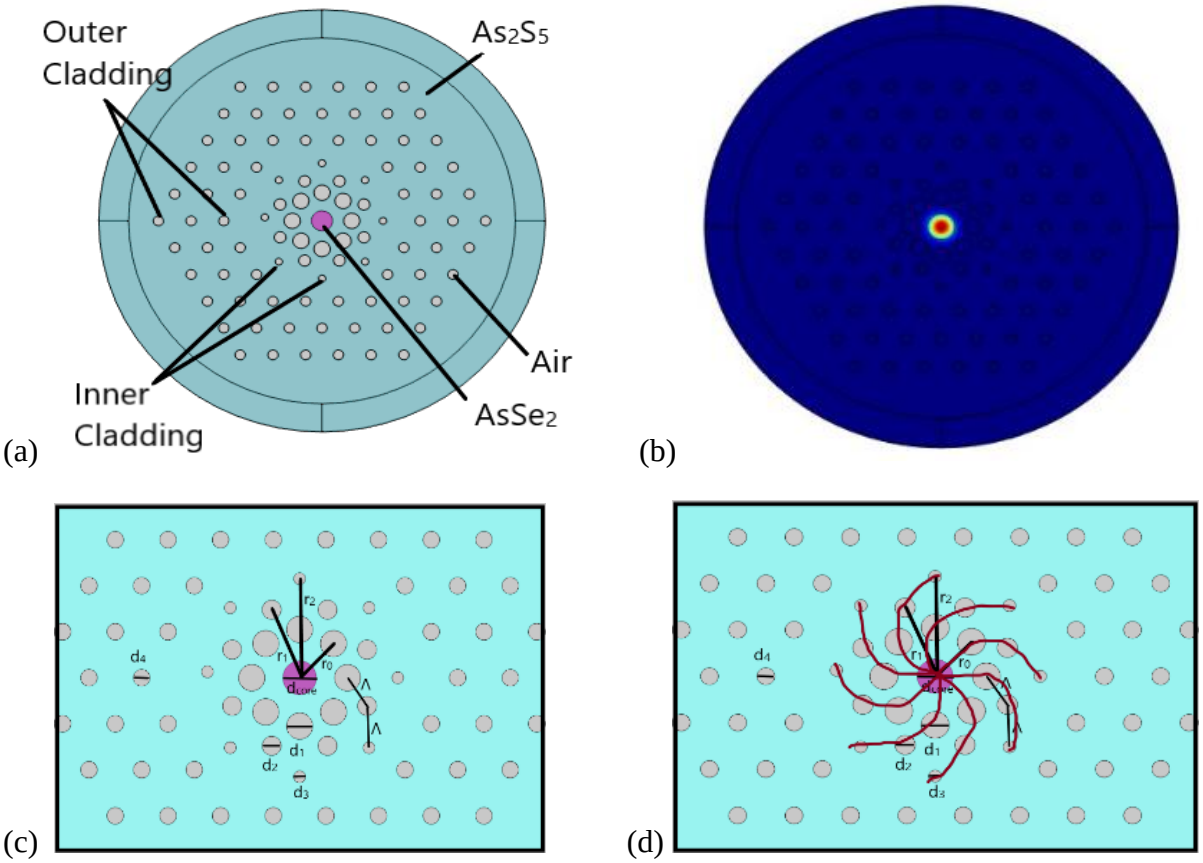

Figure 4.1 (a) The cross-sectional perspective of the suggested PCF in a transverse view, **(b)** the distribution of electric field for the fundamental mode at 5 µm, **(c)** structural parameters of the PCF and **(d)** displaying spiral nature of the inner cladding for better understanding.

Grading has been done in a systematic manner where 1st ring diameter is varied as (d_1= 1.10 µm, 1.30 µm, 1.50 µm), 2nd ring diameter (d_2 = 0.80 µm, 0.90 µm, 1.00 µm), 3rd ring diameter (d_3 = 0.50 µm), core diameter is also varied as (d_{core} = 1.2 µm, 1.4 µm, 1.6 µm, 1.8 µm). Successive grading is represented as D ($D = d_1 - d_2 = d_2 - d_3$ =0.30 µm, 0.40 µm, 0.50 µm).

The next three rings which forms the outer cladding region have a hexagonal shape of constant diameter (d_4 = 0.70 Thickness of PML is 2.0 µm.). The distance of first hexagonal ring from the center is 5.6 µm. The distance between the consecutive hexagonal rings is kept constant which is 1 µm. The value of structural parameters have been shown in Table 4.1 for better understanding. The cylindrical PML is applied at the periphery of the cladding for eradicating the reflection effect occurring at the boundary. Here, the thickness of perfectly matched layer is 2.0 µm. [23, 32-33].

Table 4.1. Value of parameters in the design

INNER CLADDING REGION				OUTER CLADDING REGION
1st helical ring diameter(μm) (d_1)	**2nd helical ring diameter(μm) (d_2)**	**3rd helical ring diameter (μm) (d_3)**	**D (μm) ($=d_1- d_2 = d_2 - d_3$)**	**Diameter of hexagonal air holes (μm) (d_4)**
0.50	0.50	0.50	0.00	0.70
1.10	0.80	0.50	0.30	0.70
1.30	0.90	0.50	0.40	0.70
1.50	1.00	0.50	0.50	0.70

Achieving a profile with all-normal dispersion (ANDi) as well as nearly zero dispersion is the purpose of designing such a structure. Since, it helps in achieving broader SCG and low noise. Simulated electric field distribution of travelling mode in proposed PCF design has been illustrated in Fig. 4.1(b). From the fabrication point of view, the reported PCF structure can be fabricated using the well-known rod in tube fabrication technique [34].

4.3 Results and discussions

For a PCF structure the broadening in the supercontinuum spectrum primarily depend upon the nonlinearity of material and the dispersion characteristics [13]. We have optimized the core diameter of the proposed design for d_{core} (1.2 μm, 1.4 μm, 1.6 μm and 1.8 μm) as shown in Fig.4.2(a). Dispersion profile shows all normal dispersion behavior for all d_{core} except for 1.8 μm. Soliton fission process along with the emission of the dispersive waves is responsible for the broadening in the supercontinuum spectrum if pumped in the anomalous dispersion region.

The SCG by the process of soliton fission is vulnerable to the laser shot noise which makes supercontinuum unstable. As depicted in Fig.4.2 (a) for d_{core} =1.6 μm, d_1=1.10 μm , d_2 =0.80 μm, d_3 =0.50 μm, D = 0.30 μm and pitch=2.2 μm, the profile is more flat and all normal with minimum value of dispersion around 4.8 μm as compared to rest of the core diameters. So, we have opted for 1.6 μm as a core diameter. Further, the air holes in the inner cladding region has been graded in the decreasing order of diameter. Figure 4.2(b) shows dispersion for various values of D. Among the evaluated D (0.00 μm, 0.30 μm, 0.40 μm and 0.50 μm) it has been found that both D = 0.00 μm (non-graded) & D = 0.30 μm are showing all normal dispersion profile whereas others have both normal and anomalous dispersion. But between these two, we have considered D = 0.30 μm, along with being all

normal it is more flat and have less dispersion.

So it will result in more broadening as well as good coherency. Figure 4.3 shows that on changing the pitch (Λ) of the air holes in the inner cladding region there is no significant change in the nature of the profile. On changing pitch the effective refractive index of the profile has not changed much which could possibly affect dispersion curve, since it is same so the profile is also same for different pitch values.

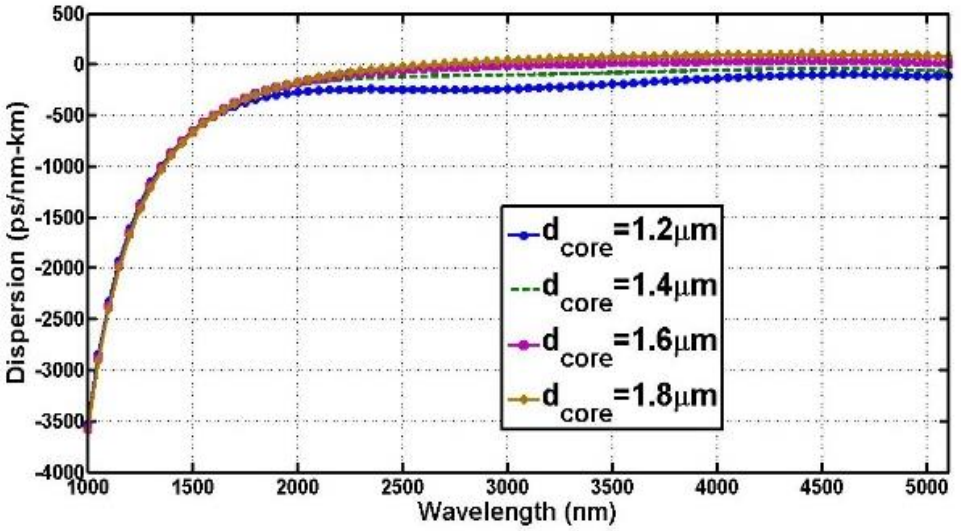

(a)

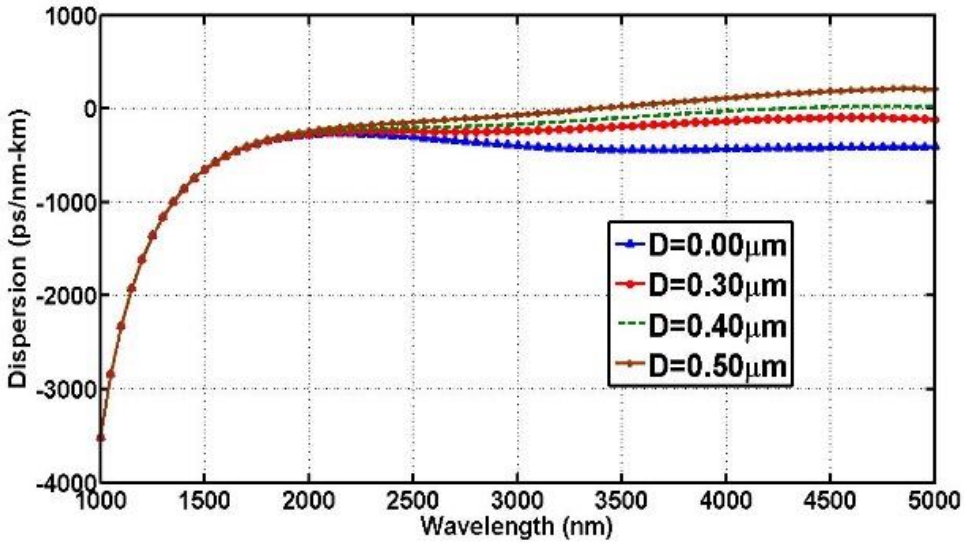

(b)

Figure 4.2 (a) Effect of core Width "d_{core}" on dispersion characteristic of the PCF with d_1=1.10 μm, d_2 =0.80 μm, d_3 =0.50 μm, D= 0.30 μm and Λ=2.2 μm, **(b)** Effect of grading on the dispersion characteristic of the PCF for d_{core} = 1.6 μm and Λ=2.2 μm.

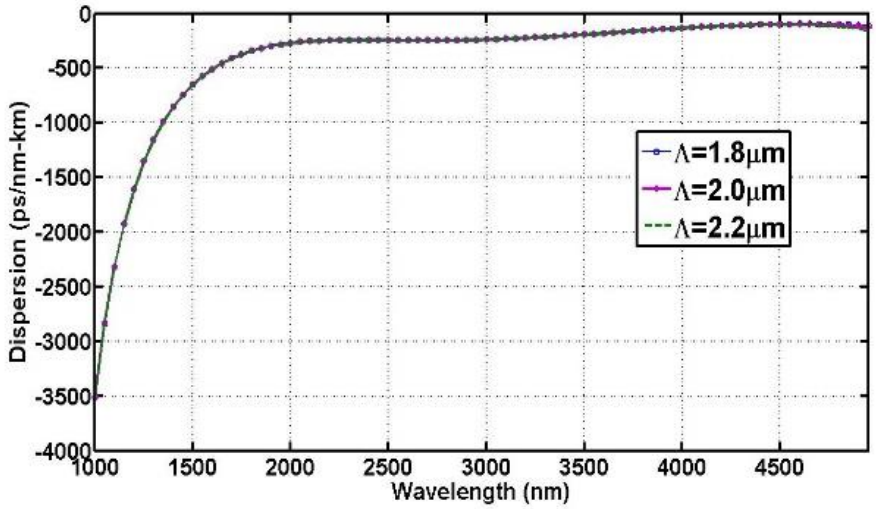

Figure 4.3 Effect of pitch on the dispersion characteristic of the PCF for d_{core} = 1.6 μm and D= 0.30 μm.

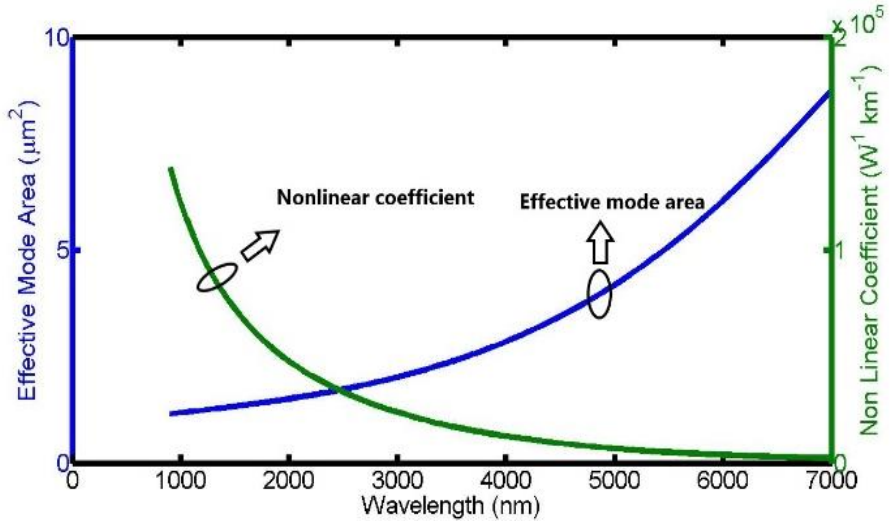

Figure 4.4 The spectral changes in the effective mode area and nonlinear coefficient are depicted with respect to wavelength for PCF.

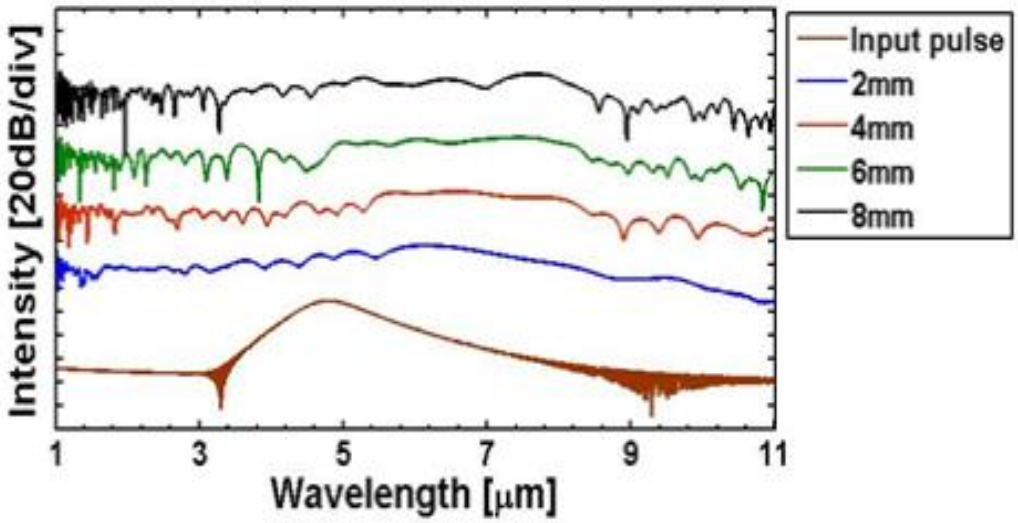

Figure 4.5 The advancement of spectral SC broadening along the length of the PCF, induced by 50 fs laser pulses with 750 W pump power at 5.0 μm.

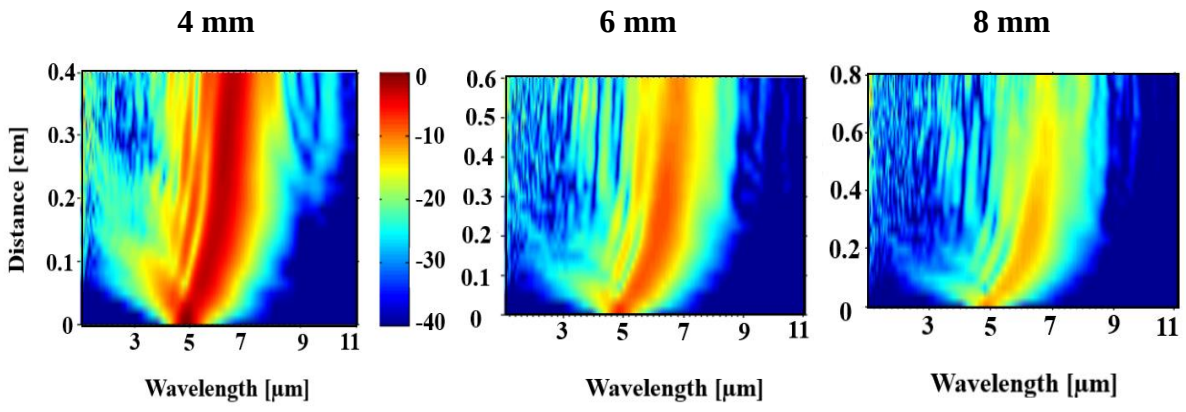

Figure 4.6 The advancement of spectral SC broadening along the length **(a)** 4 mm, **(b)** 6 mm, **(c)** 8 mm of the PCF, induced by 50 fs laser pulses with 750 W pump power at 5.0 µm.

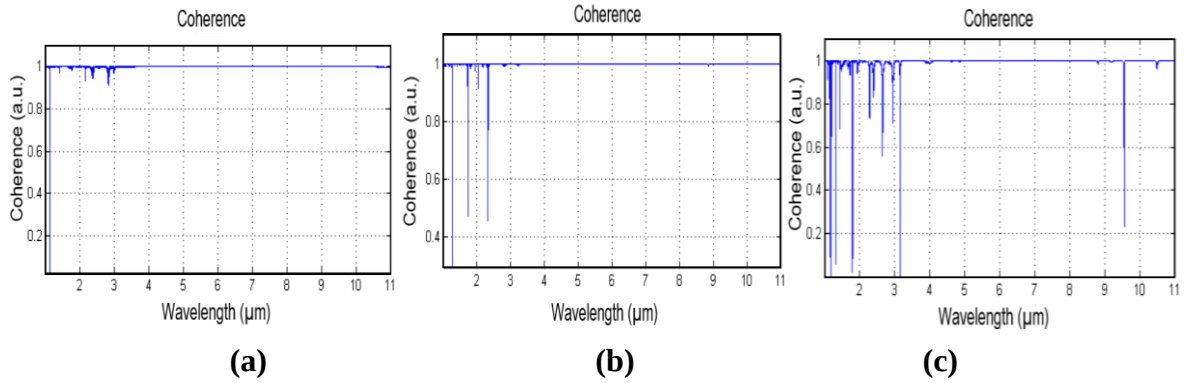

Figure 4.7 The changes in the coherence evolution at 5 µm in response to the input pulse peak power 750W, 50 fs pulse width along the length of the fiber **(a)** 4 mm, **(b)** 6 mm and **(c)** 8 mm.

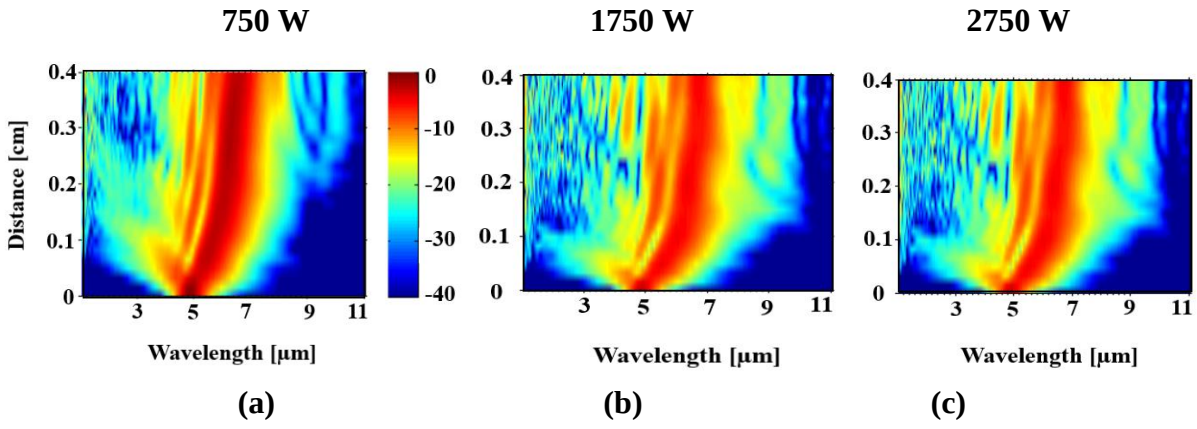

Figure 4.8 The advancement of spectral SC broadening with the pump power, **(a)** 750W, **(b)** 1750W and **(c)** 2750W, induced by 50 fs laser pulses with 4 mm fiber length at 5.0 µm.

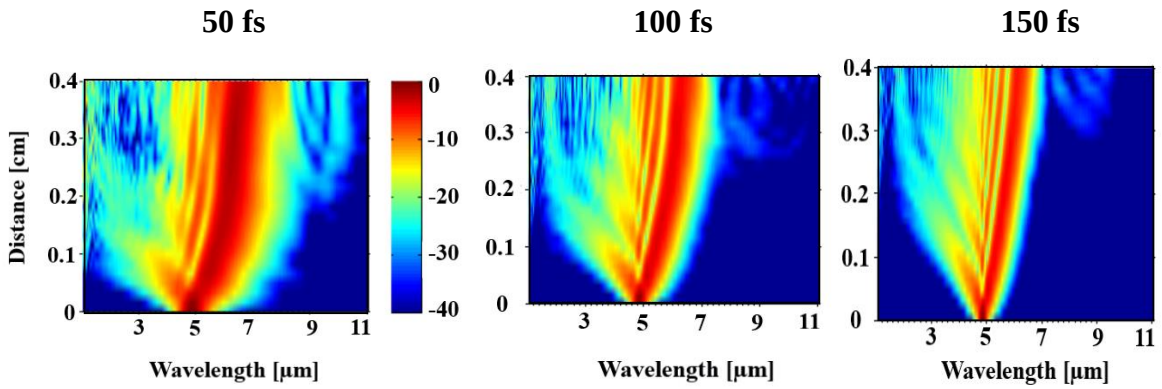

Figure 4.9 The advancement of spectral SC broadening at 5 μm induced by **(a)** 50 fs, **(b)** 100 fs and **(c)** 150 fs laser pulses at 4 mm fiber length, 750 W pump power.

Considering the availability of a commercial available laser source we have taken 5 μm as a pump wavelength. At 5μm the dispersion is -53.13 ps/nm-km for 1.6 μm core diameter, D= 0.30 μm and Λ=2.2 μm. In Fig.4.4, effective mode area vs. nonlinearity shows the obvious trend when plotted against wavelength. At 5 μm effective mode index, effective mode area and nonlinearity has been evaluated and found to be 2.278, 4.18 μm^2 and 6900 $W^{-1}Km^{-1}$ respectively.The complete loss is sum of both material and confinement loss in a fiber. The value of confinement loss is less in comparison to the material loss of the $AsSe_2$ chalcogenide glass, which shows absorption peak in the loss curve around 2.9 μm due to the OH impurity in the chalcogenide glass, and other absorption peak around 12.7 μm because of the Se-OH bonds [35].

SCG has been evaluated at pump wavelength of 5μm for various values of fiber length, pulse width and peak power with 1 kHz repetition rate. The maximum broadening is observed for 4 mm fiber length, 750W peak power and 50fs pulse width. Figure 4.5 shows variation of intensity with length from 2 mm to 8 mm, it is seen that the broadening is very less below 4 mm and above 4 mm noise is increasing. Similarly, in Fig. 4.6 the length variation in a spectrum from 4mm to 8mm depicts that on increasing the length at-40 dB power level the spectrum is experiencing a shift towards longer wavelength region. In the beginning the broadening has occurred due to SPM which is later dominated by (OWB) optical wave breaking. Further increase in length add undesirable fluctuations in the supercontinuum spectrum and deteriorate coherence. So we have considered 4 mm as optimum fiber length. Also, in Fig.4.7 coherence has been evaluated and it is evident that on increasing length the coherence is also getting disturbed. In Fig.4.8, as the pump power is incremented from 750 W to 2750 W the spectrum gets shifted towards the longer wavelength region. As the pumping power was further increased the SC started to degrade due to absorption at the coating [36]. In Fig.4.9, it can be

observed as the value of T_{FWHM} is increased from 50 fs to 150 fs the resultant spectra began to get (thinner) narrow down. This is due to the Self phase modulation effect. It is worth noting that shorter pulses tend to get broader SC spectra. Hence, 50 fs pulses are giving stable spectrum. For 50 fs laser pulse at 5 μm, β_2 is 1.15 $\times 10^{-25}$; ($T_0 = T_{FWHM}/1.763$) ; the nonlinear length ($L_{NL} = (\gamma P_0)^{-1}$) and dispersion length ($L_D = (\beta_2/T_0^2)^{-1}$) for proposed PCF are 1.9 $\times 10^{-4}$ m and 2.17$\times 10^{-2}$ m respectively. In order to achieve a broader supercontinuum generation, it is desirable to have a nonlinear length that is comparable to or shorter than the dispersion length. This ensures that nonlinear effects play a significant role in shaping the spectrum of the input pulse, while dispersion does not excessively broaden the pulse before nonlinear effects can take place. The soliton order, $N \approx L_D/L_{NL} \approx 10$ and the soliton fission length, $L_{fiss} = L_D/N \approx 2.17$ mm is evaluated using these relations. In the starting phase of pulse propagation, self -phase modulation (SPM) is responsible for spectral broadening whereas at longer wavelength optical wave breaking is responsible for broadening. Finally we conclude that our proposed structure is able to generate broader and comparable SCG bandwidth with lower pump power in comparison to previously reported work, mentioned in Table 4.2.

As can be inferred from the table $As_{38.8}\,Se_{61.2}$ PCF [37] and As_2S_5 – Borosillicate PCF [38] has a limited broadening up to 5 μm, As_2Se_3 PCF [39] and $Ga_8Sb_{32}S_{60}$ PCF [27] has broadening around 1 to 10 μm but the peak power used is quite high around 20kW. In $GeSe_2$-As_2Se_3-PbSe PCF [36] the broadening is comparable but the peak power used is higher as 0.95kW with 10mm fiber length as compared to 0.75kW and 4mm fiber length in our case. In reference [40] and [41], the material used is tellurite which shows very less broadening using high peak power.

Since the focus of this work is to produce greater broadening with low peak power as it offers several advantages in SCG. It leads to better performance in applications where spectral stability is crucial, such as OCT and spectroscopy. With lower peak power, the supercontinuum spectrum tends to be more stable over time. It enhances Signal-to-Noise ratio which improves the quality of measurements and imaging in various applications. It reduces photodamage. Also, it often corresponds to longer pulse durations, which can be beneficial for certain applications that require longer interaction times with the sample, such as material processing and biomedical imaging. Overall, using lower peak power in supercontinuum generation can result in more stable, high-quality spectra with reduced nonlinear effects and improved safety for sensitive samples.

Table 4.2. Comparison against previously documented outcomes of SC spectrum in chalcogenide PCFs

References	Chalcogenide Type	Pump Wavelength (μm)	Fiber length	Peak power (kW)	SCG bandwidth (μm)
[37]	$As_{38.8}Se_{61.2}$ PCF	3.7	5cm	0.88	2.9 – 4.575
[38]	As_2S_5 – Borosillicate PCF	2.5	4mm	28.16	1-5
[39]	As_2Se_3 PCF	2.5	10mm	20	1-10
[27]	$Ga_8Sb_{32}S_{60}$ PCF	4.5	1cm	20	1.65-9.24
[36]	$GeSe_2$-As_2Se_3-PbSe PCF	3.1	10mm	0.95	1-11
[40]	PCF (Core:TeO_2-Li_2O-WO_3-MoO_3-Nb_2O_5; Cladding: TeO_2-ZnO-Na_2O-La_2O_3)	3.0	5cm,15 cm	-	1.5-4.0
[41]	PCF (60TeO_2- 20PbO-20$PbCl_2$)	2.45	5cm	5.0	2.0-4.9
Proposed work	$AsSe_2$- As_2S_5 PCF	5.0	4mm	0.75	1-11

4.4 Conclusions

In summary, the especially designed graded index hybrid PCF structure with $AsSe_2$- As_2S_5 offers all normal dispersion (ANDi) at pump wavelength of 5 μm. The essence of this work lies in the generation of mid-IR supercontinuum. An efficient broadband coherent mid-IR SC spectrum extending from 1 – 11 μm is reported in a 4 mm long PCF when subjected to 750 W, 50 fs laser pulse at a wavelength of 5 μm. From an application standpoint, the utilization of a PCF-based broadband coherent NIR to MIR SC light holds great significance in various critical domains, including early cancer diagnostics, food quality control, security, sensing, and the recognition of a sustained optical frequency comb for enabling high-precision spectroscopy and optical coherence tomography. Additionally, the reported PCF, which generates NIR to MIR SC light, has the potential to significantly expand the range of functionalities achievable in future photonic integrated circuits.

REFERENCES

[1] Y Qu, W Sun, J Cao, H Chen and H Jia, "Coherent ultrabroad orbital angular momentum supercontinuum generation in an $AsSe_2$ -As_2S_5 microstructured fiber with all-normal dispersion", Optics Communication, 497, 127191 (2021). https://doi.org/10.1016/j. optcom.2021.127191

[2] D S Tomer and A Kumar, "Design and numerical modeling of chalcogenide parabolic - core waveguide for on - chip supercontinuum generation extending from near - IR region to mid - IR region", Microwave and Optical Technology Letters, 66(3), e34105 (2024). https://doi.org/10.1002/mop.34105

[3] R R Alfano and S L Shapiro, "Emission in the region 4000 to 7000 å via four-photon coupling in glass", Physical Review Letters, 24, 584–587 (1970). https://doi.org/10.1103/PhysRevLett.24.584

[4] P Chauhan, A Kumar and Y Kalra, "A dispersion engineered silica-based photonic crystal fi ber for supercontinuum generation in near-infrared wavelength region", Optik - International Journal of Light and Electron Optics, 187, 230–237 (2019). https://doi.org/10.1016/j. ijleo.2019.03.107

[5] T S Saini, A Kumar and R K Sinha, "Broadband mid-infrared Supercontinuum spectra spanning 2–15 μm using As_2Se_3 chalcogenide glass triangular-core graded-index photonic crystal fiber", Journal of Light Technology, 33, 3914–3920 (2015). https://doi.org/10.1109/ JLT.2015.2418993

[6] J K Ranka, R S Windeler and A J Stentz, "Visible continuum generation in air–silica microstructure optical fibers with anomalous dispersion at 800 nm" Optics Letters, 25, 25 (2000). https://doi. org/10.1364/ol.25.000025

[7] W. Yuan, "2–10 μm mid-infrared supercontinuum generation in As_2Se_3 photonic crystal fiber", Laser Physics Letters, 10, 095107 (2013). https://doi.org/10.1088/1612-2011/10/9/095107

[8] Weiqing and Gao, "Supercontinuum generation in a step-index chal cogenide fiber with $AsSe_2$ core and As_2S_5 cladding", Japenese Journal of Applied Physics, 55 (2016). https://doi.org/10.7567/JJAP.55.122201

[9] S Ankita, B Bissa, A Suthar and Bhargava, "Study transmission characteristics of graded photonic crystal as low pass filter", Journal of Physics: Conference Series, 2603, 012046 (2023). https://doi. org/10.1088/1742-6596/2603/1/012046

[10] S Ankita, B Bissa, A Suthar and Bhargava, "High pass filter based on one-dimensional graded photonic crystal high pass filter based on one-dimensional graded photonic", Journal of Physics: Conference Series, 2335, 012006 (2022). https://doi.org/10.1088/1742-6596/2335/1/012006

[11] S Bissa, B Suthar, C Nayak and A. Bhargava, "Results in optics an improved optical biosensor design using defect / metal mul tilayer photonic crystal for malaria diagnosis", Results in Optics, 9, 100304 (2022). https://doi.org/10.1016/j.rio.2022.100304

[12] M Sharma, F Amirkhan, S K Mishra, D Sengupta, Y Mes saddeq, F Blanchard and B Ung, "Annular core photonic crystal fiber for transmission of endlessly mono-radial vortex beams", in OSA Advanced Photonics Congress (AP) (IPR, NP, NOMA, Networks, PVLED, PSC, SPPCom,SOF), L. Caspani, A. Tauke Pedretti, F. Leo, and B. Yang, eds., OSA Technical Digest (Optica Publishing Group, 2020), paper SoM3H.7, (2020) https://doi. org/10.1364/SOF.2020.SoM3H.7

[13] J M Dudley, G. Genty and S Coen, "Supercontinuum generation in photonic crystal fiber", Reviews of Modern Physics, 78, 1135–1184 (2006). https://doi.org/10.1103/RevModPhys.78.1135

[14] M Sharma, F Amirkhan, S K Mishra, D Sengupta, Y Mes saddeq, F Blanchard and B Ung, "Transmission of Orbital Angular Momentum and Cylindrical Vector beams in a large-bandwidth annular core Photonic Crystal Fiber", Fibers, 8(4), 22 (2020). https://doi.org/10.3390/fib8040022

[15] B Suthar and A Bhargava, "Enhanced optical sensor for waterborne bacteria-based photonic crystal using graded thickness index", Applied Nanoscience, 13, 5399–5406 (2023). https://doi.org/10.1007/ s13204-023-02809-2

[16] S Ankita, B Bissa, A Suthar and Bhargava, "Graded photonic crystal as improved sensor for nanophotonic application", Macromolecular Symposia, 401, 2100319 (2022). https://doi.org/10.1002/ masy.202100319

[17] S Ankita, B Bissa, A Suthar and Bhargava, "Optical sensor for biomedical application based on photonic crystal with double defect", Materials Today: Proceedings, 62(Part 8), 5407–5410 (2022). ISSN 2214 7853. https://doi.org/10.1016/j.matpr.2022.03.616

[18] A Kumar, T S Saini and R K Sinha, “Design and analysis of photonic crystal biperiodic waveguide structure based optofluidic gas sensor”, Optik, 126(24), 5172–5175 (2015).

[19] L B Shaw, P A Thielen, F H Kung, V Q Nguyen, J S Sanghera, and I D Aggarwal, "IR Supercontinuum Generation in As-Se Photonic Crystal Fiber," in Advanced Solid-State Photonics, Technical Digest (Optica Publishing Group), 10–12 (2005) paper TuC5 https://doi.org/10.1364/ASSP.2005.TuC5

[20] H Jonathan, R Curtis, L Menyuk, J S Brandon Shaw, Sanghera and I D Aggarwal, “Maximizing the bandwidth of supercontinuum generation in As_2Se_3 chalcogenide fibers”, Optics Express. 18, 6722–6739 (2010). https://doi.org/10.1364/OE.18.006722

[21] T.S. Saini, A. Kumar and R.K. Sinha, “Broadband mid-infrared supercontinuum spectra spanning 2–15 μm using As_2Se_3 chalcogenide glass triangular-core graded-index photonic crystal fiber”, Journal of Lightwave Technology, 33(18), 3914–3920 (2015). https://doi.org/10.1109/JLT.2015.2418993

[22] M Seifouri and M R Alizadeh, “Supercontinuum generation in a highly nonlinear chalcogenide/ MgF_2 hybrid photonic crystal fiber”, International Journal of Optics and Photonics, 12(1), 69–78 (2018). http://ijop.ir/article-1-277-en. html

[23] T S Saini, A Baili, A Kumar and R Cherif, “Design and analysis of equiangular spiral photonic crystal fiber for mid-infrared super continuum generation”, Journal of Modern Optics, 62(19), 1570–1576 (2015). https://doi.org/10.1080/09500340.2015.1051600

[24] A Ben Salem, R Cherif and M Zghal, “Tapered As_2Se_3 chalcogenide photonic crystal fiber for broadband mid-infrared supercontinuum generation”, Optical Engineering, 1, 9–10 (2011).https://doi.org/10.1364/ FIO.2011.FMG6

[25]T S Saini, A Kumar and R K Sinha, “Design and modelling of dispersion-engineered rib waveguide for ultra-broadband mid-infrared supercontinuum generation”, Journal of Modern Optics, 64, 143–149 (2017). https://doi.org/10.1080/09500340.2016.1216190

[26] J W Choi, Z Han, B Sohn, G F R Chen, C Smith, L C Kimer ling, K A Richardson, A M Agarwal and D T H Tan, “Nonlinear characterization of GeSbS chalcogenide glass waveguides”,Nature Publishing Group, Scientific Report 6, 39234 (2016). https://doi.org/10.1038/srep39234

[27] A Medjouri, D Abed and Z Becer, “Numerical investigation of a broadband coherent supercontinuum generation in $Ga_8\ Sb_{32}\ S_{60}$ chalcogenide photonic crystal fiber with all-normal dispersion”, Opto-Electronics Review, 27, 1–9 (2019). https://doi.org/10.1016/j.opelre.2019.01.003

[28] E Polytechnique and F De Lausanne, “Linearly chirped mid-infrared supercontinuum in all-normal-dispersion chalcogenide photonic crystal fibers”, Optics Express, 26, 2423–2428 (2018) https://doi. org/10.1364/OE.26.019627

[29] S Vyas, T Tanabe, G Singh and M Tiwari, “Broadband supercontinuum generation and Raman response in $Ge_{11.5}As_{24}Se_{64.5}$ based chalcogenide photonic crystal fiber”, International Conference on Computational Techniques in Information and Communication Technologies, IEEE, 607–611 (2016). https:// doi.org/10.1109/ICCTICT.2016.7514651

[30] T Cheng, Y Kanou, X Xue, D Deng, M Matsumoto, T Misumi, T Suzuki and Y Ohishi, “Mid-infrared supercontinuum generation in a novel $AsSe_2$-As_2S_5 hybrid microstructured optical fiber”, Optics Express, 22, 23019–23025 (2014). https://doi.org/10.1364/ OE.22.023019

[31] L Chen, W Gao, L Chen, P Wang, C Ni, X Chen, Y Zhou, W Zhang, J Hu, M Liao, T Suzuki, and Y Ohishi, “Numerical study on supercontinuum generation by different optical modes in $AsSe_2$-As_2S_5 chalcogenide microstructured fiber," Applied Optics, 57, 382-390 (2018)

[32] S Chandru, T Shankar and A Rajesh, “Investigation on nanocore centred nonlinear PCF for high nonlinearity and low dispersion”, Ceramics International, 48, 16042–16048 (2022). https://doi.org/10.1016/j. ceramint.2022.02.148

[33] A G Chaitanya, T S Saini, A Kumar and R K Sinha, “Ultra broadband mid-IR supercontinuum generation in $Ge_{11.5}As_{24}Se_{64.5}$ based chalcogenide graded-index photonic crystal fiber: design and analysis”, Applied Optics, 55(36), 10138–10145 (2016). https://doi. org/10.1364/AO.55.010138. PMID: 28059256

[34] T Cheng, T H Tuan, L Liu, X Xue, M Matsumoto, H Tezuka, T Suzuki and Y Ohishi, “Mid-infrared Dispersive Waves Generation in an All-solid $AsSe_2$-As_2S_5 Microstructured Optical Fiber”, Frontiers in Optics, OSA Technical Digest (online) (Optica Publishing Group, 2016), paper JTh2A.38 (2016). https://doi.

org/10.1364/FIO.2016.JTh2A.38

[35] U Sharma, E W Chang, S H Yun, "Long-wavelength optical coherence tomography at 17 μm for enhanced imaging depth", Optics Express, 16, 19712 (2008). https://doi.org/10.1364/ OE.16.019712

[36] P Chauhan, A Kumar and Y Kalra, "Numerical exploration of coherent supercontinuum generation in multicomponent $GeSe_2$-As_2Se_3-PbSe chalcogenide based photonic crystal fiber", Optical Fiber Technology, 54, 102100 (2020). https:// doi.org/10.1016/j.yofte.2019.102100

[37] M Diouf, A Salem, R Cherif, H Saghaei and A Wague, "Super-flat coherent supercontinuum source in $As_{38.8}$ $Se_{6.12}$ chalcogenide photonic crystal fiber with all-normal dispersion engineering at a very low input energy", Applied Optics, 56(2), 163–169 (2017). https://doi.org/10.1364/AO.56.000163

[38] A Ben Salem, "Ultraflat-top mid-infrared coherent broadband supercontinuum using all normal As_2S_5 - borosilicate hybrid photonic crystal fiber", Optical Engineering, 55, 5–12 (2016). https://doi. org/10.1117/1.OE.55.6.066109

[39] M Kalantari, A Karimkhani and H Saghaei, "Ultra-Wide mid-IR supercontinuum generation in As_2S_3 photonic crystal fiber by rods filling technique", Optik, 158, 142-151 (2018).

[40] F Xu, C Mei, J Yuan, F Li, Z Kang, B Yan, K Wang, X Sang, X Zhou, K Zhong, C Yu, "Supercontinuum generation in an all-Normal dispersion tellurite photonic crystal fiber", Conference on Lasers and Electro-Optics/Pacific Rim, Optical Society of America, W3A–30(2018).

[41] T Huang, P Huang, Z Cheng, J Liao, X Wu, J Pan, "Design and analysis of a hexagonal tellurite photonic crystal fiber with broadband ultra-flattened dispersion in mid-IR", Optik 167 ,144–149 (2018).

CHAPTER 5: ETHANOL-INFILTRATED CIRCULAR PHOTONIC CRYSTAL FIBER FOR LOW PEAK POWER SUPERCONTINUUM GENERATION FROM NEAR-INFRARED TO MID-INFRARED REGION *

5.1 Introduction

In this chapter, our focus is to highlight the influence of liquid infiltration in a PCF for supercontinuum generation [1-5]. Because of the incredible linear and nonlinear properties of PCF, make them a popular choice among researchers. [6-10]. All normal dispersion (ANDi) profile of PCFs offer several advantages, including the preservation of ultrashort pulses, characterized by a uniform power spectral density and temporal profile. The absence of modulation instability (MI) due to soliton dynamics minimizes noise effects, facilitating the generation of coherent flat spectra. This characteristic is advantageous for applications in spectroscopy, metrology, and optical tomography systems including OCT [11,12]. But the disadvantage with them they require high input power which can lead to photo thermal effect which can damage the fiber.

However, if we use anomalous dispersion regime with lesser input power broad spectra can be achieved, but coherency will be compromised. In order to balance out this soft glasses like chalcogenide was used [13-15]. However, they exhibit steep normal dispersion and a long ZDW in NIR, which restricts the flatness of the dispersion curve and the spectral bandwidth of supercontinuum generation.

To overcome these shortcomings recently liquid infiltrated PCFs are designed which have high nonlinear refractive index like CS_2 where $n_2 = 2.2 \times 10^{-18}$ m^2 W^{-1} at 1032 nm [16] which is quite large in comparision to silica. The advantage of using liquids in the air holes enable high nonlinear and tunable properties. The enhancement of nonlinear properties result in a broader SC spectrum with low pump power and low attenuation. They also provide extra degree of freedom.

Some of the recent published work shows where Chemnitz et al, who reported on experimental evidence for dynamics of hybrid solitons, a new type of solitary wave, by using a CS_2-filled liquid

** **D.S. Tomer** and A. Kumar, "Ethanol-infiltrated circular photonic crystal fiber for low peak power supercontinuum generation from near-infrared to mid-infrared region", Journal of Optics 1-9 (2024). https://doi.org/10.1007/s12596-024-02152-x*

core optical fiber [17]. Kedenburg et al, demonstrated that the PCF filled with CS_2 is capable of generating a spectral broadening ranging from 1.2 to 2.4 μm [18]. Similary, Pniewski et al, numerically demonstrated that the PCF filled with toluene can generate a broadband spectrum over 1000 nm [19]. Dai et al, measured a stimulated Raman scattering response around 0.6 μm in a commercially available hollow silica fiber filled with a toluene/chloroform mixture [20] and Van et al, numerically investigated the broadband spectrum of 700 nm in IR wavelength ranges for all-normal dispersion in hollow core PCFs with toluene [21]. But CS_2 and toluene both are highly toxic. Other organic solvents like nitrobenzene ($C_6H_5NO_2$). tetrachloroethylene (C_2Cl_4), chloroform ($CHCl_3$), benzene (C_6H_6), carbon tetrachloride (CCl_4), and ethanol (C_2H_5OH) etc. are also used which are comparatively less toxic. Vieweg et al, who experimentally demonstrated solitonic SC generation over 600 nm bandwidth with PCFs filled with carbon tetrachloride (CCl_4) [22]. In terms of fabrication techniques multiple options for infiltration have been used depending upon the requirement like photopolymerization [22], Thermal collapse [23], splicer process or UV adhesive process [24], Micro channel milling [25].

Structures with multiple hexagonal ring arrangement around the core has been a popular choice [26,27]. But the spectral bands are not very flat even though the dispersion curve is close to zero. Various designs like square, circular, octagonal, pentagonal and spiral structures were used to overcome this limitation [28,29]. Circular PCFs demonstrate enhanced suitability for broadband SCG owing to their unique attributes, including (i) the redshift of the ZDW, which facilitates SCG in the MIR, (ii) the high design symmetry leads to the highest concentration of electromagnetic field energy in the core, (iii) a reduced dispersion slope within the anomalous dispersion region results in reduction of noise in the SCG spectrum. Also, group velocity dispersion is low in the normal dispersion regime, leading to longer dispersion lengths and a higher degree of soliton interaction [30].

In our reported design, we analyze the impact of infiltration of ethanol on supercontinuum generation. A near-infrared to mid-infrared SC spectrum is observed at a low input pump power extending form 1.25 μm - 3.0 μm at 1.55 μm pump wavelength using a fiber of length 20 cm injected with 60 fs laser pulses of 550 W. Low input power is crucial from practical point of view. Especially, with liquid infiltration in PCFs, they cannot stand high pump power as they can be evaporated if high power is used. Also, the time of operation should be minimum to keep the evaporation of liquid in control due to system heat up. A higher broadening with low input power is reported in contrast to recently reported result mentioned in Table 5.1. Furthermore, the challenge of balancing spectral broadening with maintaining coherence has been adeptly managed. The generated SC source is versatile and can be employed in a wide array of applications such as chemical analysis, explosive detection, frequency

comb generation, food quality inspection, medical diagnostics and advanced optical imaging techniques including OCT.

This chapter is organized into four main sections. The first section offers a concise introduction and an overview of the study. The second section delves into the design of PCF. The third section presents the results and discusses their implications. Finally, the fourth section concludes the paper which is followed by a list of references.

5.2 Design and analysis

Dispersion properties are not the sole determinant of the effectiveness of a nonlinear medium for SCG. It is also crucial to achieve low loss and small effective mode area. Also, the material used should have high nonlinear refractive index (n_2).These factors are influenced by the fiber structure. Figure 5.1 shows the cross-sectional view of proposed PCF. The PCF structure comprises of silica with micro structured air holes in the form of four circular rings. Each ring is having constant diameter of air holes as d= 0.7 µm. The first ring has eight air holes and other rings have larger number of air holes constituting symmetry in the structure given by $x = r\ cos\ (\theta)\ and\ y=r\ sin\ (\theta)$, where r is the distance from the center. The pitch (Λ) is the distance between the two consecutive air holes. The pitch (Λ) is 1µm. The cylindrical PML is generally 10-20% of the diameter of the cladding region, which is implemented at the edges of the cladding for eradicating reflections at the boundary. Thickness of PML is 2.0 µm.

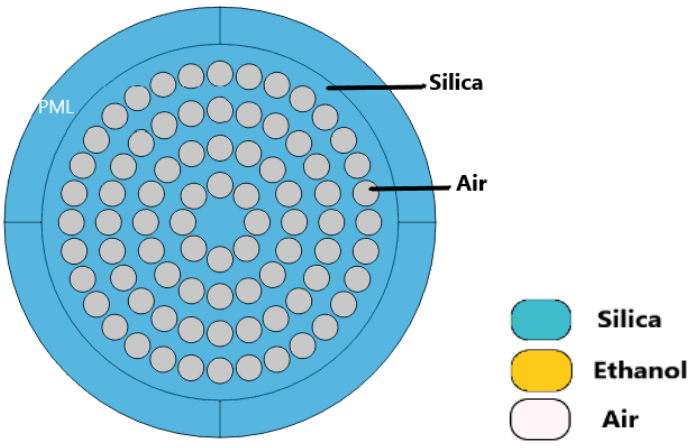

(a)

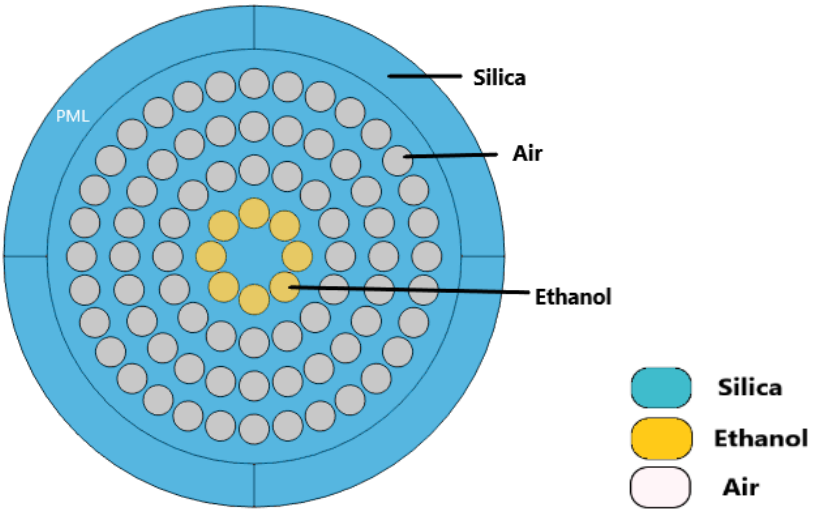
PML
Silica
Air
Ethanol
Silica
Ethanol
Air

(b)

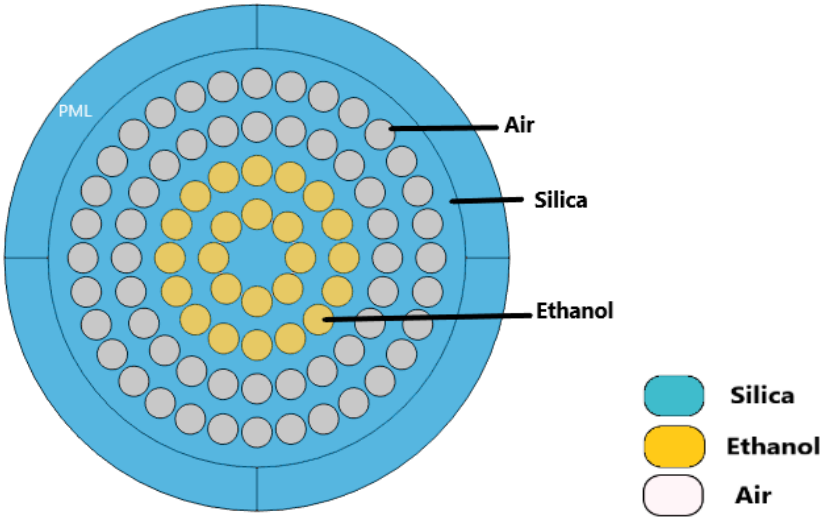
PML
Air
Silica
Ethanol
Silica
Ethanol
Air

(c)

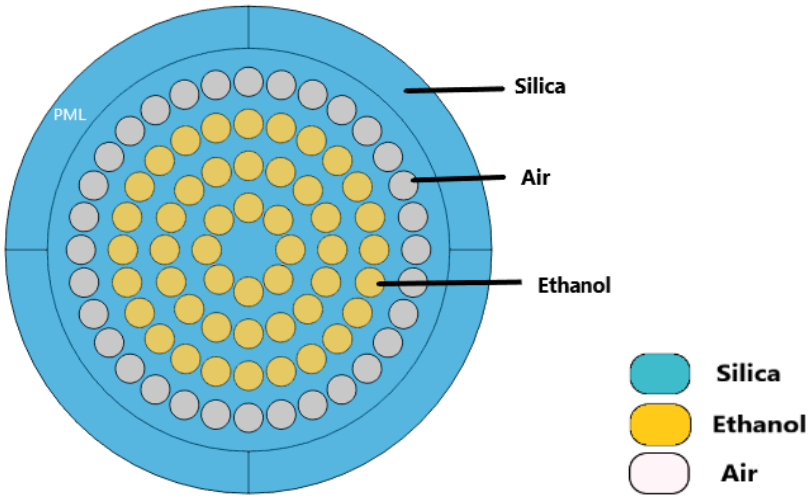
PML
Silica
Air
Ethanol
Silica
Ethanol
Air

(d)

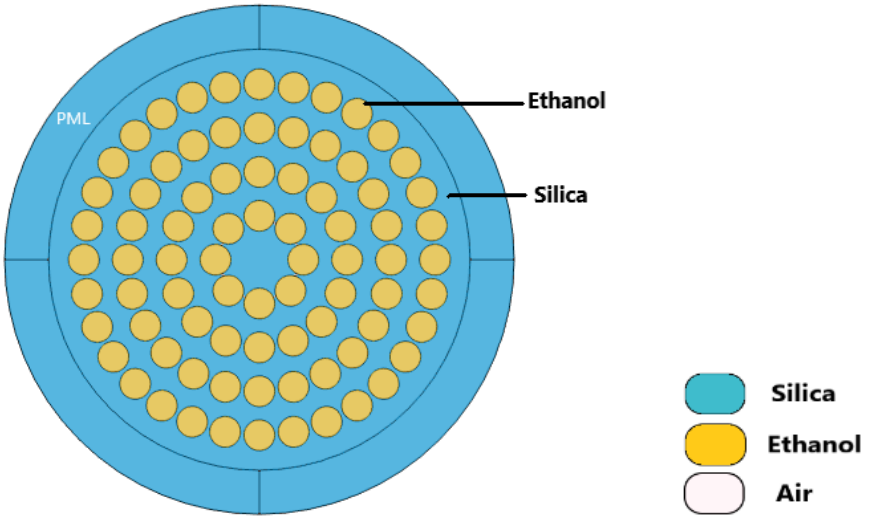

(e)

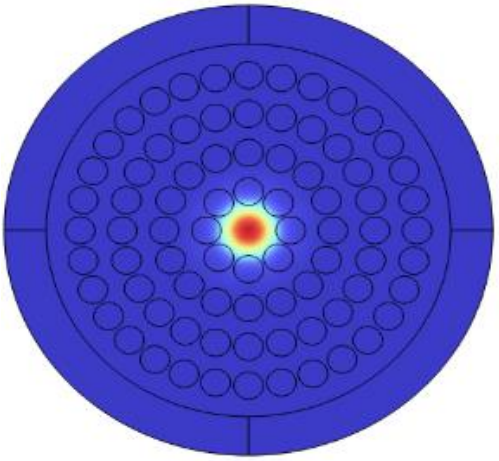

(f)

Figure 5.1 (a), (b), (c), (d), (e) depicts the cross-sectional view of the suggested PCF and **(f)** depicts the dispersal of electric field for the principal mode at 1.55 μm.

The circular rings are infiltrated with ethanol gradually (one ring → two rings → three rings → four rings) and its impact is studied.

5.3 Results and discussion

In a PCF structure the broadening in the supercontinuum spectrum primarily depend upon the nonlinearity of material and the dispersion characteristics [31]**.** Figure 5.2 depicts the values of dispersion for different rings. The plot with all air has one ZDW around 1.3 μm and a dispersion compensating nature. It has been observed that the behaviour of plot has largely been changed after infiltration, it has resulted into a more flat and smoother curve. Also the value of dispersion has greatly been reduced. It can be seen for one ring with d=0.7 μm and the pitch (Λ) =1.0 μm it has two ZDWs one at 1.8 μm and another at 2.5 μm. The profile mostly being in the normal and near zero anomalous dispersion region leading to enhancement of the coherent characteristics. Now, again the infiltration

was performed for more circular rings two rings, three rings and four rings gradually. The nature of the plot is similar but they all have only one ZDW around 1.8 μm with large value of dispersion as compared to one ring infiltration. Also, they have both normal and anomalous regime. One ring with ethanol is having better dispersion control and hence has been considered for further study. Also, from the practical perspective one ring infiltration is simpler. In Fig.5.3, Λ is optimized for 1.0 μm, 2.0 μm and 3.0 μm. It is observed that the profile with Λ =1.0 μm has lesser value of dispersion as compared to Λ =2.0 μm and Λ =3.0 μm. So the former was considered. In Fig.5.4 while doing the optimization of *d* (=0.6 μm, 0.7 μm and 0.8 μm), *d*=0.7 μm has shown comparatively more flat profile with less dispersion. A flat, normal and lesser dispersion valued profile gives a broader as well as coherent SC spectra. So, as a structural parameter we have considered *d* = 0.7 μm as air hole diameters and pitch as 1 μm with one ring infiltration of ethanol. The value of dispersion is +30.231ps/nm-km for *d* = 0.7 μm and Λ =1.0 μm. Effective mode area (A_{eff}) & nonlinearity (γ) possesses inverse relation with each other, the trend can be seen in Fig.5.5 when both plotted with wavelength. The value of A_{eff} and γ at 1.55μm is 4.16 μm^2 and 281.4 $W^{-1}Km^{-1}$ respectively. Keeping in mind the availability of a standard commercial femtosecond laser system, 1.55 μm Er- Fiber laser with 100 MHz repetition rate is used.

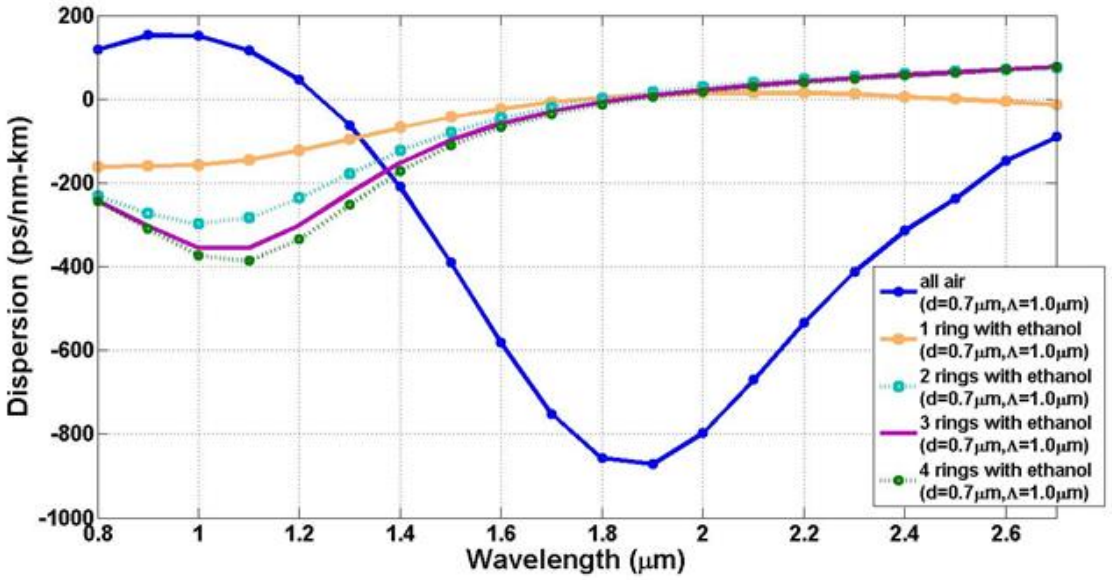

Figure 5.2. Effect of subsequent ring infiltrations with Λ=1 μm on dispersion characteristic of the PCF with *d*=0.7 μm.

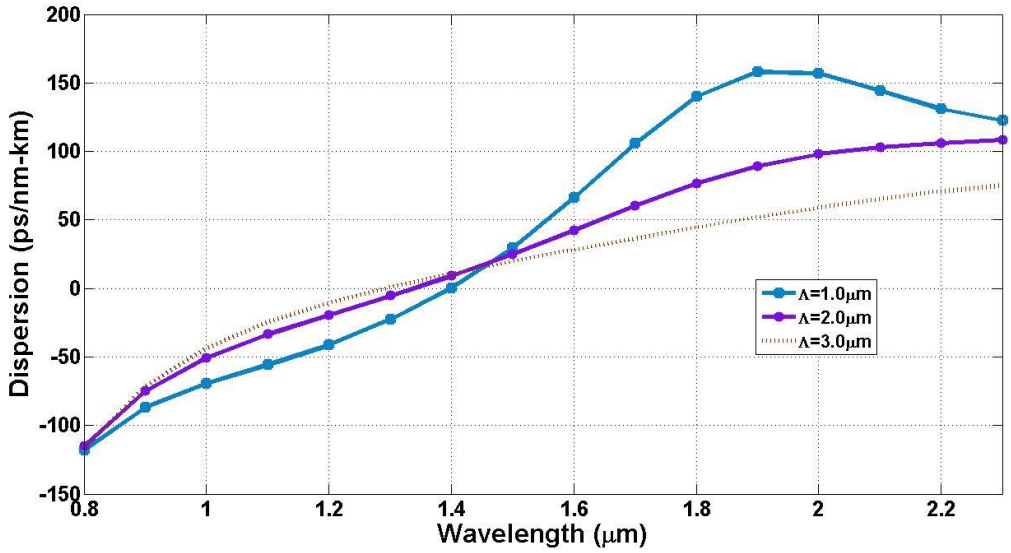

Figure.5.3. Effect of Pitch variation on one ring infiltration with Λ=1 μm, 2 μm and 3 μm and *d*=0.7 μm.

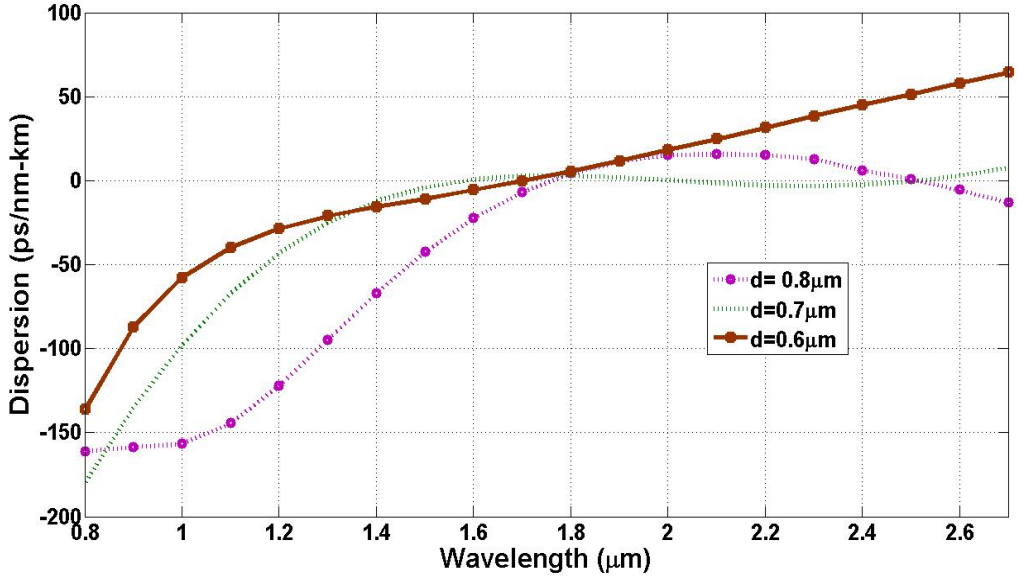

Figure 5.4. Effect of air hole diameter variation on the dispersion characteristic of the PCF with one ring infiltration for *d*= 0.6 μm, 0.7 μm & 0.8 μm with Λ=1 μm.

For multiple values of fiber length, pulse width and pump power, SCG has been assessed at a wavelength of 1.55 μm with 100 MHz repetition rate at −40 dB power level. SCG has been observed for various fiber length 5 cm, 10 cm and 20 cm in Figs. 5.6 & 5.7. The spectrum is getting broader with increasing length.

Self-phase modulation and soliton formation play fundamental roles in spectral broadening during nonlinear pulse propagation in optical fibers. SPM arises from the intensity-dependent refractive

index (Kerr effect), where the instantaneous phase of an optical pulse is modulated by its own power, generating new frequency components and symmetrically broadening the spectrum around the central wavelength.

As the pulse propagates in the anomalous dispersion regime, the interplay between group velocity dispersion and nonlinear phase modulation can lead to soliton formation. A soliton maintains its shape due to the balance between dispersion and nonlinearity, but higher-order solitons can undergo fission, breaking into fundamental solitons and emitting dispersive waves. This process significantly enhances and extends spectral broadening, particularly toward longer and shorter wavelengths. Together, SPM initiates the spectral expansion, while soliton dynamics and fission further amplify and redistribute the generated frequencies, enabling broadband supercontinuum generation. The phenomenon responsible for this broadening is SPM. Additionally, to assess the coherence level of the obtained spectra, we have performed a coherence calculation for 20 cm fiber length, 550 W pump power and 60 fs pulse width in Fig. 5.8. The spectrum is coherent for the entire SC broadening range 1.25 - 3.0 μm. We have computed the Degree of coherence especially to examine the wavelength dependence of the coherence [32].

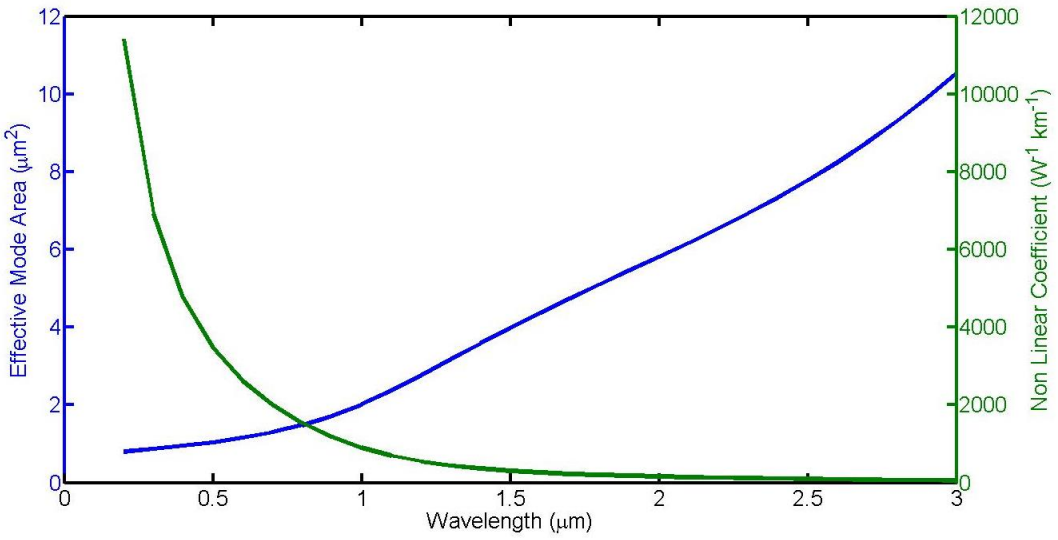

Figure 5.5. The variation of the effective mode area and nonlinear coefficient are illustrated across different wavelengths for the PCF.

In Fig. 5.9 the peak power is changed from 450 W to 650 W, the spectrum gets shifted towards the longer wavelength region. The symmetrical broadening of SC spectrum is mainly occurred due to the nonlinear SPM effect along the shorter and longer wavelength regions. Simultaneously, at higher peak power, the SC started to deteriorate and the coherency has also started to degrade as noise is increasing. This happened due to the absorption at the coating [33]. Then, the impact of increased pulse widths on SC has been analyzed. In Fig. 5.10, it is evident that as the T_{FWHM} value increases

from 60 fs to 80 fs, the resulting spectra narrow down. It is noteworthy that shorter pulses typically yield broader supercontinuum spectra. Therefore, the 60 fs pulses exhibit a stable spectrum. The maximum broadening, ranging from 1.25 to 3.0 μm, is observed with the length of fiber as 20 cm, 550 W peak power, and a pulse width of 60 fs.

For 60 fs laser pulse at 1.55 μm, β_2 is 1.21×10^{-26}, ($T_0 = T_{FWHM}/1.763$), the nonlinear length ($L_{NL} = (\gamma P_0)^{-1}$) and dispersion length ($L_D = (\beta_2/T_0^2)^{-1}$) for proposed PCF are 6.49×10^{-3} m and 2.975×10^{-1} m respectively. The order of soliton $N \approx L_D/L_{NL} \approx 45$ and the fission length of soliton calculated as $L_{fiss} = L_D/N \approx 6.6$ mm are determined using these relationships. To achieve a wider SCG, it is advantageous to have $L_{NL} \leq L_D$.

This ensures that nonlinear effects significantly influence the spectrum of the input pulse, while preventing excessive broadening of the pulse by dispersion before nonlinear effects can occur. Initially, during pulse propagation, spectral broadening primarily occurs due to SPM, where the intensity alters the pulse phase. As the pulse progresses to longer wavelengths, broadening is increasingly influenced by optical wave breaking, a phenomenon where the intensity of the pulse or shape changes due to nonlinear effects in the medium.

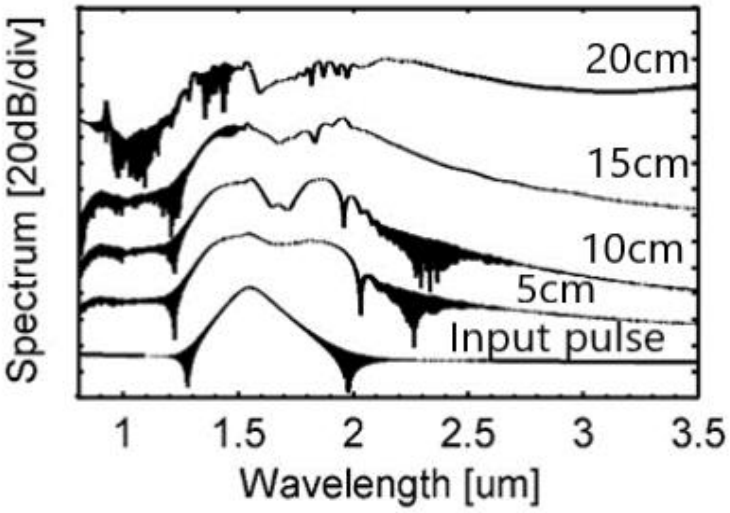

Figure 5.6. The progression of spectral supercontinuum (SC) broadening at 1.55 μm due to varying fiber lengths of 5 cm, 10 cm, 15 cm, and 20 cm under conditions of 60 fs and 550 W.

In conclusion, our proposed structure demonstrates the capability to achieve a broader and comparable bandwidth for SCG using lower pump power compared to previously documented results, as outlined in Table 5.1. As can be seen in reference [34] has comparable peak power but have lesser broadening range, in references [35-39] the peak power used is very high and the broadening range is also less as compared to the proposed design.

This study focuses on achieving substantial spectral broadening with low peak power, providing multiple benefits for supercontinuum generation. Operating at lower peak power significantly reduces noise, thereby enhancing the quality of measurements and imaging. Additionally, lower peak power typically results in longer pulse durations, which can be advantageous for applications that require prolonged interaction with the sample, including material processing and biomedical imaging. In summary, employing a lower value of peak power in SCG can produce more stable, high-quality spectra and offers increased safety for sensitive samples.

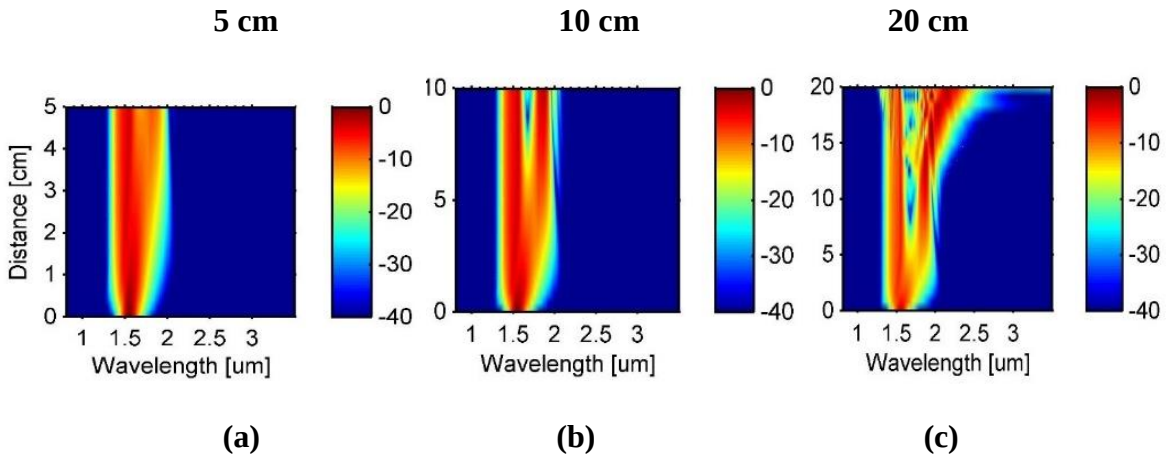

Figure 5.7 The spectral evolution of SCG at 1.55 µm induced by 60 fs, 550 W and length variation of **(a)** 5 cm, **(b)** 10 cm and **(c)** 20 cm respectively.

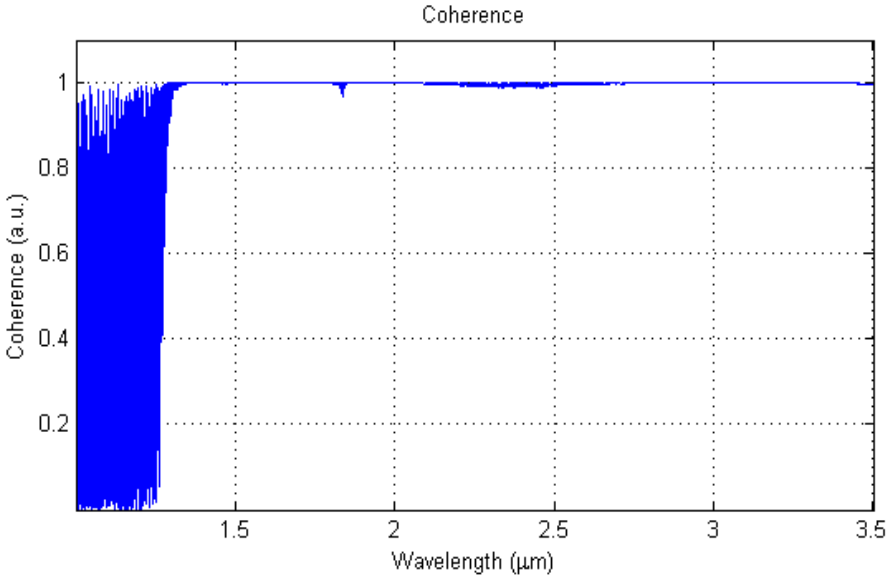

Figure 5.8 The coherence evolution at 1.55 µm using 550W, 60 fs pulse width along the fiber length of 20 cm.

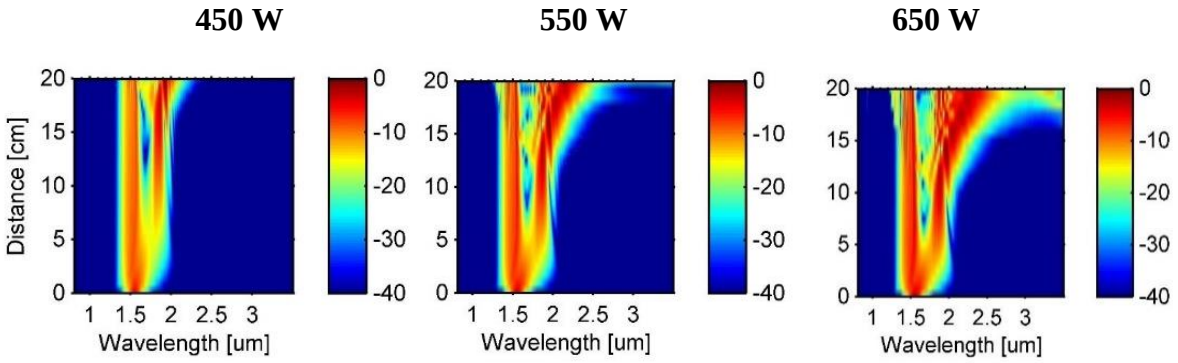

Figure 5.9 The spectral evolution of SCG at 1.55 µm induced by peak power variation of **(a)** 450W, **(b)** 550W and **(c)** 650W at 60 fs & 20 cm.

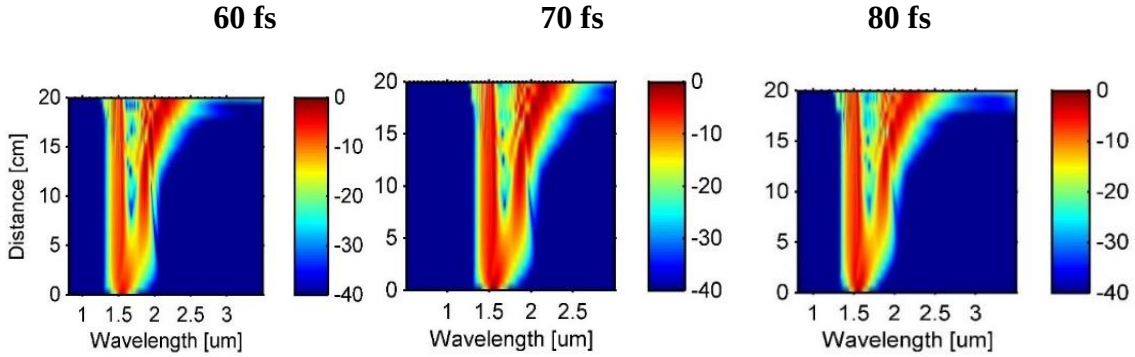

Figure 5.10 The spectral evolution of SCG at 1.55 µm induced by pulse width variation of **(a)** 60 fs, **(b)** 70 fs and **(c)** 80 fs at 20 cm fiber length and 550 W pump power.

Table 5.1. Comparison with earlier documented findings of supercontinuum spectra in infiltrated PCFs

References	#PCF	Pump Wavelength (µm)	Peak power (kW)	Fiber length	SCG bandwidth (µm)
[34]	$C_6H_5NO_2$,#F_2	1.56	5.55	5cm	0.8 – 2.1
[34]	$C_6H_5NO_2$, #F_3	1.56	0.66	5cm	1.3-2.3
[35]	C_7H_8	1.03	25	10cm	0.95-1.1
[36]	C_6H_6, #F_1	1.56	55	1cm	0.7-2.0
[37]	C_2Cl_4 ,#F_1	1.56	16.67	5cm	0.8-2.0
[37]	C_2Cl_4 ,#F_2	1.56	16.67	10cm	1.0-2.0
[37]	C_2Cl_4 ,#F_3	1.03	20.83	10cm	0.7-2.4
[38]	$C_2H_4Br_2$, #F_1	1.03	12.5	10cm	0.64-1.7
[38]	$C_2H_4Br_2$, #F_2	1.03	0.75	15cm	0.7-2.4
[39]	C_7H_8 , # I_3_0.3	1.55	7.14	10cm	1.1-1.75

[39]	C_7H_8 , # I_3_0.35	1.55	6.67	10cm	1.0-1.75
Proposed work	C_2H_6O	1.55	0.55	20cm	1.25-3.0

5.4 Conclusion

In conclusion, our proposed structure demonstrates the capability to achieve a broader and a comparable bandwidth for supercontinuum generation using lower pump power of 0.55kW. Furthermore, the challenge of balancing spectral broadening with maintaining coherence has been adeptly managed. The core focus of this work centres on generation of near to mid-IR supercontinuum with a coherent SC spectrum extending from 1.25 – 3.0 μm in a PCF of 20 cm length, when subjected to 550 W and 60 femtosecond laser pulse at 1.55 μm. From an application perspective, leveraging a PCF-based broadband coherent supercontinuum light source spanning from the near-infrared to the mid-infrared spectrum is profoundly impactful across several vital fields. These applications encompass early cancer detection, food quality monitoring, security applications, and sensing technologies. Additionally, the technology facilitates the creation of a stable optical frequency comb essential for precise OCT and spectroscopy.

REFERENCES

[1] Y Qu, W Sun, J Cao, H Chen and H Jia, "Coherent ultrabroad orbital angular momentum supercontinuum generation in an $AsSe_2$ -As_2S_5 microstructured fiber with all-normal dispersion", Optics Commununications, 497, 127191 (2021). https://doi.org/10.1016/j.optcom.2021.127191.

[2] D S Tomer and A Kumar, "Design and numerical modeling of chalcogenide parabolic - core waveguide for on - chip supercontinuum generation extending from near - IR region to mid - IR region", Microwave and Optical Technology Letters, 66(3), e34105 (2024). https://doi.org/10.1002/mop.34105

[3] R Sharma, S Kaur, P Chauhan and A Kumar, "Computational design & analysis of $GeSe_2$-As_2Se_3-PbSe based rib waveguide for mid infrared supercontinuum generation", Optik, 220, 0030–4026 (2020). https://doi.org/10.1016/j.ijleo.2020.165032

[4] T S Saini, A Kumar and R K Sinha, "Design and modelling of dispersion-engineered rib waveguide for ultra-broadband mid infrared supercontinuum generation", Journal of Modern Optics, 64(2), 143–149 (2016). https://doi.org/10.1080/09500340.2016.1216190

[5] R R Alfano and S L Shapiro, "Emission in the region 4000 to 7000 å via four-photon coupling in glass", Physics Review Letters, 24, 584–587 (1970). https://doi.org/10.1103/PhysRevLett.24.584

[6] P Chauhan, A Kumar and Y Kalra, "A dispersion engineered silica-based photonic crystal fiber for supercontinuum generation in near-infrared wavelength region" Optik - International Journal for Light and Electron Optics, 187, 230–237 (2019). https://doi.org/10.1016/j. ijleo.2019.03.107

[7] T S Saini, T H Tuan, T Suzuki et al., "Coherent mid-IR super continuum generation using tapered chalcogenide step-index optical fiber: experiment and modelling", Scientific Reports, 10, 2236 (2020). https://doi.org/10.1038/s41598-020-59288-6

[8] T S Saini, T H Tuan, L Xing, N P T Hoa, T Suzuki and Y Ohishi, "Coherent mid-infrared supercontinuum spectrum using a step-index tellurite fiber with all-normal dispersion", Applied Physics Express, 11, 102501 (2018). https://doi. org/10.7567/APEX.11.102501

[9] M Sharma, F Amirkhan, S K Mishra, D Sengupta, Y Messaddeq, F Blanchard and B Ung, "Transmission of Orbital Angular Momentum and Cylindrical Vector beams in a large-bandwidth annular core Photonic Crystal Fiber", Fibers, 8(4), 22 (2020). https://doi.org/10.3390/fib8040022

[10] M Sharma, F Amirkhan, S K Mishra, D Sengupta, Y Messaddeq, F Blanchard and B Ung, "Annular core photonic crystal fiber for propagation of optical vortices, in Conference on Lasers and Electro-Optics", OSA Technical Digest, Optica Publishing Group, STu3R.2 (2020). https://doi.org/10.1364/CLEO_SI.2020.STu3R.2

[11] T Sylvestre, E Genier, A N Ghosh, P Bowen, G Genty, J Troles, A Mussot, A C Peacock, M Klimczak and A M Heidt, "Recent advances in supercontinuum generation in specialty optical fibers", Journal of Optical Society of America B, 38, F90 (2021). https://doi. org/10.1364/JOSAB.439330

[12] J M Dudley, G Helsinki and S Coen, "Supercontinuum generation in photonic crystal fiber", Review of Modern Physics, 78, 1135 (2006). https:// doi.org/10.1103/RevModPhys.78.1135

[13] M Diouf, M L M Mandeng, C Tchawoua and M Zghal, "Numerical investigation of supercontinuum generation through $AsSe_2$/ As_2S_5 chalcogenide photonic crystal fibres and rib structures", Journal of Lightwave Technology, 37(22), 5692–5698 (2019). https://doi. org/10.1109/JLT.2019.2934034

[14] C Heuteu, S K Boukar, L M Mandeng and C Tchawoua, "Supercontinuum generation of truncated airy pulses in a cubic-quintic $AsSe_2$/As_2S_5 optical waveguide with rib-like structure", Journal of Optics, 23(09), 095503 (2021). https://doi.org/10.1088/2040-8986/ac0ff4

[15] C V Lanh and L T B Tran, "Low peak power broadband supercon tinuum spectra generated in a square lattice toluene core photonic crystal fiber with different air hole diameters", Laser Physics, 33, 095102, (2023).10.1088/1555–6611/ace24d

[16] S Kedenburg, A Steinmann, R Hegenbarth, T Steinle and H Giessen, "Nonlinear refractive indices of nonlinear liquids: wavelength dependence and influence of retarded response", Applied Physics B, 117, 803–816 (2014). https://doi.org/10.1007/s00340-014-5833-y

[17] M Chemnitz, M Gebhardt, C Gaida, F Stutzki, J Kobelke, J Limpert, A Tünnermann and Schmidt, "Hybrid Soliton dynamics in liquid-core fibres", Nature Communications, 8, 42 (2017). https://doi.org/10.1038/s41467-017-00033-5

[18] S Kedenburg, T Gissibl, T Steinle, A Steinmann and H Giessen, "Towards integration of a liquid-filled fiber capillary for supercontinuum generation in the 1.2–2.4 μm range", Optics Express, 23, 8281–8289 (2015). https://doi.org/10.1364/OE.23.008281

[19] J Pniewski, T Stefaniuk, H L Van, V C Long, L C Van, R Kasztelanic, G Stepniewski, A Ramaniuk, M Trippenbach and R Buczynski, "Dispersion engineering in nonlinear soft glass photonic crystal fibers infiltrated with liquids", Applied Optics, 55, 5033-5040 (2016). https://doi.org/10.1364/AO.55.005033

[20] F Dai, Y Xu and X Chen, "Enhanced and broadened SRS spectra of toluene mixed with chloroform in liquid-core fiber", Optics Express, 17, 19882–19886 (2009). https://doi.org/10.1364/OE.17.019882

[21] L C Van, A Anuszkiewicz, A Ramaniuk, R Kasztelanic, K D Xuan, ,V C Long, M Trippenbach and R Buczynski, "Supercontinuum generation in photonic crystal fibers with core filled with toluene", Journal of Optics, 19, 125604 (2017). https://doi.org/10.1007/ s11082-021-02820-3

[22] M Vieweg, T Gissibl, S Pricking, B T Kuhlmey, D C Wu, B J Eggleton and H Giessen, "Ultrafast nonlinear optofluidics in selectively liquid-filled photonic crystal fibers", Optics Express, 18, 25232–25240 (2010). https://doi.org/10.1364/OE.18.025232

[23] S A Adnan, A W Abdulwahhab and S N Ismail, "Fusion splicing: the penalty of increasing the collapse length of the air-holes in ESM-12B photonic crystal fibers", Optica Applicata, 46(2), 265-275 (2016). https://doi.org/10.5277/oa160211

[24] X Lin, H Yan, Y Ma and Z Zhou, "A construction method of the quasi-monolithic compact interferometer based on UV adhesives bonding", Review of Scientific Instruments, 94, 074501 (2023). https://doi. org/10.1063/5.0155637

[25] P Fürjes, "Controlled focused ion beam milling of composite solid state nanopore arrays for molecule sensing", Micromachines, 10(11), 774 (2019). https://doi.org/10.3390/mi10110774

[26] V T M Ngoc, C V Lanh, N T H Phuong, H V Thuy, N T Hue and L V Hieu, "Supercontinuum generation in a square-lattice photonic crystal fiber using carbon disulfide infiltration", Optik 286, 171049 (2023). https://doi.org/10.1016/j.ijleo.2023.171049

[27] N T Thuy, H T Duc and C V Lanh, "Comparison of supercontinuum spectral widths in CCl_4-core PCF with square and circular lattices in the claddings", Laser Physics, 33, 055102 (2023). https://doi.org/10.1088/1555-6611/acc240

[28] A G N Chaitanya, T S Saini, A Kumar, R K Sinha, "Ultra broadband mid-IR supercontinuum generation in $Ge_{11.5}As_{24}Se_{64.5}$ based chalcogenide graded-index photonic crystal fiber: design and analysis", Applied Optics, 55, 10138–10145 (2016). https://doi.org/10.1364/ao.55.010138

[29] T S Saini, A Baili, A Kumar, R Cherif, M Zghal and R K Sinha, "Design and analysis of equiangular spiral photonic crystal fiber for mid infrared supercontinuum generation", Journal of Modern Optics, 62(19), 1570-1576 (2015). https://doi.org/10.1080/09500340.2015.1051600

[30] A Rjeb, H Fathallah, S Chebaane and M Machhout, "Design of novel circular lattice photonic crystal fiber suitable for transporting 48 OAM modes", Optoelectronics Letter, 17 (2021). https://doi.org/10.1007/s11801-021-0158-7

[31] J M Dudley, G Genty and S Coen, "Supercontinuum generation in photonic crystal fiber", Review of Modern Physics, 78, 1135–1184 (2006). https://doi.org/10.1103/RevModPhys.78.1135

[32] L C Van, K Borzycki, K D Xuan, V T Quoc, M Trippenbach, R Buczyński and J Pniewski, "Supercontinuum generation in photonic crystal fibers infiltrated with nitrobenzene", Laser Physics, 30(3), 035105 (2020). https://doi.org/10.1007/s12648-023-02830-9

[33] P Chauhan, A Kumar and Y Kalra, "Numerical exploration of coherent supercontinuum generation in multicomponent $GeSe_2$ -As_2Se_3 -PbSe chalcogenide based photonic crystal fiber", Optical Fiber Technology, 54, 102100 (2020). https://doi.org/10.1016/j. yofte.2019.102100

[34] H V Thuy et al., “All-normal dispersion supercontinuum generation in photonic crystal fibers with large hollow cores infiltrated with toluene”, Optical Material Express, 8(11), 3568 (2018). https://doi.org/10.1364/OME.8.003568

[35] C V Lanh, H V Thuy, K Borzycki, D X Khoa, T Q Vu, M Trippenbach, R Buczyn´ski and J Pniewski, “Broadband supercontinuum generation with low peak power in controllable C_7H_8-core photonic crystal fibers of characteristic quantities”, Laser physics, 30, 035105 (2020). https://doi.org/10.1007/s12648-023-02830-9

[36] L C Van, H V Thuy, V C Long, K Borzycki, K D Xuan, V T Quoc, M Trippenbach, R Buczyn´ski and, J Pniewski, “Broadband supercontinuum generation with low peak power in controllable C_7H_8-core photonic crystal fibers of characteristic quantities”, Optical Engineering, 60, 116109 (2021). https://doi.org/10.1007/ s12648-023-02830-9

[37] L V Hieu, H V Thuy, N T Hue, C L Van, R Buczyn´ski and R Kasztelanic, “Supercontinuum generation in photonic crystal fibers infiltrated with tetrachloroethylene”, Optical Quantum Electronics, 53, 187 (2021). https://doi.org/10.1007/s11082-021-02820-3

[38] Le H Van, V T Hoang, Le T Canh, Q H Dinh, H T Nguyen, N V Thi Minh, M Klimczak, R Buczynski and R Kasztelanic, “Silica-based photonic crystal fiber infiltrated with 1,2-dibromo ethane for supercontinuum generation”, Applied Optics, 60(24), 7268–7278 (2021). PMID: 34613015. https://doi.org/10.1364/ AO.430843

[39] L C Van, A Anuszkiewicz, A Ramaniuk, R Kasztelanic, K D Xuan, V C Long, M Trippenbach and R Buczynski, “Supercontinuum generation in photonic crystal fibres with core filled with toluene” Journal of Optics, 9, 125604 (2017). https://doi.org/10.1088/2040-8986/ aa96bc

CHAPTER 6: PHOTONIC CRYSTAL FIBERS INFILTRATED WITH NITROBENZENE FOR LOW PEAK POWER SUPERCONTINUUM GENERATION IN NIR TO MIR REGION *

6.1 Introduction

In this chapter, we present a comparative analysis of the effects of nitrobenzene infiltration on SC generation across two different designs. Unlike CS_2 and toluene, nitrobenzene is less toxic. Nitrobenzene has stronger nonlinear optical properties than benzene. The presence of the nitro group in nitrobenzene increases its polarizability, making it more responsive to intense light fields. Utilizing liquids within the air holes offer tunable properties and high nonlinearity, which enhances the bandwidth of SC spectrum with lower pump power and reduced attenuation. One design features a symmetrical structure, while the other incorporates elliptical air holes, introducing birefringence due to asymmetry. Polarization effects are another essential aspect of the dynamics of SCG in MOFs [1].

Polarization-dependent dispersion in polarization-maintaining fibers originates from deliberate birefringence, which leads to two orthogonal polarization modes known as the fast and slow axes. They possess different propagation constants and dispersion coefficients (such as β_2 and β_3). Consequently, each polarization component propagates with a different group velocity and undergoes distinct pulse broadening, soliton evolution, and phase-matching behavior. In supercontinuum generation, where spectral broadening strongly depends on dispersion characteristics, these differences can substantially affect soliton fission dynamics, dispersive wave formation, and the resulting spectral profile. If the input light is not accurately aligned with one principal axis, both polarization modes may be simultaneously excited, leading to temporal walk-off, spectral distortions, increased intensity noise, and reduced coherence. Hence, precise polarization control and appropriate fiber design are crucial for achieving stable, low-noise, and repeatable broadband performance in polarization maintaining supercontinuum sources [2].

*__D.S. Tomer__ *and A. Kumar, "Photonic crystal fibres infiltrated with nitrobenzene for low peak power supercontinuum generation in NIR to MIR region", Journal of Modern Optics, 72(4–6), 175–187 (2025). https://doi.org/10.1080/09500340.2025.2478641*

The birefringent fibers for SCG has demonstrated to be quite useful, as it keeps the polarization state preserved along the propagation for all the spectral components. Ortigosa-Blanch et al have observed that the birefringence can be achieved either by making the PCF design non symmetrical or by introducing a birefringent material [3]. Elliptical air holes have also been utilized in MOFs to provide increased birefringence effect [4].

A SC spectrum ranging from NIR to MIR is generated using a symmetrical graded design at low input pump power. This spectrum extends from 1.3 μm to 2.0 μm when pumped at a wavelength of 1.55 μm, utilizing a 10 mm long fiber and injecting 50 fs laser pulses at a power of 650 W. In another design on using same pump power, same fiber length and same 50fs laser pulse broadening around 0.9 μm – 2.3 μm is obtained with *x*-polarization and broadening around 1.0 μm – 2.4 μm is obtained with *y*-polarization.

From the perspective of practical implication low input power is crucial. In case of liquid infiltration in PCFs, they are unstable at high temperatures and high power. They can be easily vaporized if high power is used. The produced SC source can be utilized in wide range of applications such as monitoring food quality, biomedical diagnostics, chemical detection & analysis, frequency comb generation, explosive detection, and advanced optical imaging techniques including OCT. A wide supercontinuum spectrum with low input peak power is presented, in comparison to the lately reported results summarized in Table 6.1. Moreover, the difficulty of harmonizing SC broadening along with preserving coherence has been efficiently resolved.

This chapter is organized into four main sections, each addressing a critical aspect of the study. Section one serves as an introduction, providing a brief yet comprehensive overview of the research objectives and the scope of the study. Section two focuses on the design of PCF, outlining the theoretical framework and the design principles employed. The section three presents the results obtained from the study, offering an in-depth discussion of their significance and potential implications for the field. Finally, section four concludes the paper, summarizing the key findings and suggesting directions for future research, followed by a comprehensive list of references.

6.2 Geometrical parameters of PCF

Achieving low loss and small effective mode area is crucial for determination of the efficacy of a nonlinear medium for supercontinuum generation. At the same time dispersion properties are equally important. These factors are largely shaped by the geometry of the fiber. Along with these factors, the material used in the fabrication of PCF should have high nonlinear refractive index (n_2). The structural view of proposed circular PCF is shown in Figs. 6.1(a) & 6.1(b). This design is symmetrical

with circular rings of air holes which have been graded for better confinement of light within the core. The amount of grading (δD) = d_1- d_2 = d_2 - d_3 = d_3 – d_4 has been kept constant as 0.50 µm between two consecutive rings.

Each ring of air holes is designed with a unique diameter: the first ring surrounding the core has a diameter of d_1= 2.0 µm, second ring d_2= 1.5 µm, third ring d_3= 1.0 µm and the fourth ring d_4= 0.5 µm. The diameter of core is constant as d_{core} =1.0 µm.

The first ring contains eight air holes, while the outer rings have a greater number of air holes, creating a symmetrical structure described by $x = r\ cos\ (\theta)\ and\ y = r\ sin\ (\theta)$, where r represents the radial distance from the center and (θ) varies from 0° to 360°. The pitch (Λ) is defined as the distance between two adjacent air holes, is set to 1 µm.

To eradicate reflections at the boundary a cylindrical PML is implemented at the edges of the cladding. The PML is generally 10% to 20% of the whole cladding diameter. Here, it is 1.8 µm. The core is infiltrated with nitrobenzene. Figure 6.1(c) shows the electric field distribution of the principal mode at pump wavelength.

Similarly, Figs. 6.2(a) & 6.2(b) show a similar design but with an elliptical first ring around the core. The rest of the design parameters are kept the same. Instead of circular symmetrical ring of constant diameter d_1= 2.0 µm, elliptical air holes are introduced with major axis, a = 2.0 µm and minor axis as b = 1.0 µm.

Figure 6.2(c) & 6.2(d) show the distribution of electric field for the principal mode at pump wavelength along x-direction as (#EX) & along y-direction as (#EY) respectively. Again, the core is infiltrated with nitrobenzene. The Circular symmetric design is represented as #C, whereas x-polarization of elliptical design is represented as #EX and y-polarization of elliptical design is represented as #EY. Both designs are being studied for comparative study.

Figure 6.3 shows the variation of refractive index (n) of silica and nitrobenzene with wavelength. For better confinement of light within the core the refractive index of nitrobenzene must be greater than silica which is visible from Fig.6.3.

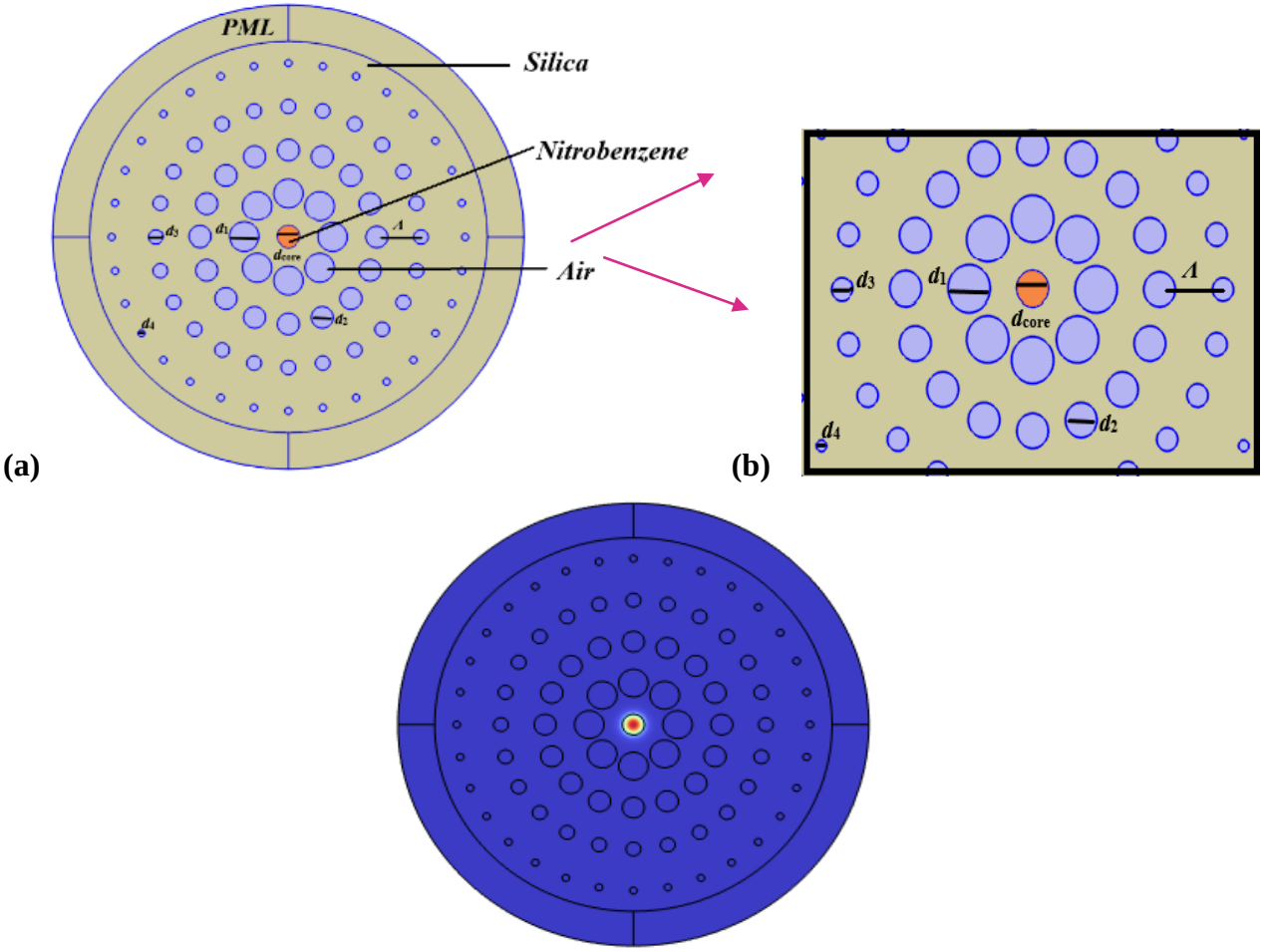

Figure 6.1 (*a*) Cross-sectional view of the circular PCF (#C), **(b)** displaying the cladding region for better understanding and **(c)** at 1.55 μm the electric field distribution for the fundamental mode within the PCF.

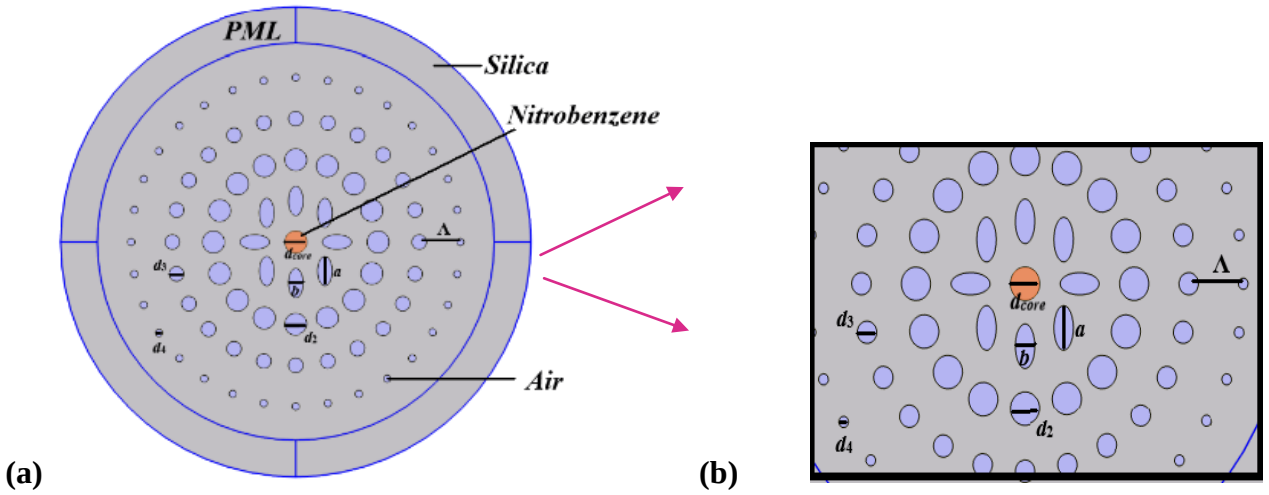

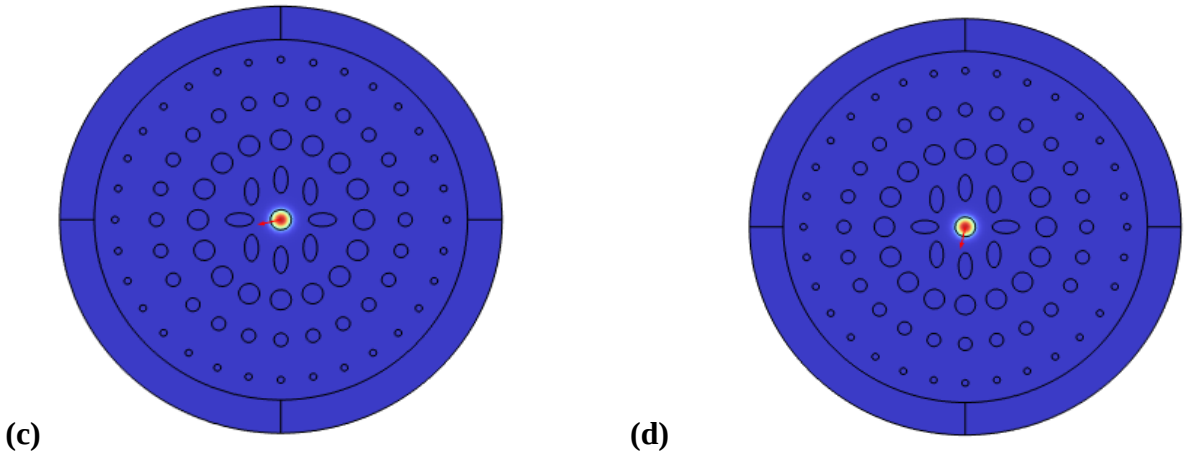

Figure 6.2 (*a*) Cross-sectional view of the elliptical PCF (#E), **(b)** displaying the cladding region for better understanding & at 1.55 μm the distribution of electric field for the principal mode along **(c)** *x*-direction as (#EX) and **(d)** *y*-direction as (#EY).

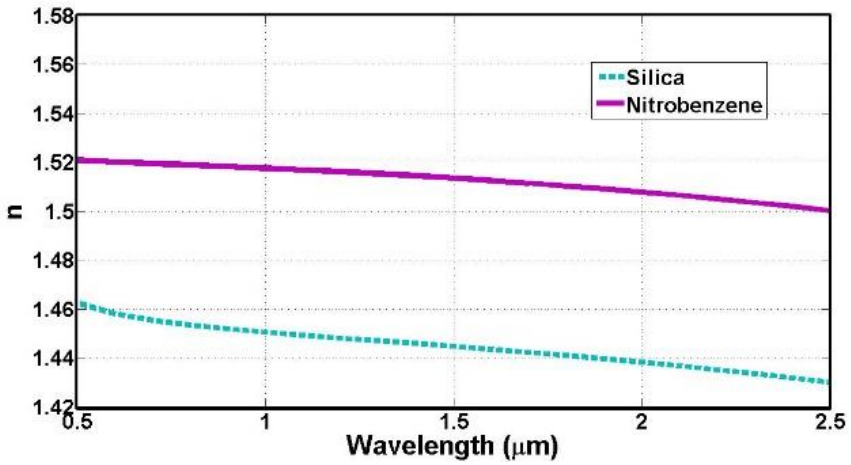

Figure 6.3 Characteristics of the refractive index (*n*) of silica and nitrobenzene.

6.3 Results and discussion

In a PCF structure the broadening in SC spectrum primarily relies upon the nonlinearity of material and the dispersion characteristics [5]. Figure 6.4(a) depicts the values of dispersion for design #C with different core size as d_{core} = 1.0 μm, 1.2 μm and 1.4 μm. The plot shows no major difference in the dispersion values for all chosen d_{core} values. The design is robust. So, d_{core} = 1.0 μm has been preferred as lower area will result into more nonlinearity. Again, in Fig.6.4 (b) for optimization, the pitch (Λ) has been changed as 2.4 μm, 2.8 μm and 3.2 μm. Λ= 2.4 μm is having no ZDW, Λ= 2.8 μm is having ZDW around 1.2 μm and Λ= 3.2 μm is having ZDW around 1.6 μm. ZDW is the wavelength where the dispersion value exhibited by the waveguide transitions from normal to anomalous dispersion regime i.e. passes zero [6]. It provides an insight to choose a suitable pumping

wavelength which will influence SCG process. As if pumped in the anomalous dispersion region, the soliton fission process along with the emission of the dispersive waves is responsible for the broadening in the SC spectrum.

On the other end, if pumped in normal dispersion regime SPM will be prevalent phenomenon for broadening. The value of Λ = 3.2 μm is giving more negative dispersion on shorter wavelength side and on longer wavelength side it is having less positive dispersion as compared to other values. It is also giving minimum dispersion value around 1.55 μm. So, for #C, Λ= 3.2 μm has been picked up as pitch. Figure 6.5(a) shows dispersion profile for different d_{core} (= 1.0 μm, 1.2 μm and 1.4 μm) for elliptical profile. The dispersion values are distinct for *x* and *y*-polarization. #EX and #EY represents *x* and *y*-polarization of the elliptical design respectively. The pattern is almost similar for all three profiles of different d_{core} values where the difference in dispersion values for *x* and *y*-polarization is becoming prominent at higher wavelengths. Since asymmetrical design leads to birefringence hence this trend is obvious. So, choosing a smaller core diameter as 1 μm will be better since it will lead to greater nonlinearity.

Figure 6.5(b) shows dispersion profile for different values of Λ as 2.4 μm, 2.8 μm and 3.2 μm for elliptical profile with d_{core} =1.0 μm. Λ= 2.4 μm is having no ZDW, Λ= 2.8 μm is having ZDW around 1.5 μm and Λ= 3.2 μm is having ZDW around 1.8 μm. Λ= 2.8 μm has been selected as it is giving minimum dispersion value around 1.55 μm.

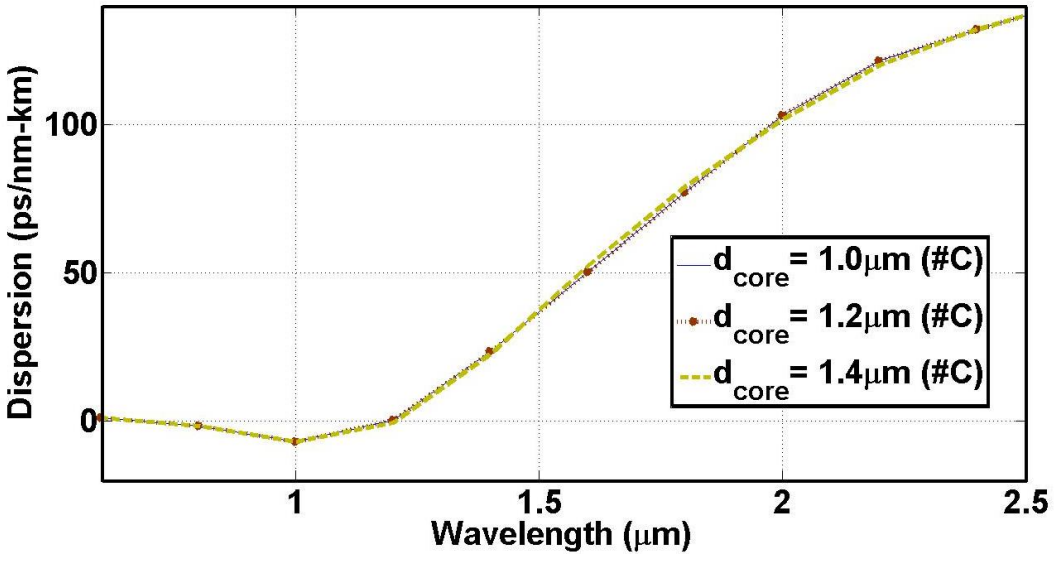

(a)

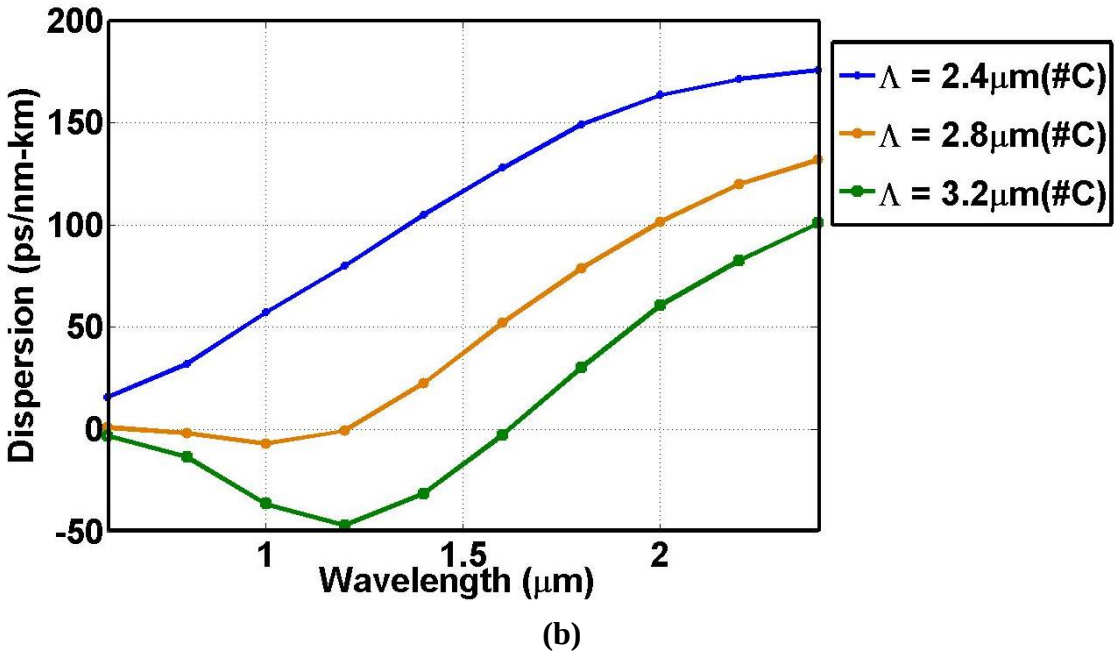

(b)

Figure 6.4 Study of dispersion characteristics of #C with variation of **(a)** d_{core} and keeping Λ= 3.2 μm as constant and **(b)** Λ and keeping d_{core} = 1.0 μm as constant.

It is found that changing core diameter has not impacted much to the circular design but it has significantly impacted the dispersion profile in the elliptical geometry on the higher wavelength region. Figure 6.6(a) shows the variation of birefringence with respect to wavelength. It can be seen that as the value of wavelength increases the difference in the values of effective mode index between the two states of polarization increases. Birefringence = | n_x - n_y|, where n_x & n_y are the *x* and *y* components of effective mode index respectively [1]. The value of birefringence at 1.55 μm is 1.3×10^{-3}.

Figure 6.6 (b) shows the variation of effective mode area and nonlinearity for #C, #EX & #EY. EMA & γ holds inverse relation, and this behavior can be observed when both plotted with respect to the wavelength. The value of A_{eff} at 1.55 μm is 4.13 μm^2 for #C, 4.55 μm^2 for #EX & 4.60 μm^2 for #EY respectively. Similarly, the nonlinear coefficient for #C, #EX & #EY are 1962.0 $W^{-1}Km^{-1}$, 1780.9 $W^{-1}Km^{-1}$ and 1761.5 $W^{-1}Km^{-1}$ respectively. Our reported dispersion value is less than previous documents works [7-9].The effective mode area is smaller than other studies with values of 6.67 μm^2 [10] and 7.76 μm^2 [11]. Also, the value of nonlinear coefficient is higher than the results mentioned in other document works [12-14]. In Fig. 6.7(a) a more flat dispersion profile is found for #EX & #EY polarization as compared to #C, which is preferable for obtaining a broad SC spectrum. In Fig. 6.7(b) confinement loss for different designs has been shown. Beyond 2.5μm the loss is large due to limited transparency of silica. According to the measurements in reference [22], nitrobenzene is transparent in visible and NIR region with an absorption maximum at 1.67

μm. Our chosen pump wavelength is 1.55μm at which nitrobenzene is transparent around 90%, offering negligible losses. This assumption does not influence dispersion characteristics, which are taken into account in all simulations [19].

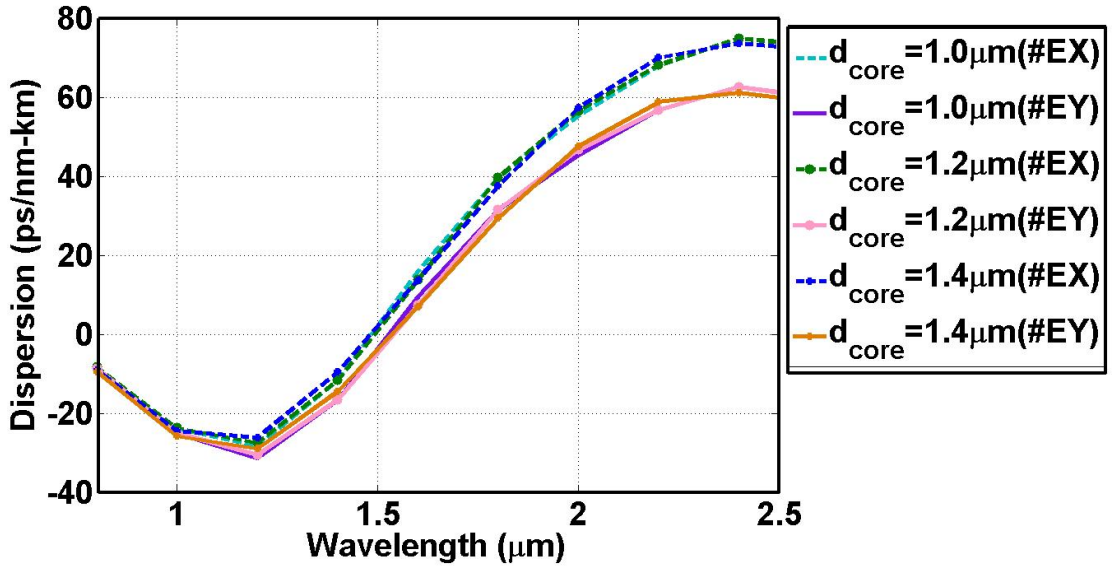

(a)

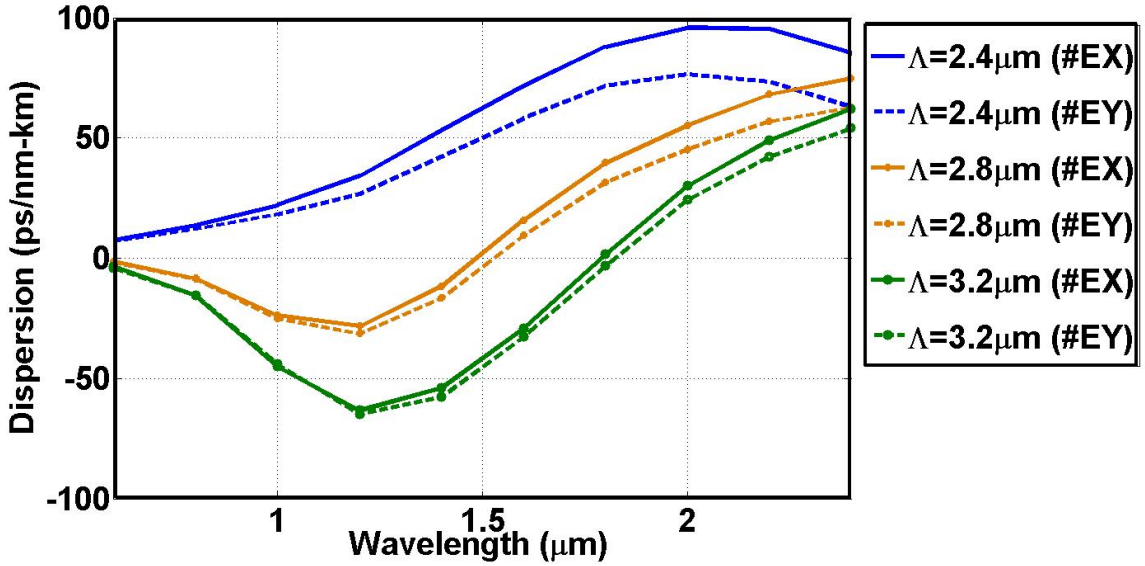

(b)

Figure 6.5 Study of dispersion characteristics of #EX & #EY with variation of **(a)** d_{core} and keeping Λ = 2.8 μm as constant, and **(b)** Λ and keeping d_{core} = 1.0 μm as constant.

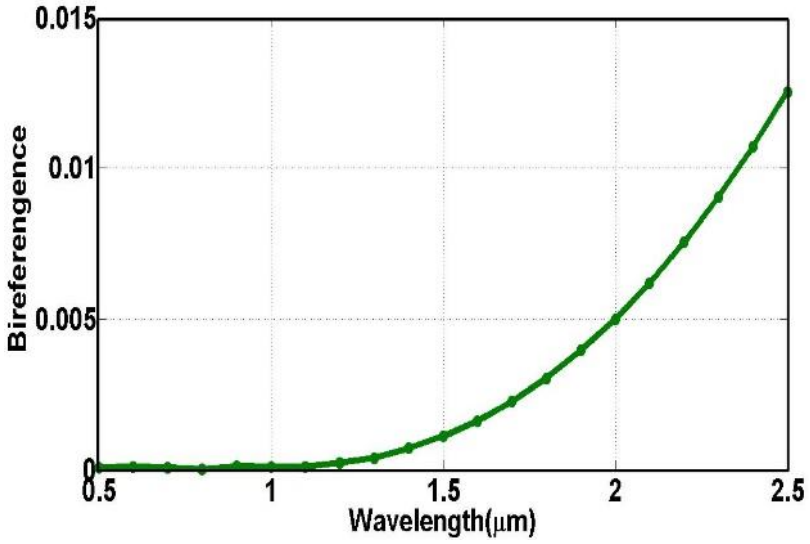

(a)

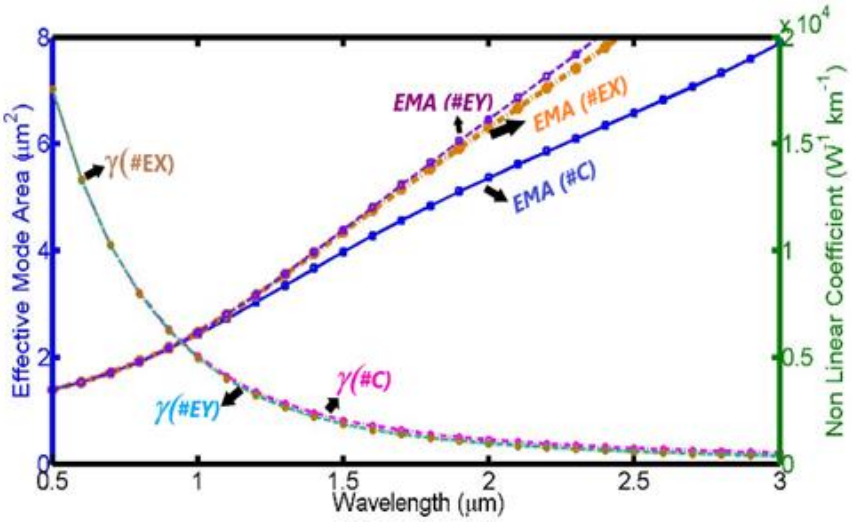

(b)

Figure 6.6 (a) Birefringence for elliptical design and **(b)** the variation of effective mode area (EMA) and nonlinearity (γ) of #C, #EX & #EY with wavelength.

SCG has been systematically evaluated across a range of parameters, including fiber length, pulse width, and pump power, specifically at a wavelength of 1.55 μm with a repetition rate of 100 MHz and a power level set at -20 dB. The results illustrate that SCG has been successfully observed for different fiber lengths, spanning from 5 mm to 20 mm. This data is presented in Figures 6.8(a), (b) and (c), which correspond to samples #C, #EX and #EY respectively. As the fiber length increases, the spectrum undergoes significant broadening. At a fiber length of 5 mm, the spectral broadening is minimal, indicating limited extension of the SC. However, the broadest spectral expansion is achieved at a fiber length of 10 mm across all three configurations, #C, #EX and #EY. This length-dependent behaviour highlights the critical role of SPM in expanding the SC as fiber length increases. With further increase in length beyond 10 mm the noise is becoming more prominent and

spectrum started to get deteriorate.

The coherence is also getting disturbed. The coherence is also evaluated for 650 W pump power, 50 fs pulse width and 10 mm fiber length in Fig.6.9.

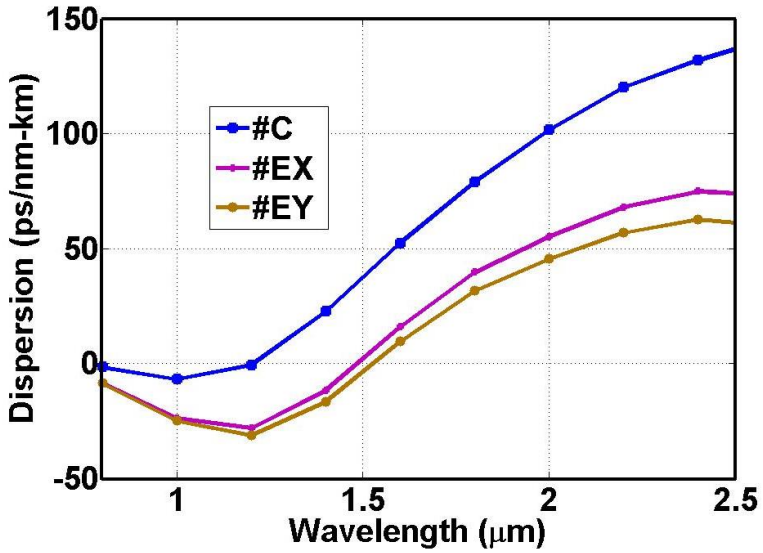

(a)

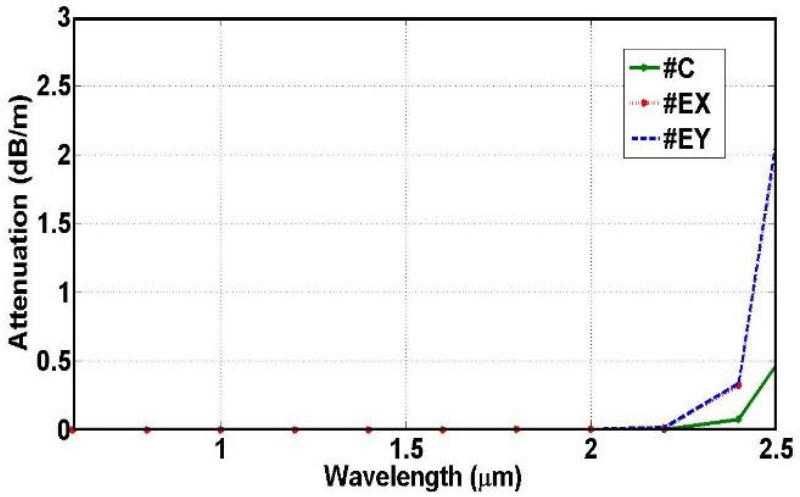

(b)

Figure 6.7 (a) Optimized dispersion characteristics of #C (d_{core} = 1.0 μm, Λ= 3.2μm) #EX & #EY (d_{core} = 1.0 μm, Λ= 2.8μm) with wavelength and **(b)** confinement loss of #C, #EX & #EY

Furthermore, the conducted coherence calculation illustrated in Fig. 6.9 revealed that the spectrum remains coherent throughout the entire SC broadening range: from 1.3 μm to 2.0 μm for sample #C, from 0.9 μm to 2.3 μm for sample #EX, and from 1.0 μm to 2.4 μm for sample #EY. Beyond 2.5 μm the coherence plot has started to deteriorate as the spectrum shows large noise this is due to the limited transparency window of silica. This coherence assessment is crucial as it demonstrates the stability and quality of the SC spectra across different samples, indicating that the generated

light maintains a consistent phase relationship within these specified wavelength ranges.

In Figs.6.10, 6.11 & 6.12 the peak power is changed from 450 W to 850 W, with increasing power the spectrum gets shifted towards the shorter as well as longer wavelength region for #C, #EX & #EY. The broadening of the SC spectrum appears symmetrically, primarily due to nonlinear SPM effects across both smaller and larger values of wavelength. At higher peak power, however, the SC spectrum starts to degrade, with a noticeable decrease in coherence as noise increases. This degradation is attributed to absorption occurring in the coating [15]. For #C, #EX & #EY with 450 W the broadening is less and for 850 W noise is large. The maximum & a stable broadening is obtained at 650 W. Subsequently, the effect of increasing pulse widths on the SC has been examined.

Figures 6.13, 6.14 and 6.15 illustrate that as the T_{FWHM} rises from 50 fs to 150 fs, the resulting spectra become narrower for configurations #C, #EX, and #EY. It is important to note that shorter pulse durations generally produce broader SC spectra. Consequently, the 50 fs pulses display a more stable spectrum. The maximum spectral broadening at -20 dB for configurations #C, #EX and #EY reaches 1.3 μm to 2.0 μm, 0.9 μm to 2.3 μm and 1.0 μm to 2.4 μm respectively, with a peak power of 650 W, fiber length of 10 mm and a pulse width of 50 fs. For 50 fs laser pulse at 1.55 μm, β_2 for #C is 3.21×10^{-26} s^2/m, ($T_0 = T_{FWHM}/1.763$), the nonlinear length ($L_{NL} = (\gamma P_0)^{-1}$) and dispersion length ($L_D = (\beta_2/T_0^2)^{-1}$) for proposed PCF are 7.8×10^{-4} m and 2.25×10^{-2} m respectively. The order of soliton $N \approx L_D/L_{NL} \approx 28$ and the fission length of soliton are calculated as $L_{fiss} = L_D/N \approx 0.8$ mm. Similarly, for #EX β_2 is 5.95×10^{-26} s^2/m, $L_{NL} = 8.6\times10^{-4}$ m and $L_D = 1.35\times10^{-2}$ m respectively. $N \approx 15$ & $L_{fiss} = 0.9$ mm. For #EY β_2 is 7.12×10^{-26} s^2/m, $L_{NL} = 8.7\times10^{-4}$ m and $L_D = 1.12\times10^{-2}$ m respectively. $N \approx 12$ & $L_{fiss} = 0.93$ mm.

To obtain a broader SCG, it is beneficial to have a nonlinear length less than or equal to dispersion length for the proposed fiber. This observation confirms that nonlinear effects play a crucial role in the broadening of the input pulse, while simultaneously preventing excessive broadening due to dispersion before these nonlinear interactions can take place. At the initial stage of pulse propagation, the broadening of the spectrum is primarily influenced by SPM, a nonlinear optical effect where the intensity of the pulse induces changes in its phase. This phase alteration causes a broadening of the pulse's spectral content, leading to the generation of new frequencies. As the pulse continues to propagate and shifts toward longer wavelengths, the broadening becomes dominated by a process known as optical wave breaking. This phenomenon occurs when the nonlinear effects within the medium become strong enough to significantly modify the intensity profile or shape of the pulse.

On comparing the circular and elliptical design we have found that a broader SC spectra is obtained for elliptical design as compared to circular design when subjected to the same values of fiber length, pump power and pulse width. Among *x* & *y* polarized states the broadening is more at lower wavelength region in *x*-polarization and whereas for *y*-polarization the broadening is more at higher wavelength region.

In summary, the designs we have proposed exhibit a strong potential to achieve a wider and comparable bandwidth for supercontinuum generation while operating at a lower pump power than what has been reported in prior studies. This improvement in performance highlights the efficiency and potential of our approach in enhancing SCG bandwidth without the need for high-power input, as detailed in Table 6.1. This advancement underscores the effectiveness of our designs in addressing the demands of SCG applications requiring broad spectra at lower energy costs. Also at pump wavelength both the proposed designs have very low attenuation. It can be seen, the SCG in reference [16] has been evaluated at -40 dB with higher peak power.

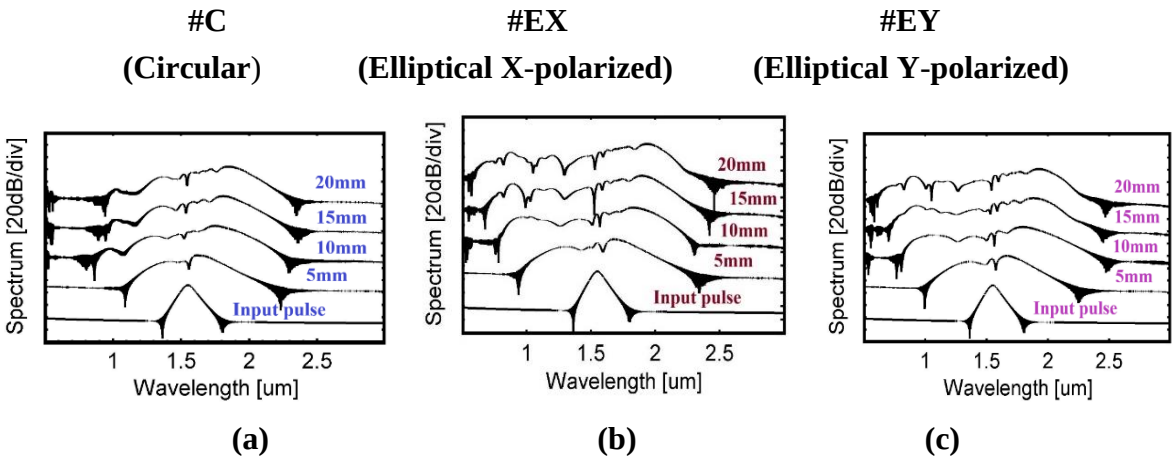

Figure 6.8. The broadening of SC spectrum at 1.55 µm due to varying fiber lengths of 5 mm, 10 mm, 15 mm and 20 mm under conditions of 50 fs and 650 W.

This study aims to achieve significant spectral broadening at low peak power, offering several advantages for SCG. Operating at reduced peak power minimizes noise levels, which in turn improves the quality of measurements and imaging. Additionally, lower peak power typically results in longer pulse durations, which can be advantageous for applications that require prolonged interaction with the sample, including material processing and biomedical imaging [21].

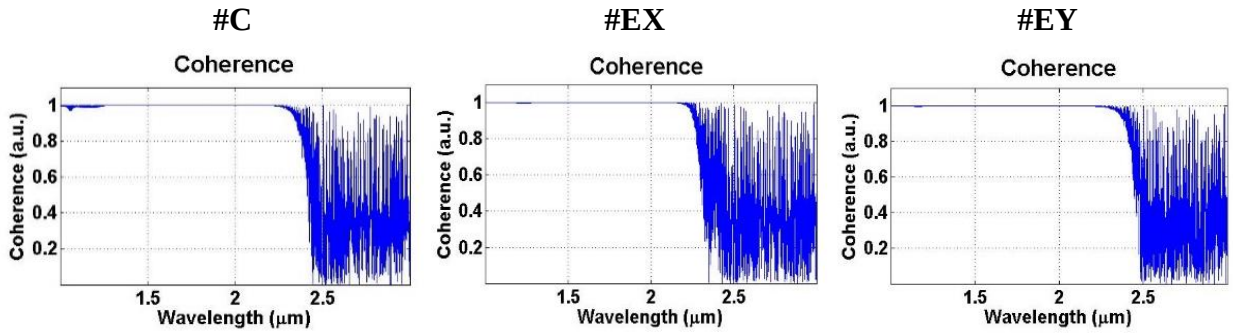

Figure 6.9. The coherence evolution using 650 W, 50 fs pulse width at 1.55 μm along the fiber length of 10 mm.

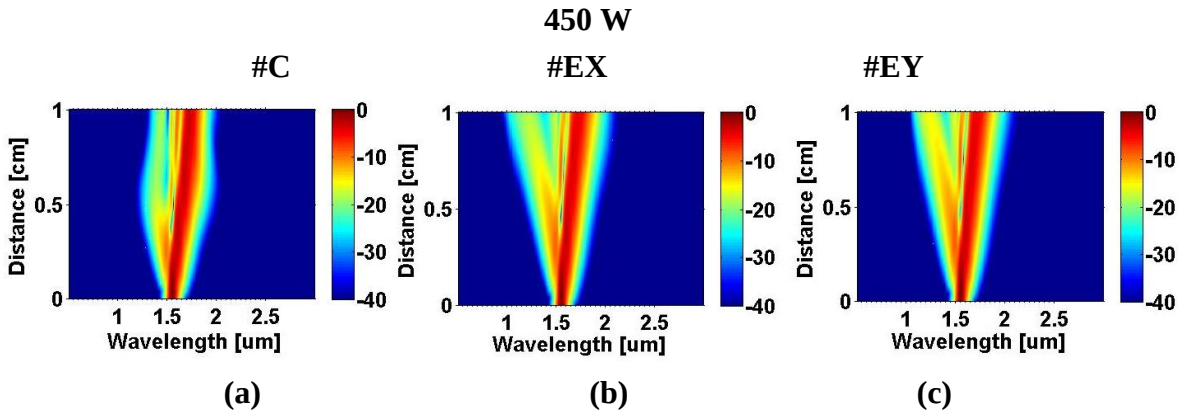

Figure 6.10. The spectral advancement of SCG at 1.55 μm in **(a)**, **(b)**, **(c)** with peak power of 450 W at 50 fs & 10 mm.

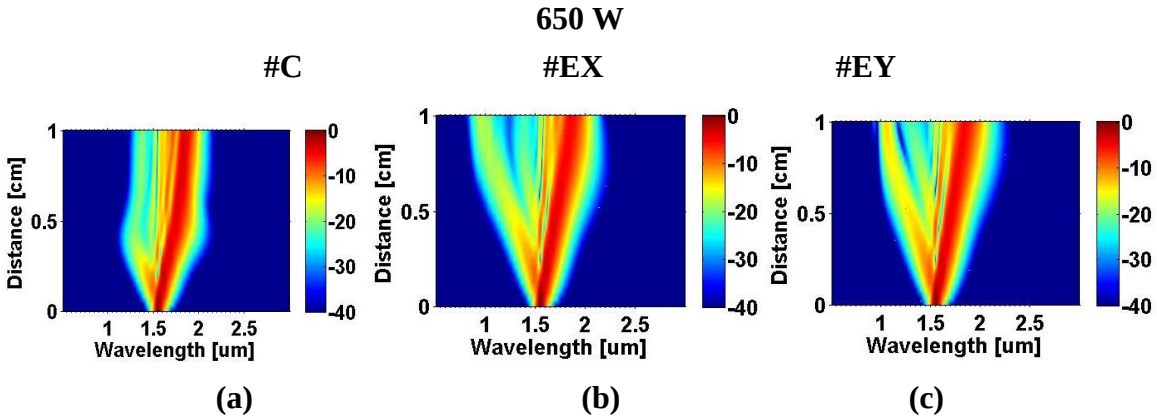

Figure 6.11. The spectral advancement of SCG at 1.55 μm in **(a)**, **(b)**, **(c)** at length of 10 mm, pulse width 50 fs & power 650W.

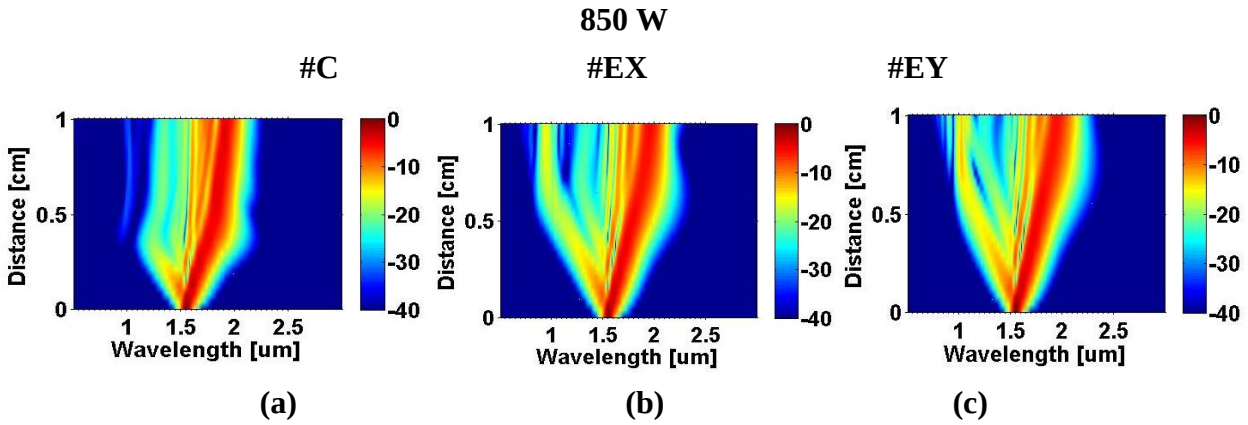

Figure 6.12. The spectral advancement of SCG at 1.55 µm induced in **(a)**, **(b)**, **(c)** with 850 W pump power, pulse width of 50 fs at 10 mm fiber length.

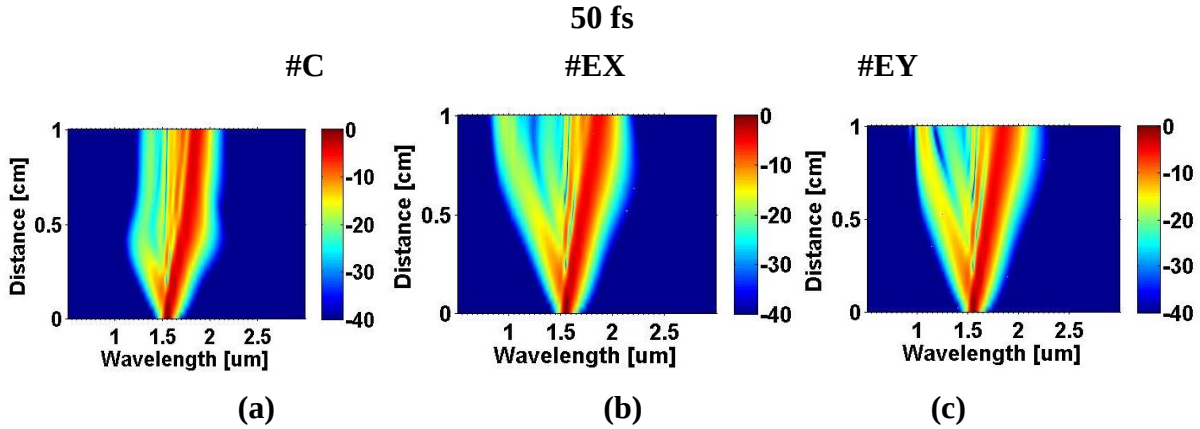

Figure 6.13. The spectral advancement of SCG at 1.55 µm induced in **(a)**, **(b)**, **(c)** with pulse width of 50 fs at 10 mm fiber length and 650 W pump power.

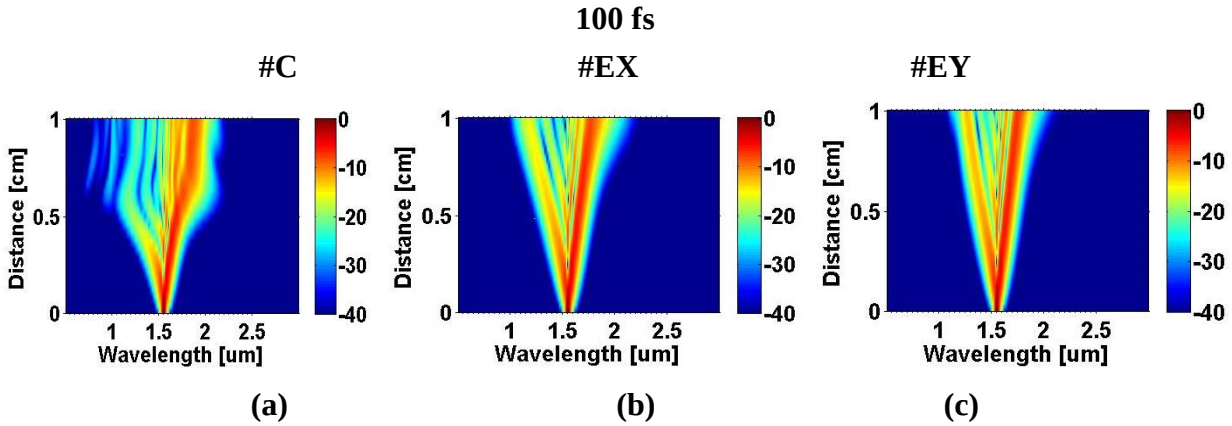

Figure 6.14. The spectral advancement of SCG at 1.55 µm induced in **(a)**, **(b)**, **(c)** with pulse width of 100 fs at 10 mm fiber length and 650 W pump power.

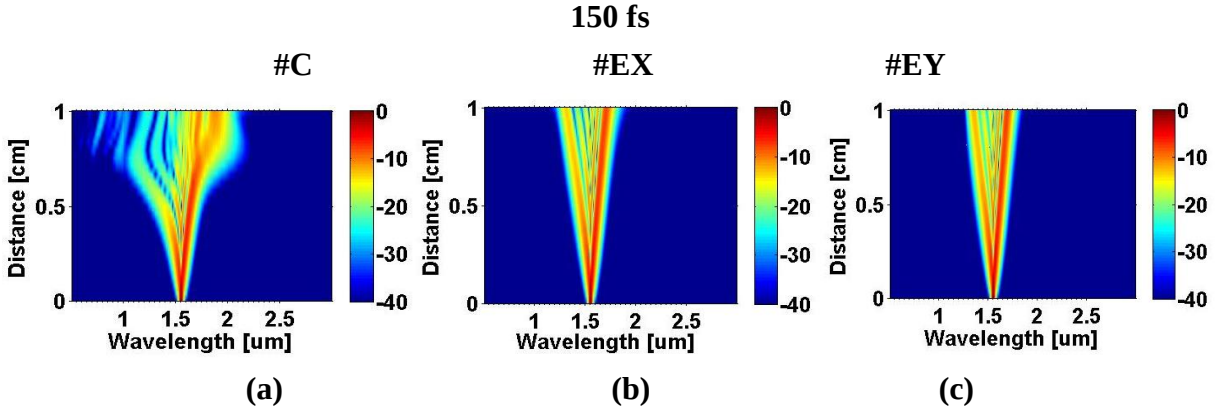

Figure 6.15. The spectral advancement of SCG at 1.55 µm induced in **(a)**, **(b)**, **(c)** pulse width of 150 fs at 10 mm fiber length and 650 W pump power.

For this fiber, the broadening is more as compared to #C which is evaluated at -20 dB in our case, but still lesser than #EX & #EY at -20 dB. Similarly, the designs mentioned in references [17-19] is using higher peak power at -20 dB but have lesser broadening range than #EX & #EY. The peak power used is high in the designs mentioned in references [19,20] and the broadening range has also been evaluated at -60 dB & -40 dB respectively. At these dB values both the designs #C & #E have greater broadening. At -40 dB the SC broadening in our proposed designs is 0.90 µm - 2.3 µm for #C, 0.79 µm - 2.4 µm for #EX and 0.88 µm - 2.46 µm for #EY respectively.

In conclusion, utilizing a lower peak power in SCG leads to the production of spectra that are more stable and of high quality, while also enhancing safety for sensitive samples as it mitigates the risk of damage that can occur from excessive energy exposure.

Table 6.1. Comparison with previously recognized results of PCFs

References	**#PCF**	**Pump Wavelength (µm)**	**Peak power (kW)**	**Pulse width (fs)**	**Fiber length**	**SCG bandwidth (µm)**	**Dispersion (ps/nm/km)**	**Nonlinearity ($W^{-1}km^{-1}$)**
[16]	Cs_2	1.55	2.0	500	10cm	1.35-2.11	-114.26	3327
[17]	CCl_4	1.03	62.5	400	20cm	0.85-1.25	-150	22
[18]	$CHCl_3$,#F_1	1.03	0.83	400	10cm	0.6-1.26	-7	1290
[18]	$CHCl_3$,#F_2	1.03	4.16	400	10cm	0.6-1.40	-7.6	440
[19]	$C_6H_5NO_2$,#F_1	1.03	0.83	120	5cm	1.8 – 2.8	33.7	-
[19]	$C_6H_5NO_2$,#F_2	1.56	5.55	90	5cm	0.8 – 2.1	-2.2	-

[19]	$C_6H_5NO_2$, $\#F_3$	1.56	0.66	90	5cm	1.3-2.3	-	-
[20]	$C_6H_5NO_2$	1.81	1	50	5cm	1.3-2.8	-	-
[20]	$C_6H_5NO_2$	1.55	1	50	5cm	1.3-2.8	-	-
Proposed work	$C_6H_5NO_2$, #C	1.55	0.65	50	10mm	1.3-2.0	30.211	1962
Proposed work	$C_6H_5NO_2$, #EX	1.55	0.65	50	10mm	0.9-2.3	-10.852	1780.9
Proposed work	$C_6H_5NO_2$, #EY	1.55	0.65	50	10mm	1.0-2.4	-8.356	1761.5

6.4 Conclusion

In conclusion, the designs we have proposed exhibit a remarkable ability to achieve both a broader and comparable bandwidth for SCG while operating at a lower pump power of just 0.65 kW. This achievement not only enhances the efficiency of the SCG process but also signifies a significant advancement in the field. Moreover, we have successfully navigated the inherent challenge of balancing the need for spectral broadening with the critical requirement of maintaining coherence. This careful management ensures that the quality and stability of the generated SC light are preserved, paving the way for more effective applications in various fields.

This work is primarily focused on a comparative analysis of #C, #EX, and #EY configurations for generating supercontinuum in the near- to mid-infrared range. Results show that an elliptical design produces a broader SC spectrum compared to a circular design, given the same fiber length, pump power, and pulse width. Specifically, a coherent SC spectrum spanning 1.3 µm to 2.0 µm for #C, 0.9 µm to 2.3 µm for #EX and 1.0 µm to 2.4 µm for #EY is achieved with a 10 mm fiber length, 650 W peak power and 50 femtosecond pulse width. Both designs demonstrate low confinement loss at the pump wavelength. Leveraging PCF-based broadband SC light source that covers NIR to MIR spectrum has significant applications in various fields. In practical terms, these technologies facilitate the development of a stable optical frequency comb, which is crucial for high-precision optical coherence tomography (OCT) and spectroscopy. Additionally, they contribute to advancements in biomedical diagnostics, food quality assessment, security, and sensing technologies.

REFERENCES

[1] E R Martins, D H Spadoti, M A Romero and B H V Borges, "Theoretical analysis of supercontinuum generation in a highly birefringent D-shaped microstructured optical fiber", Optics Express, 15(22), 14335-14347(2007).

[2] C Wang, K Lin, S Cao, G Feng, J Wang, A N Abdalla, "Polarized supercontinuum generation in CS_2-core all-normal dispersion photonic crystal fiber", IEEE Photonics Journal, 14(6), 3061607-3061613 (2022).

[3] Ortigosa-Blanch, J C Knight, W J Wadsworth, J Arriaga, B J Mangan, T A Birks and P S J Russell, "Highly birefringent photonic crystal fibers", Optics letters, 25(18),1325-1327 (2000).

[4] M J Steel and R M Osgood Jr, "Elliptical-hole photonic crystal fibers", Optics Letters, 26(4), 229-231 (2001).

[5] J M Dudley, G Genty and S Coen, "Supercontinuum generation in photonic crystal fiber", Reviews of modern physics, 78(4), 1135-1184 (2006). https://doi.org/10.1103/RevModPhys.78.1135

[6] D Garg and A Kumar, "Highly coherent on-chip mid-infrared supercontinuum generation from 1.5 to 25 μm in CdTe-based Rib waveguide", Optical Quantum Electronics, 57, 96 (2025). https://doi.org/10.1007/s11082-024-08007-w

[7] L Chu Van, B T Le Tran, T Nguyen Thi et al, "Comparison of supercontinuum generation spectral intensity in benzene-core PCFs with different types of lattices in the claddings", Optical Quantum Electronics, 54, 840 (2022). https://doi.org/10.1007/s11082-022-04218-1

[8] C V Lanh and L T B Tran , "Low peak power broadband supercontinuum spectra generated in a square lattice toluene-core photonic crystal fiber with different air hole diameters", Laser Physics, 33, 095102 (2023).

[9] C V Lanh, N T Thuy, H T Duc, L T B Tran, V T M Ngoc, D V Trong, L C Trung, H D Quang and D Q Khoa, "Comparison of supercontinuum spectrum generating by hollow core PCFs filled with nitrobenzene with different lattice types", Optical Quantum Electronics, 54, 300 (2022).

[10] N T Thuy, H T Duc, L T B Tran, D V Trong and C V Lanh, "Optimization of optical properties of toluene-core photonic crystal fibers with circle lattice for supercontinuum generation", Journal of Optics, 51, 678 (2022).

[11] C V Lanh, A Anuszkiewicz, A Ramaniuk, R Kasztelanic, D X Khoa, M Trippenbach and R Buczyński, "Supercontinuum generation in photonic crystal fibers with core filled with toluene", Journal of Optics, 19, 125604 (2017).

[12] C V Lanh, H V Thuy, C L Van, K Borzycki, D X Khoa, T Q Vu, M Trippenbach, R Buczyński and R Pniewski, "Optimization of optical properties of photonic crystal fibers infiltrated with chloroform for supercontinuum generation", Laser Physics, 29, 075107(2019).

[13] L V Hieu, H V Thuy, H T Nguyen, C L Van, R Buczyński and R Kasztelanic, "Supercontinuum generation in photonic crystal fibers infiltrated with tetrachloroethylene", Optical and Quantum Electronics, 53, 187 (2021).

[14] G P Agrawal, "Nonlinear fiber optics", In Nonlinear Science at the Dawn of the 21st Century, Springer, Berlin Heidelberg, 195-211 (2000). https://doi.org/10.1016/B978-0-12-817040-3.00007-9

[15] P Chauhan, A Kumar and Y Kalra, "Numerical exploration of coherent supercontinuum generation in multicomponent $GeSe_2$-As_2Se_3-PbSe chalcogenide based photonic crystal fiber", Optical Fiber Technology, 54, 102100 (2020). https://doi.org/10.1016/j.yofte.2019.102100

[16] Z Guo, J Yuan, C Yu, X Sang, K Wang, B Yan, L Li, S Kang and X Kang, "Highly coherent supercontinuum generation in the normal dispersion liquid-core photonic crystal fiber", Progress In Electromagnetics Research M, 48, 67-76 (2016).

[17] V T Hoang, R Kasztelanic, A Filipkowski, G Stępniewski, D Pysz, M Klimczak, S Ertman, V C Long, T R Woliński, M Trippenbach and K D Xuan, "Supercontinuum generation in an all-normal dispersion large core photonic crystal fiber infiltrated with carbon tetrachloride", Optical Materials Express, 9(5), 2264-2278 (2019).

[18] C Van Lanh, K Borzycki, K D Xuan, V T Quoc, M Trippenbach, R Buczyński and J Pniewski, "Optimization of optical properties of photonic crystal fibers infiltrated with chloroform for supercontinuum generation", Laser Physics, 29(7), 075107 (2019).

[19] L C Van, K Borzycki, K D Xuan, V T Quoc, M Trippenbach, R Buczyński and J Pniewski, "Supercontinuum generation in photonic crystal fibers infiltrated with nitrobenzene", Laser Physics, 30(3), 035105 (2020). https://doi.org/10.1007/s12648-023-02830-9

[20] J Wen, B Liang, W Qin, W Sun, C He and K Xiong, "High coherent supercontinuum generation in nitrobenzene liquid-core photonic crystal fiber with elliptical air-hole inner ring", Optical and Quantum Electronics, 54(12), 817 (2022).

[21] J Wen, B Liang, W Sun, C He, K Xiong, H Yu, H Zhang, Z Wu and Q Wang, "Coherence analysis of supercontinuum generation in nitrobenzene liquid-core photonic crystal fiber based on adaptive step-size methods", Optical and Quantum Electronics, 56(4), 619 (2024).

[22] R Zhang, J Teipel and H Giessen, "Theoretical design of a liquid-core photonic crystal fiber for supercontinuum generation", Opt. Express 14, 6800–12(2006).

CHAPTER 7: A COMPARATIVE STUDY OF PHOTONIC CRYSTAL FIBERS FILLED WITH ORGANIC LIQUIDS FOR LOW PEAK POWER SUPERCONTINUUM GENERATION *

7.1 Introduction

The work in this chapter centers on attaining significant spectral broadening while maintaining low peak power. It offers several key advantages as the SCG process becomes more efficient, leading to enhanced precision in measurements and imaging. A major benefit of this approach is the reduction of noise, which significantly improves the overall quality and accuracy of the results. Additionally, operating at low peak power can be advantageous in scenarios where sustained energy delivery or extended temporal interaction with the target material is critical. This characteristic is particularly beneficial in applications such as precision material processing and biomedical imaging, where prolonged exposure enhances the interaction efficiency and minimizes the risk of damage associated with high-intensity pulses. SCG is a complex process in which interactions among various nonlinear effects within an optical fiber produce new frequency components, transforming a narrow input spectrum into a significantly broader and continuous one.

The performance of SCG depends on the pump wavelength, fiber nonlinearity, input pulse energy, fiber length and pulse duration [1]. It is affected by attenuation, effective mode area, and dispersion characteristics of a PCF. Preferably, a flat curve and near zero dispersion value with minimum attenuation constant and effective mode area is required. These parameters can be controlled by changing geometrical parameters of the PCF.

The effectiveness of the SC is measured by three main indicators: bandwidth, coherence, and flatness [2,3]. A variety of approaches have been developed for SC generation, with particular emphasis on leveraging high optical nonlinearities and low dispersion profiles, both of which are critical to facilitating efficient spectral broadening [4]

A general approach for this is to utilize PCFs made of silica or highly nonlinear soft glasses. Silica can be used for visible to NIR region but not for MIR due to limited transparency up to 2.5 μm.

*__D.S. Tomer__ and A. Kumar, *"A comparative study of photonic crystal fibers filled with organic liquids for low peak power supercontinuum generation", Journal of Nonlinear Optical Physics and Materials. https://doi.org/10.1142/S021886352550050X*

Another approach which can be used is to use tellurite, bismuth-gallate or chalcogenide glasses but they also have compatibility issues with silica for fusion splicing [5]. Such glasses possess few more limitations like difficulty in fabrication of complex fiber structure that may require high thermal power which can lead to crystallization, requirement of complex pump systems and limitation in power handling. These glasses may be mechanical weak and may have restricted spectral SCG broadening due to steep normal dispersion profile [6].

To address these limitations, liquid-infiltrated PCFs have been developed, incorporating materials with high nonlinear refractive indices such as carbon disulfide (CS_2), which has a nonlinear refractive index of $n_2 = 2.2 \times 10^{-18}$ m²/W at 1032 nm [7] significantly higher than that of silica. Recent studies highlight the potential of such structures. For instance, using a CS_2-filled liquid-core optical fiber, Chemnitz et al. experimentally verified the existence of hybrid soliton dynamics, representing a new type of solitary wave behavior [8]. In another study, Pniewski et al. numerically showed that toluene-filled PCFs can produce a broadband spectrum exceeding 1000 nm [9]. Van et al. numerically investigated broadband spectral generation of approximately 700 nm within the infrared range using toluene-filled hollow-core PCFs designed for all-normal dispersion [10]. However, CS_2 and toluene pose significant toxicity risks. Other organic solvents like chloroform ($CHCl_3$), nitrobenzene ($C_6H_5NO_2$), tetrachloroethylene (C_2Cl_4), carbon tetrachloride (CCl_4), ethanol (C_2H_5OH) and benzene (C_6H_6) etc. are utilized due to their reduced toxicity [11].

Vieweg et al. reported the experimental realization of solitonic SC generation with a spectral bandwidth exceeding 600 nm, achieved through the infiltration of photonic crystal fibers with carbon tetrachloride (CCl_4) [12]. A variety of infiltration methodologies have been employed, tailored to specific application needs, including photo-polymerization techniques [12], thermally induced fiber collapse [13], fusion splicing or UV-curable adhesive bonding [14], and precision micro channel milling [15].

Among various structures, the helical structure offers a range of advantages over traditional square or circular PCF structures, primarily due to its distinctive geometry. First, the helical shape enhances light confinement within the core, allowing for more efficient guidance and reducing the chances of energy leakage, especially over long distances. This improvement in confinement can lead to lower losses and higher transmission efficiency. Also it provides superior control over dispersion properties of the fiber. This enables better phase matching over a broader range of wavelengths, which is essential for applications like supercontinuum generation.

In our reported work, we have done a comparative study of the impact of infiltration of a single organic liquid as nitrobenzene on SC spectra and in other design along with nitrobenzene another

nonlinear organic liquid ethanol is used. Using liquids in the air holes has proven to be advantageous as it enables tunable properties and high nonlinearity. The increment in nonlinear properties contribute towards achieving a broad spectral bandwidth of SC spectrum. This spectrum requires low input pump power and offers low attenuation.

NIR to MIR coherent SC spectrum is observed for a helical graded design with silica (#A) at a very low input peak power. In other designs #B, #C & #D infiltrated with nonlinear organic liquids broader SC spectra are observed. From the perspective of practical implication low input power is crucial. In case of liquid infiltration in PCFs, they are unstable at high temperatures and high power. They can be easily vaporized if high power is used. The generated supercontinuum source is versatile and suitable for a broad spectrum of applications, including food quality monitoring, biomedical diagnostics, chemical detection and analysis, frequency comb generation, explosive detection, and advanced optical imaging techniques such as OCT. A broad supercontinuum spectrum is achieved with low input peak power, outperforming recently reported results summarized in Table 7.1.

This chapter is structured into four main sections, each addressing a key component of the study. Section one serves as an introduction, providing a brief yet comprehensive overview of the research objectives and the scope of the study. Section two focuses on the design of PCF, outlining the theoretical framework and the design principles employed. Section three presents the results obtained from the study, offering an in-depth discussion of their significance and potential implications for the field. Finally, section four concludes the paper, summarizing the key findings and suggesting directions for future research, followed by a comprehensive list of references.

7.2 Structural parameters of the proposed fiber

Minimizing loss and achieving a small effective mode area are critical for assessing the efficiency of a nonlinear medium in SCG. Equally important are the dispersion characteristics, both of which are predominantly influenced by the fiber's geometry. In addition to geometric optimization, the material used in fabricating PCF should possess a high nonlinear refractive index (n_2) to enhance nonlinear interactions. The structural view of proposed PCF is shown in Figure 7.1. The design shown in Fig.7.1 (a) is termed as (#A). The diameter of first ring is given as d_1 = 2.0 µm, second ring as d_2 =1.7 µm, third ring as d_3 = 1.4 µm and fourth ring as d_4 =1.1 µm.

Grading is presumed for effective detention of light within the core [16]. The geometry consists of eight helical patterns and each of which comprises four air holes. The layers of the suggested helical shape with graded – index (GI) are arranged as $d_1 > d_2 > d_3 > d_4$ where diameter of first, second, third and fourth ring are d_1, d_2, d_3 & d_4 respectively. The amount of grading has been considered as (δD) =

d_1- d_2 = d_2 - d_3 = d_3 – d_4 between two consecutive rings. The amount of grading, δD is 0.30 µm. The distance between the two successive air holes is pitch (Λ), taken as 2.8 µm. The design shown in Fig. 7.1(b) is termed as (#B) which is infused with liquid nitrobenzene in the core.

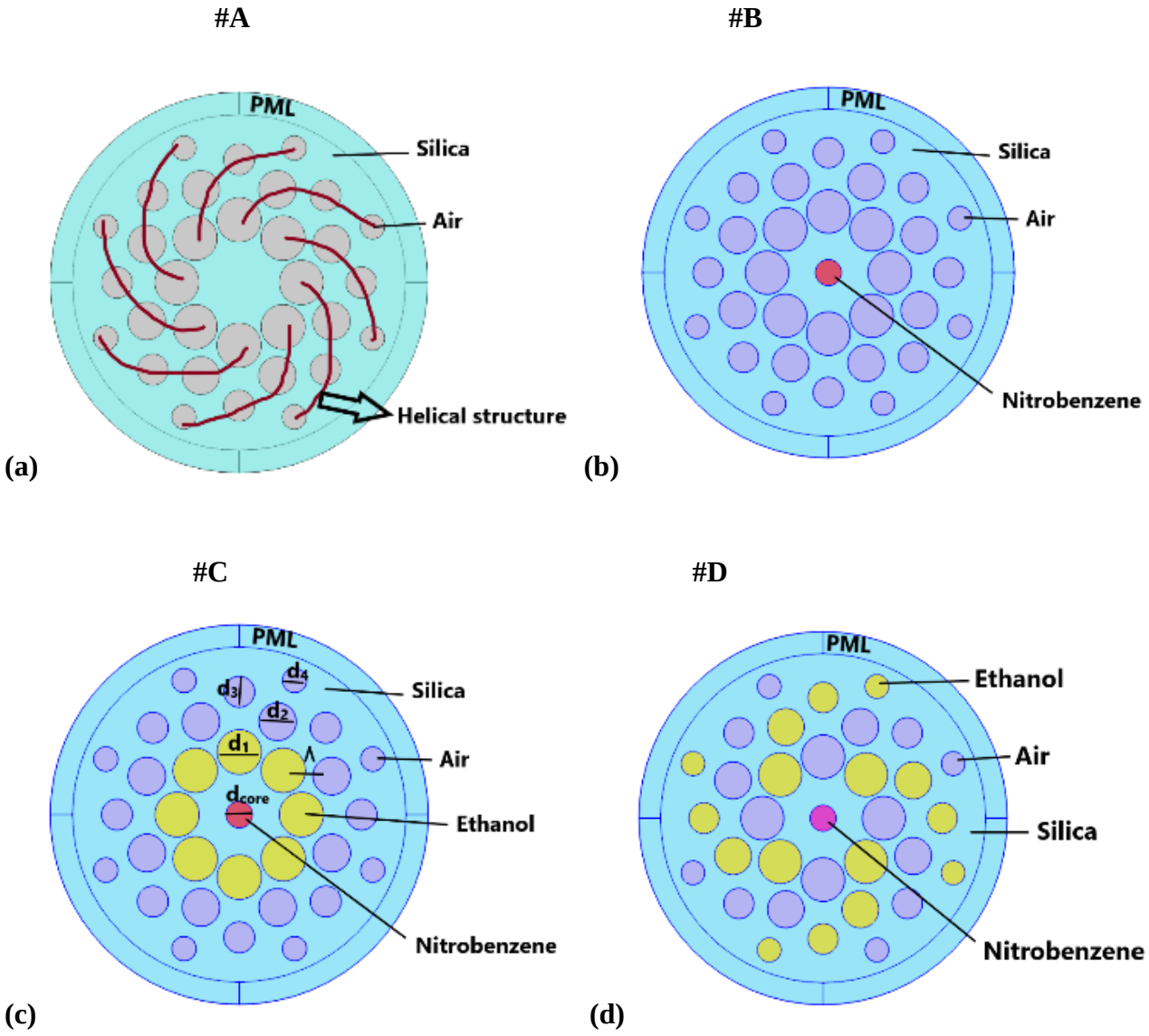

Figure 7.1. (a) Cross-sectional view of the suggested PCF (#A), **(b)** PCF (#B), **(c)** PCF (#C) and **(d)** PCF (#D).

The core diameter (d_{core}) is 1.4 µm. Rest of the design parameters are kept same. In Fig. 7.1(c) & 7.1(d) along with infusion of nitrobenzene in the core, ethanol has been infiltrated in the first ring around the core. In Fig. 7.1(d) ethanol has been infiltrated alternatively in the helical structure. The designs shown in Figs.7.1(c) & 7.1(d) are termed as (#C) & (#D) respectively.

To ensure reflection-free boundaries, PML is incorporated around the cladding perimeter of the cylindrical model. Thickness of PML is 1.0 µm. Figures 7.2(a), 7.2(b), 7.2(c) & 7.2(d) shows the electric field distribution of the principal mode at pump wavelength for design (#A), (#B), (#C) & (#D) respectively.

All the four designs are being studied for comparative study. Figure 7.3 shows refractive index profile for the materials used.

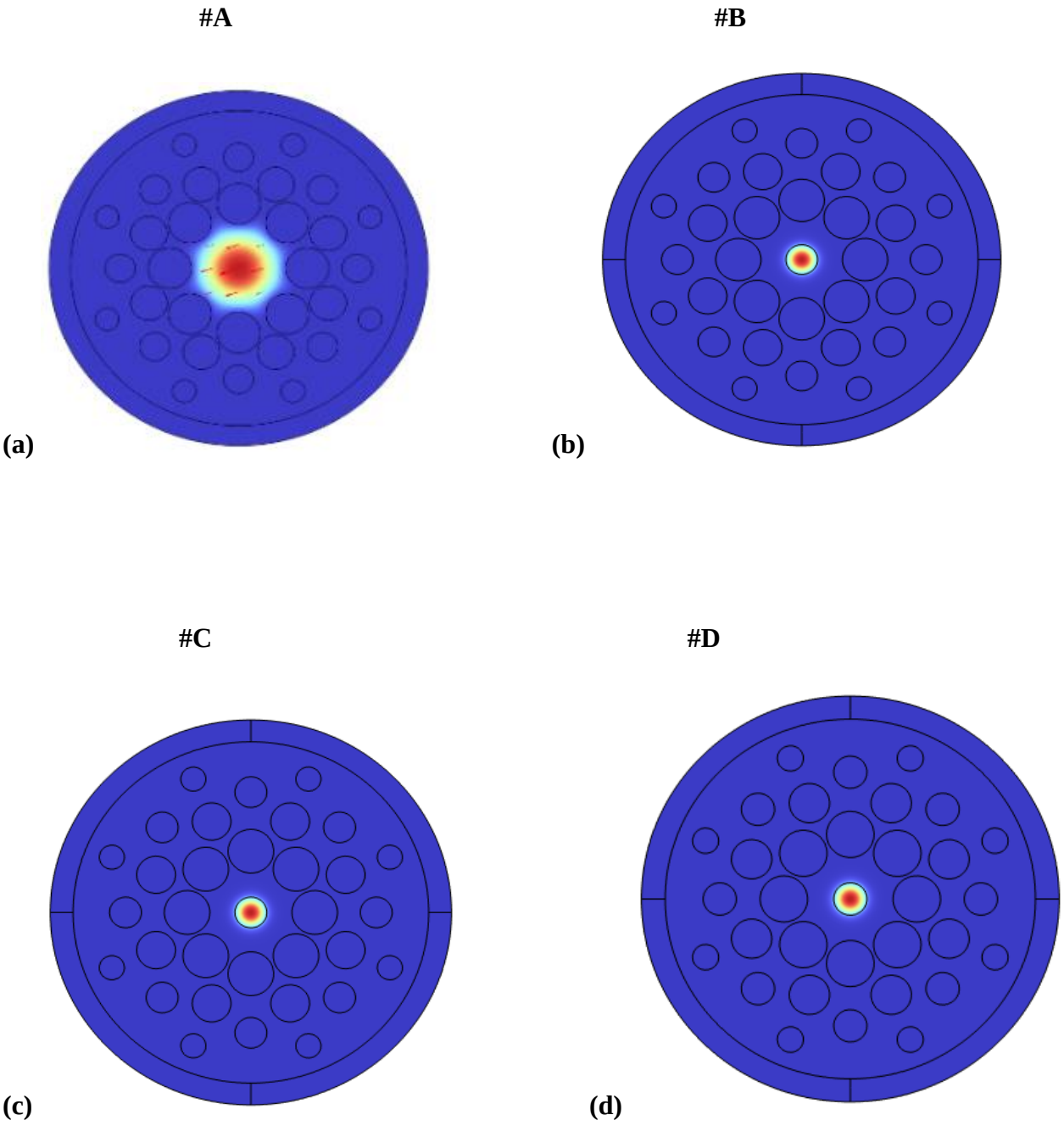

Figure 7.2. (a) Cross-sectional the electric field distribution for the principal mode at 1.55 μm for suggested PCF (#A), **(b)** PCF (#B), **(c)** PCF (#C) and **(d)** PCF (#D).

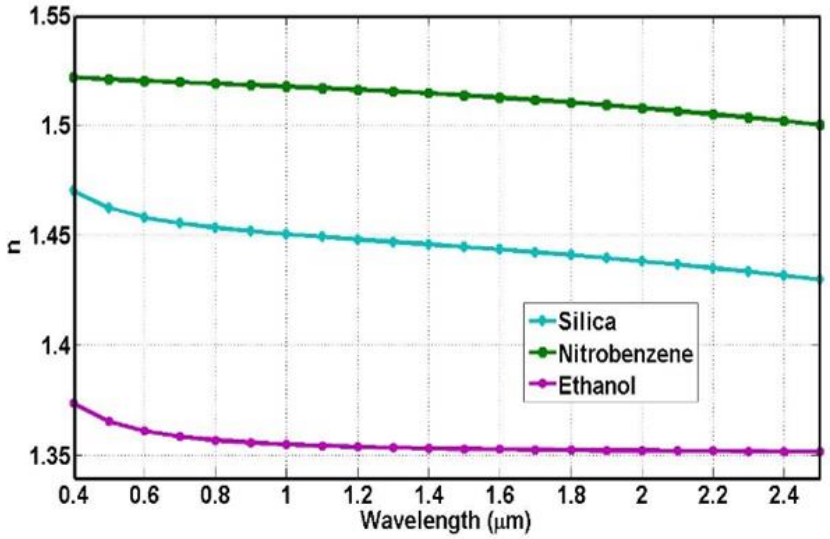

Figure 7.3. Refractive index (n) profile of silica, nitrobenzene and ethanol.

7.3 Results and discussion

In a PCF structure the extent and characteristics of SC spectral broadening are largely determined by two fundamental parameters: the nonlinear refractive index of the material and the dispersion characteristics of the fiber [3]. In Fig.7.4(a), the dispersion characteristics of #A, #B, #C & #D has been shown with δD = 0.30 μm, Λ= 2.8 μm and d_{core} = 1.4 μm . It has been observed that design #A with air holes embedded in silica has large negative dispersion at lower values of wavelength and at higher values of wavelength it is having large positive dispersion. It has one ZDW around 1 μm. Design #B which has a core infiltrated with nitrobenzene has both normal and anomalous dispersion profile with one ZDW around 1.3 μm. Design #C with core of nitrobenzene and one ring around core filled with ethanol has no ZDW. It has all normal dispersion profile. Design #D with alternative spiral arms filled with ethanol and core filled with nitrobenzene has both normal and anomalous dispersion profile. At higher wavelengths, this profile is comparatively more flat than that of design #B and it has lesser value of dispersion as well. It has one ZDW around 1.5 μm.

For optimization of structural parameters, in Fig. 7.4(b) for the designs #A, #B, #C & #D pitch has been varied as Λ= 2.8 μm, Λ= 3.0 μm & Λ= 3.2 μm. It has been observed that Λ= 2.8 μm results in minimum value of dispersion at lower wavelength region for designs #A, #B, #D. For design #C, with Λ= 2.8 μm it has minimum dispersion at lower as well as higher wavelength regions. So, Λ= 2.8 μm has been selected for #A, #B, #C & #D.

Similarly, in Fig. 7.5(a) another parameter d_{core} is optimized for #B, #C & #D having core filled with nitrobenzene. The value of core diameter has been varied as 1.0 μm, 1.2 μm & 1.4 μm. For all three designs d_{core} = 1.4 μm has minimum value of dispersion at shorter as well as longer wavelengths.

Hence, d_{core} = 1.4 μm has been opted. Again for grading optimization, δD has been varied as 0.00 μm, 0.30 μm & 0.50 μm in Fig 7.5(b). For designs #A & #B there is no significant variation in the dispersion characteristics. In #C & #D at lower wavelengths there is no significant difference in the profiles but at higher wavelengths, δD = 0.30 μm is showing less steeper and more flat profile. So, δD = 0.30 μm has been picked up for consideration.

The designs #A, #B, #C & #D with Λ= 2.8 μm, d_{core} = 1.4 μm and δD = 0.30 μm has been selected as optimized structural parameters for carrying out further analysis. On comparing the dispersion values for #A, #B, #C & #D for optimized parameters of #A (Λ= 2.8 μm, δD = 0.30 μm) and #B, #C & #D (d_{core} = 1.4 μm, Λ= 2.8 μm, δD = 0.30 μm) at pump wavelength they were found to be + 52.25 ps/nm-km, +20.81 ps/nm-km , -20.84 ps/nm-km and + 3.74 ps/nm-km respectively.

Figure 7.6(a) shows the variation of effective mode area and nonlinearity (γ) for #A and Fig. 7.6(b) shows the variation for #B, #C & #D. EMA & γ when both plotted with wavelength possesses inverse relation with each other. The value of A_{eff} at 1.55μm is around 6.57 μm^2 for #A, 1.45 μm^2 for #B, #C & #D. Similarly, the nonlinear coefficient for #A, #B, #C & #D are 1234.18 $W^{-1}Km^{-1}$, 5596.22 $W^{-1}Km^{-1}$, 5569.71 $W^{-1}Km^{-1}$ and 5584.28 $W^{-1}Km^{-1}$ respectively.

The confinement loss has been shown in Fig. 7.7. Minimal loss is observed up to 2.5 μm but beyond this value it increases significantly. The value of loss for design #B is minimum whereas for #D it increases quite rapidly and other designs #A & #C loss is coming in between. It can be seen that all the designs show low confinement loss at 1.55 μm which is relatively low in contrast to the material loss of the silica glass [17].

SCG has been thoroughly evaluated for various fiber lengths, pulse widths, and pump power levels, all centered on a wavelength of 1.55 μm. The assessment was conducted using a laser source with a 100 MHz repetition rate and a power level measured at −20 dB. By exploring a range of fiber lengths, the impact of fiber geometry on the spectral broadening and nonlinear processes was investigated. Similarly, different pulse widths were tested to understand how it influence the efficiency and dynamics of supercontinuum generation. The variation in pump power provided insights into how increasing or decreasing power levels affect the generation and stability of the supercontinuum. This comprehensive analysis across multiple parameters helped in understanding the optimal conditions for efficient SCG at the specified wavelength. SCG has been witnessed for various fiber length 4 mm, 8 mm, 12 mm and 16 mm in Figs. 7.8(a), 7.8(b), 7.8(c) & 7.8(d) for #A, #B #C & #D respectively. The pump power used is 600 W with 50 fs pulse width. The spectrum is showing maximum broadening for 4 mm length for #A in Fig. 7.8(a), the phenomenon responsible for this broadening is

SPM whereas for #B, #C & #D the maximum broadening is observed for 8 mm fiber length in Fig. 7.8(a), 7.8(b) & 7.8(c) respectively.

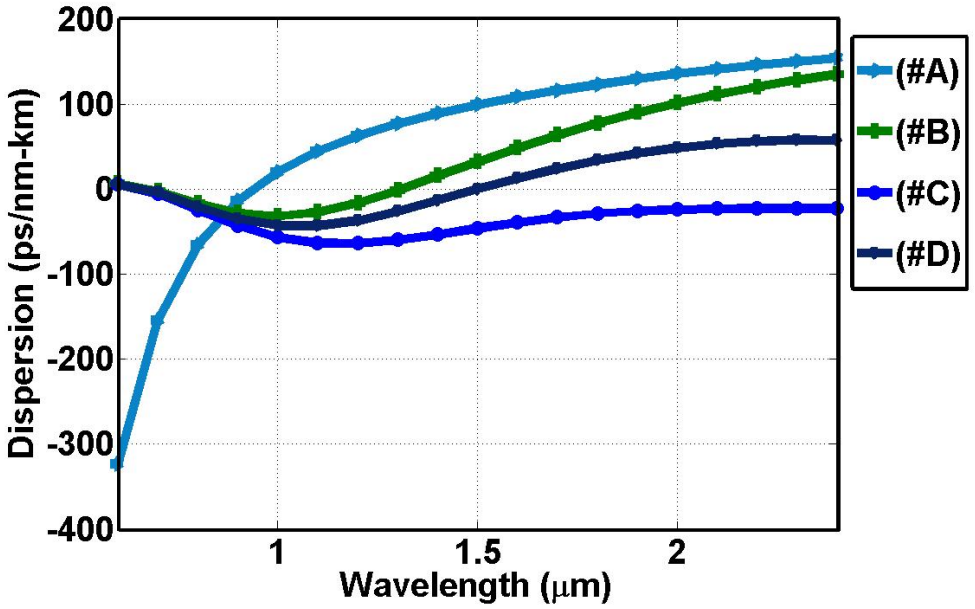

(a)

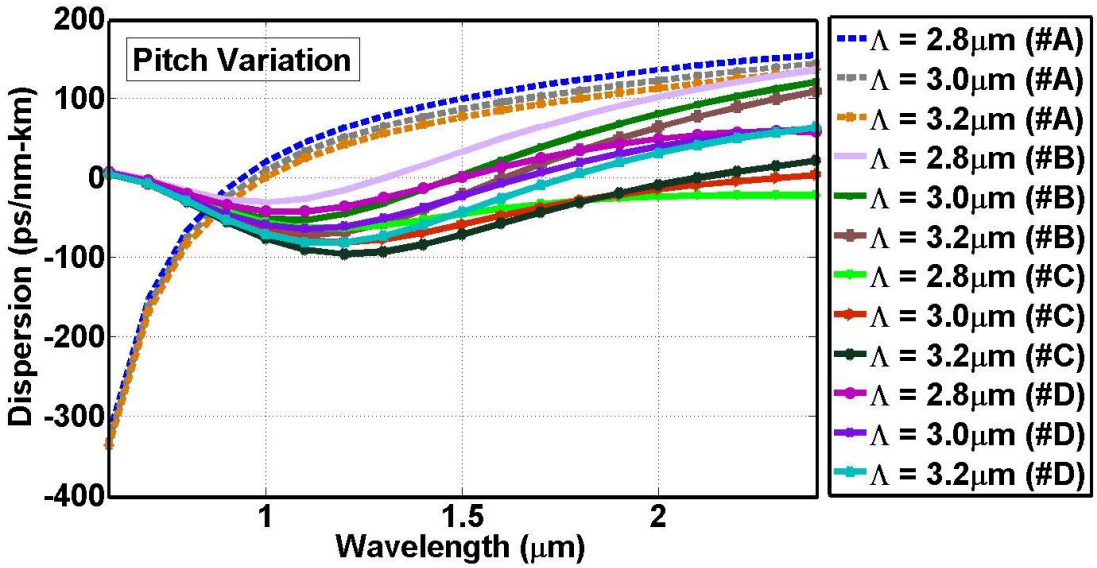

(b)

Figure 7.4. (a) Study of dispersion characteristics of #A, #B, #C & #D with δD = 0.30 μm, Λ = 2.8 μm and d_{core} = 1.4 μm , **(b)** variation of Λ for #A, #B, #C & #D with δD = 0.30 μm and keeping d_{core} = 1.4 μm as constant for #B, #C & #D.

With further increase in length beyond 8 mm the noise is becoming more prominent and spectrum started to get deteriorate. In Figs. 7.9, 7.10 & 7.11 the pump power is incremented from 400 W to 800 W. For design #A, in Fig. 7.9(a) at 400 W peak power broadening is very less. For Fig. 7.10(a) also it is quite narrow at 600 W. The maximum broadening of 1.3 μm – 1.8 μm is observed in Fig.

7.11(a) for 800 W peak power at 4 mm fiber length and 50 fs pulse width.

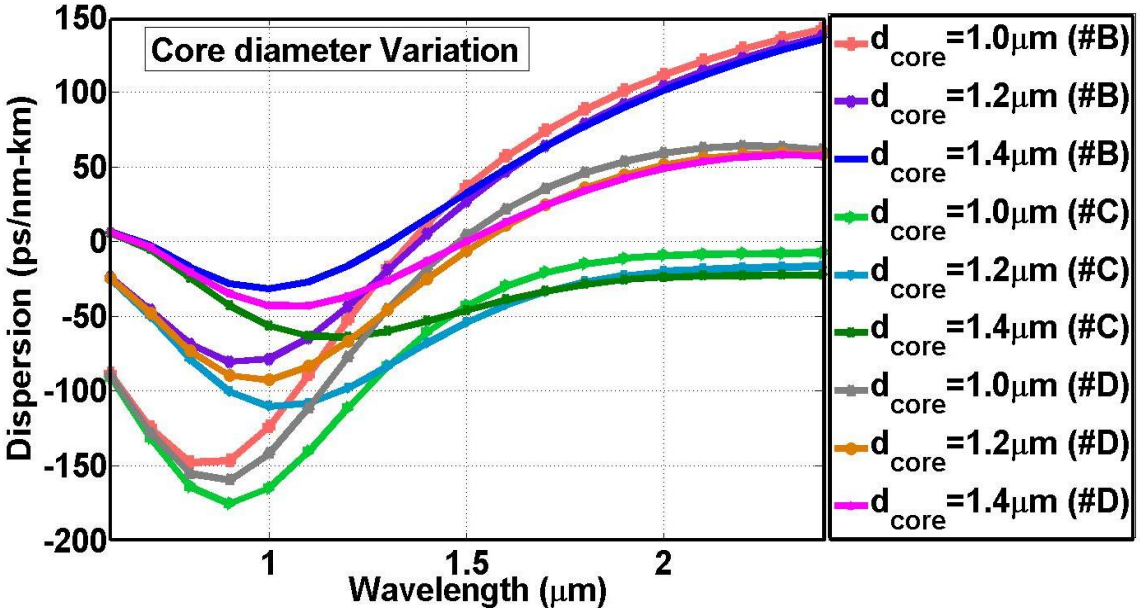

(a)

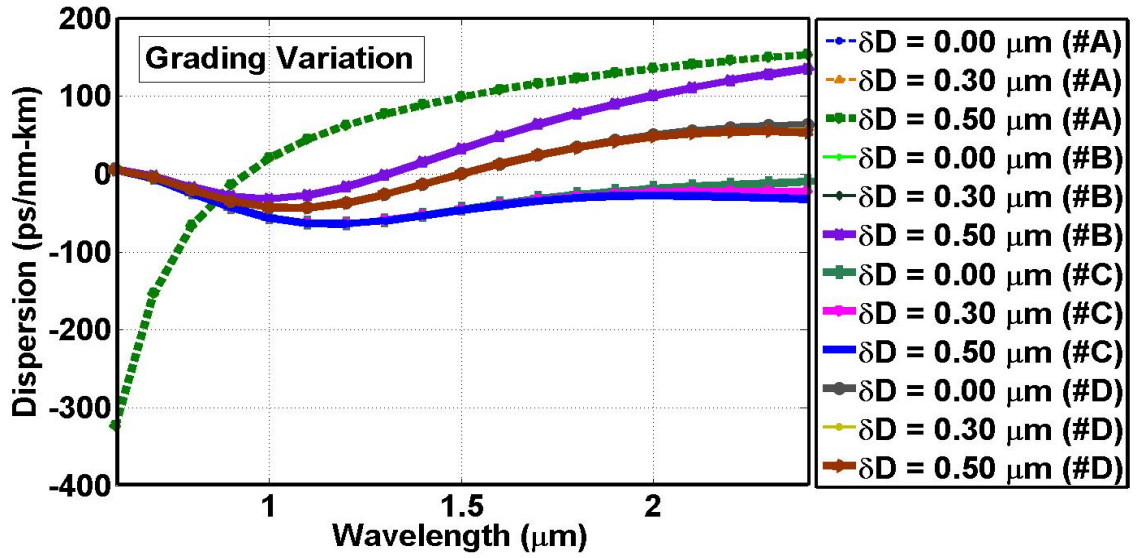

(b)

Figure 7.5. (a) Study of dispersion characteristics of #B, #C & #D with variation of d_{core} and keeping Λ= 2.8μm & δD = 0.30 μm as constant, **(b)** the dispersion characteristics of #A, #B, #C & #D with variation of δD keeping Λ= 2.8 μm for #A, #B, #C & #D and keeping d_{core} = 1.4 μm as constant for #B, #C & #D.

As the input power increases, the generated spectrum broadens significantly, extending towards both shorter (blue-shifted) and longer (red-shifted) wavelength regions. This SC broadening is primarily attributed to the nonlinear SPM effect, which plays a dominant role in inducing spectral expansion by modulating the phase of the pulse in response to intensity variations. For design #B, the broadening is symmetrical due to SPM effect. In Fig. 7.9(b) at 400 W the broadening is very less, on increasing the pump power the broadening is slightly increased in Fig. 7.10(b) at 600 W.

At 800 W in Fig. 11(b) the broadening is maximum around 1.0 µm – 2.4 µm. In Fig. 7.9(c) for design #C the broadening is not symmetrical. It is more at higher wavelengths as compared to lower wavelengths on increasing the power from 400 W to 600 W. In Fig. 7.10 (c) the broadening has increased on longer wavelength side.

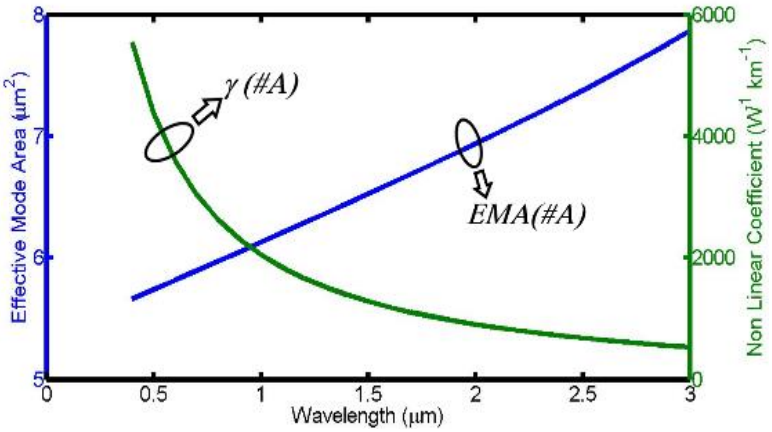

(a)

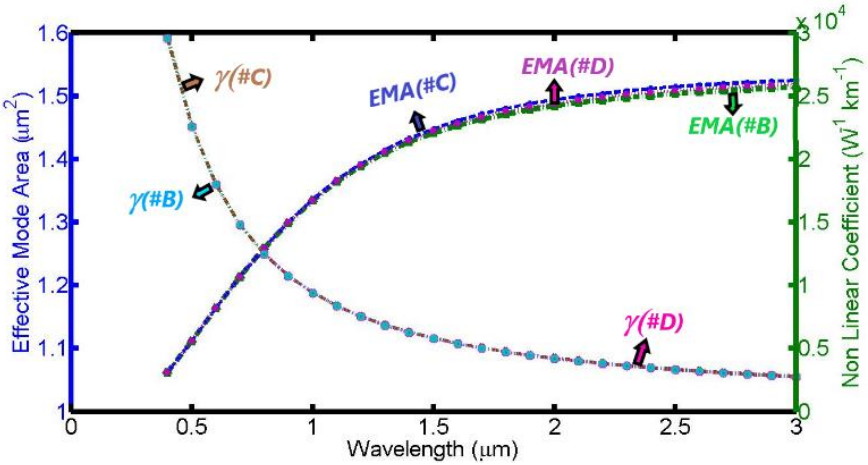

(b)

Figure 7.6. (a) Variation of effective mode area (EMA) and nonlinearity (γ) of #A and **(b)** the variation of EMA and γ of #B, #C & #D with wavelength.

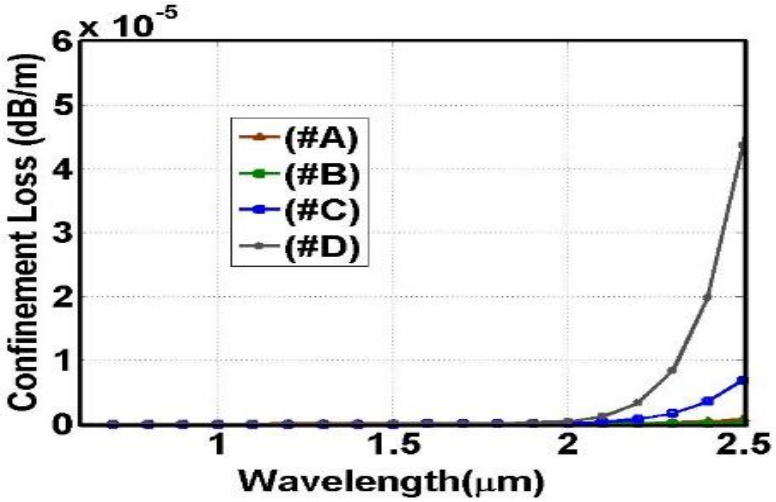

Figure 7.7. The confinement loss of #A, #B, #C & #D with wavelength.

Again, on increasing the pump power to 800W, the maximum broadening is achieved around 1.2 μm – 2.5 μm in Fig. 7.11(c). Beyond 800 W on further increasing the peak power the spectrum has become noisy and the coherence has also started to lower down as noise is aggregating. In Fig. 7.9(d), design #D shows symmetrical broadening along shorter as well as longer wavelength region. On increasing the power to 600 W (in Fig. 7.10(d)) maximum broadening of 0.9 μm – 2.5 μm is obtained. When the power is further increased to 800 W (in Fig. 7.11(d)), the SC began to worsen and coherence has started to decline as well.

Subsequently, influence of enhanced pulse widths on SC has been thoroughly investigated. As illustrated in Figs. 7.12, 7.13 & 7.14, it is apparent that as the T_{FWHM} value increases from 50 fs to 150 fs, notable changes occur in the characteristics of the generated SC spectrum. The subsequent spectra contracted down for #A, #B, #C & #D. So, 50 fs pulse width is optimum to be considered. It is interesting to note that short pulse width gives broad SC spectra. Consequently, the 50 fs pulses display stability in spectrum. The maximum broadening for #A is 1.3 μm – 1.8 μm (observed at 4 mm, 800 W, 50 fs), for #B is 1.0 μm – 2.4 μm (observed at 8 mm, 800 W, 50 fs), for #C is 1.2 μm – 2.5 μm (observed at 8 mm, 800 W, 50 fs), & #D is 0.9 μm – 2.5 μm (observed at 8 mm, 600 W, 50 fs). We have summarized the following observation, among all four designs #D requires minimum peak power and #A requires minimum fiber length for 50 fs laser pulse at 1.55 μm. The value of β_2 for #A is -1.326×10^{-25} s^2/m, ($T_0 = T_{FWHM}/1.763$), the nonlinear length ($L_{NL} = (\gamma P_0)^{-1}$) and dispersion length ($L_D = (\beta_2/T_0^2)^{-1}$) for proposed PCF are 1.01×10^{-3} m and 18.38×10^{-3} m respectively. The soliton order $N \approx \left(\frac{L_D}{L_{NL}}\right) \approx 18$ and the soliton fission length are calculated as $L_{fiss} = \left(\frac{L_D}{N}\right) \approx 1.02$ mm. Similarly, for #B, β_2 is -5.226×10^{-25} s^2/m, $L_{NL} = 2.23\times10^{-4}$ m, $L_D = 4.78\times10^{-3}$ m, $N \approx 22$ and $L_{fiss} = 0.21$ mm. For #C, β_2 is 5.315×10^{-25} s^2/m, $L_{NL} = 2.24\times10^{-4}$ m, $L_D = 4.70\times10^{-3}$ m, $N \approx 21$ and $L_{fiss} = 0.22$ mm. Similarly, for #D, β_2 is -1.106×10^{-25} s^2/m, $L_{NL} = 2.98\times10^{-4}$ m, $L_D = 22.5\times10^{-3}$ m, $N \approx 75$ and $L_{fiss} = 0.30$ mm.

To obtain a broader SCG, it is beneficial to have a nonlinear length less than or equal to dispersion length for the proposed fiber. This observation verifies that nonlinear effects are instrumental in driving the broadening of the input pulse, while also highlighting their role in mitigating premature dispersion-induced spreading before the onset of significant nonlinear interactions. At the initial stage of pulse propagation, the broadening of the spectrum is primarily influenced by SPM, a nonlinear optical effect where the intensity of the pulse induces changes in its phase. This phase alteration causes a broadening of the pulse's spectral content, leading to the generation of new frequencies. As the pulse continues to propagate and shifts toward longer wavelengths, the broadening becomes dominated by a process known as optical wave breaking. This phenomenon

occurs when the nonlinear effects within the medium become strong enough to significantly modify the intensity profile or shape of the pulse. In addition, we have employed one-photon-per-mode noise model to assess SCG coherence [18].

Coherence of the generated spectra was evaluated through calculations performed at a fiber length of 4 mm, pulse width 50fs & 800W peak power in Fig. 7.15(a) for #A. For #B & #C in Figs. 7.15(b) & 7.15 (c) with 8 mm fiber length, 50 fs , 800 W peak power and for #D in Fig. 7.15(d) with 8 mm, 50 fs and 600 W. The spectrum is coherent for the generated SC, extending from 1.3 µm – 1.8 µm for #A, 1.0 µm – 2.4 µm for #B, 1.2 µm – 2.5 µm for #C and 0.9 µm – 2.5 µm for #D respectively.

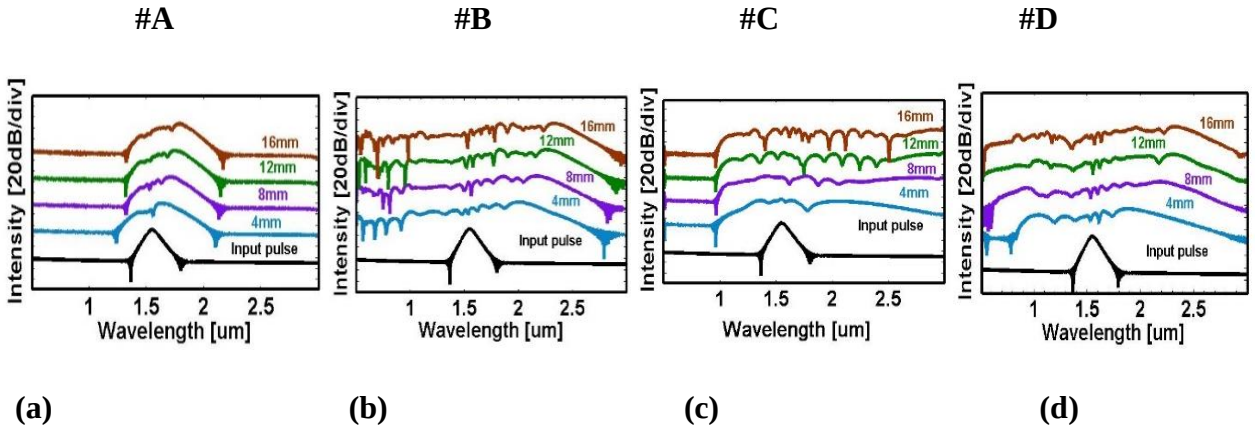

Figure 7.8. The SC spectrum due to changing fiber length as 4 mm, 8 mm, 12 mm, and 16 mm at 1.55 µm under conditions of 50 fs and 600 W for **(a)** #A, **(b)** #B, **(c)** #C & **(d)** #D.

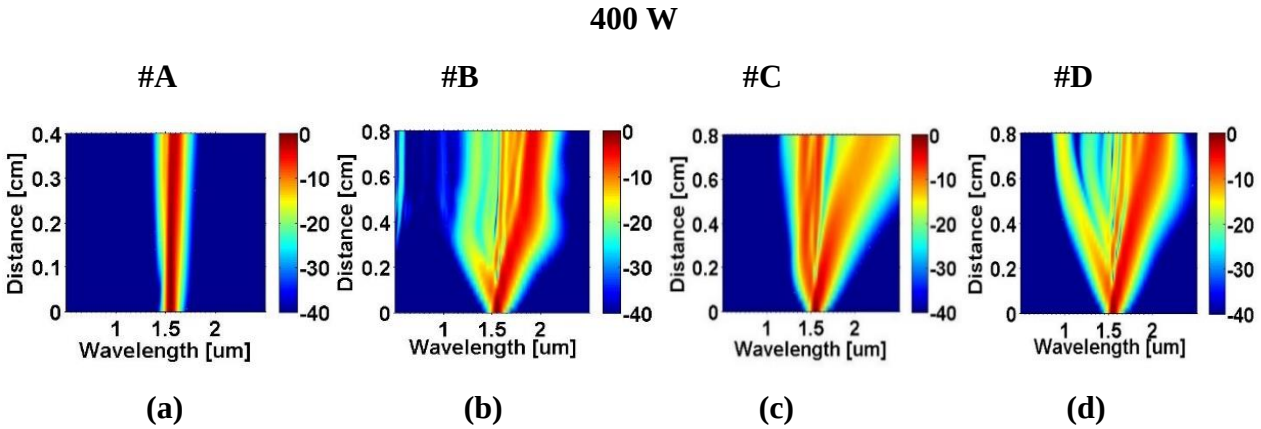

Figure 7.9. The spectral advancement at 1.55 µm using 400 W peak power with 50fs pulse width at a fiber length of **(a)** 4mm for #A and 8mm for **(b)** #B, **(c)** #C and **(d)** #D respectively.

600 W

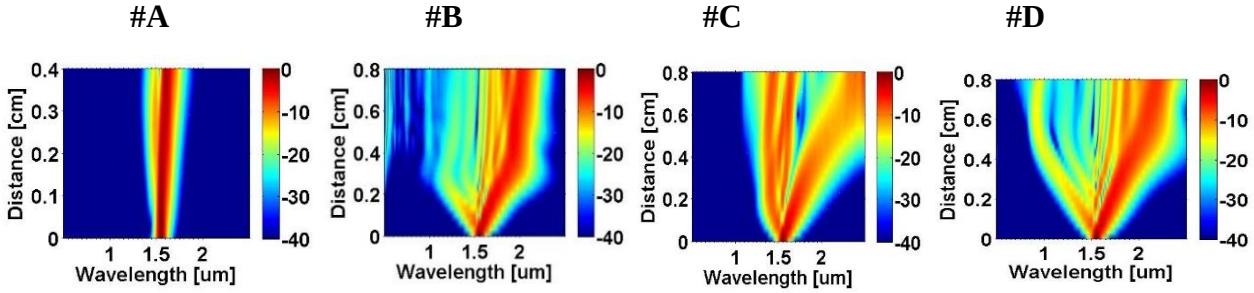

Figure 7.10. The spectral advancement at 1.55 µm using 600 W peak power with 50fs pulse width at a fiber length of **(a)** 4mm for #A and 8mm for **(b)** #B, **(c)** #C and **(d)** #D respectively.

800 W

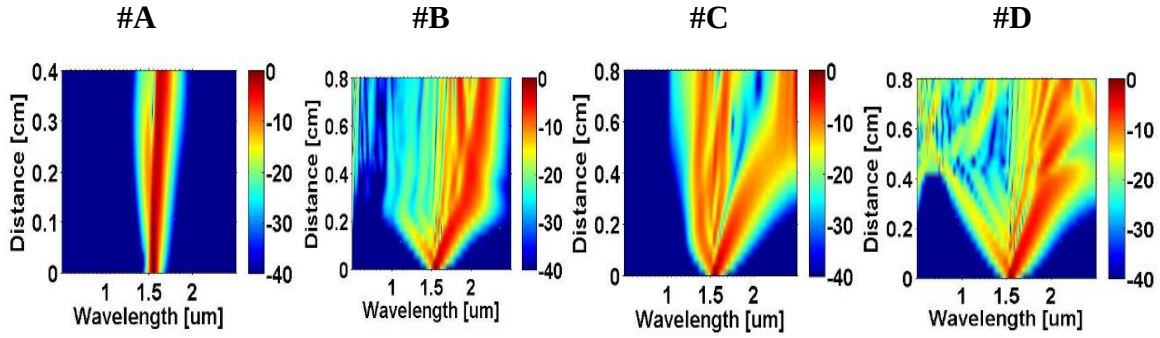

Figure 7.11. The spectral advancement at 1.55 µm using 800 W peak power with 50fs pulse width at a fiber length of **(a)** 4mm for #A and 8mm for **(b**) #B, **(c)** #C and **(d)** #D respectively.

50 fs

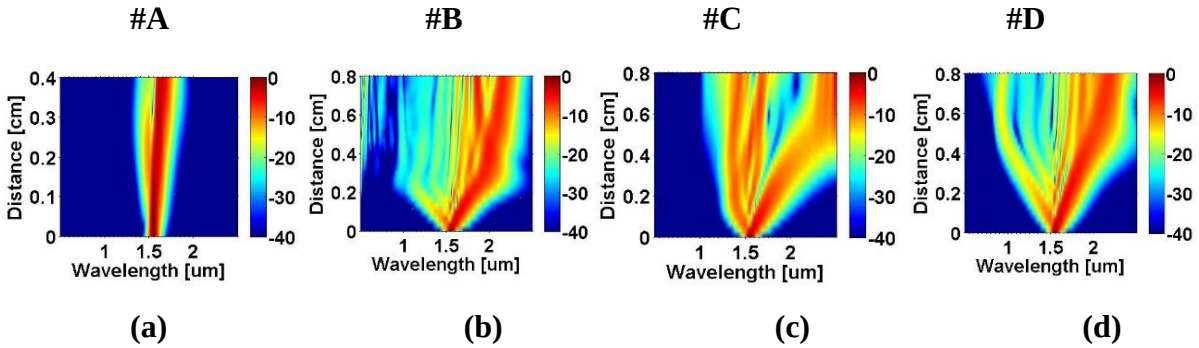

Figure 7.**12**. The spectral advancement at 1.55 µm with 50 fs pulse width of **(a)** #A at 4mm, 800 W, **(b)** #B at 8mm, 800 W, **(c)** #C at 8mm, 800 W and **(d)** #D at 8 mm & 600 W.

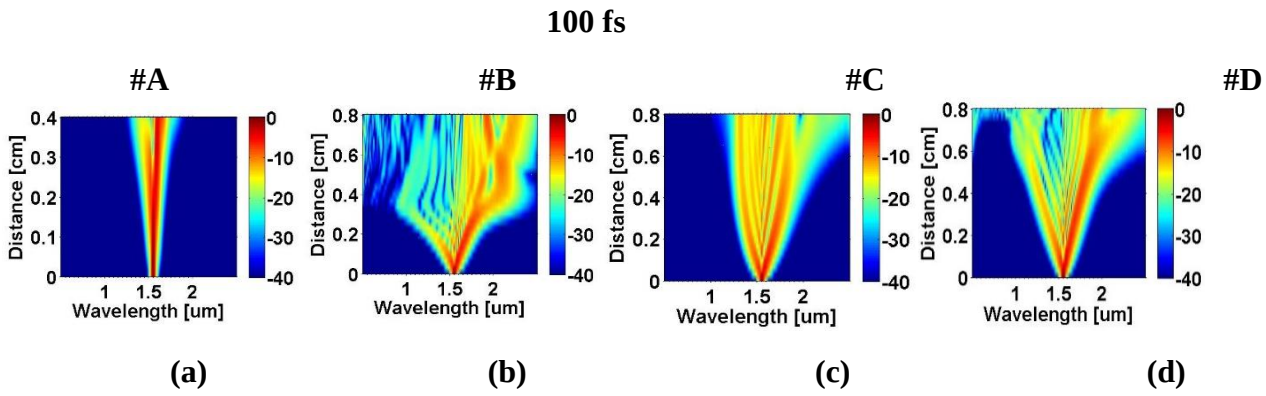

Figure 7.**13.** The spectral advancement at 1.55 µm with 100 fs pulse width of **(a)** #A at 4mm, 800 W, **(b)** #B at 8mm, 800 W, **(c)** #C at 8mm, 800 W and **(d)** #D at 8 mm & 600 W.

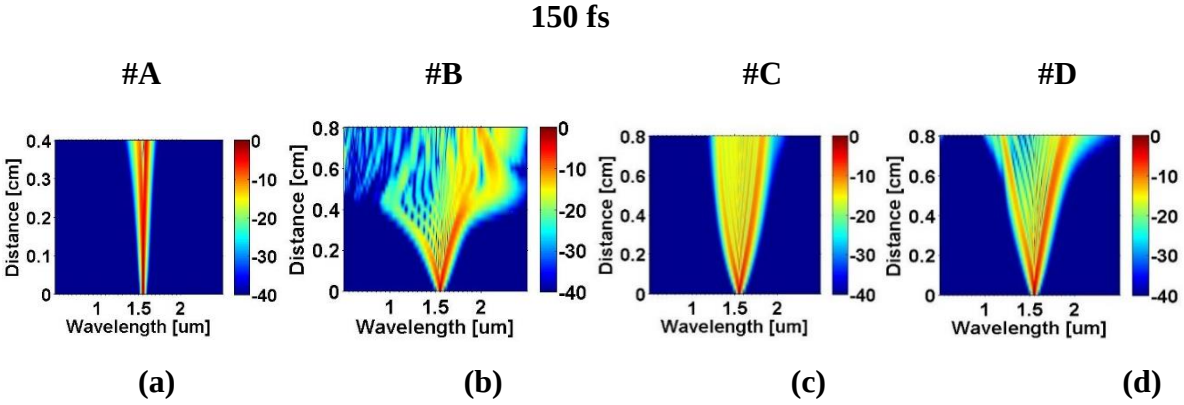

Figure 7.**14.** The spectral advancement at 1.55 µm with 150 fs pulse width of **(a)** #A at 4mm, 800 W, **(b)** #B at 8mm, 800 W, **(c)** #C at 8mm, 800 W and **(d)** #D at 8 mm & 600 W.

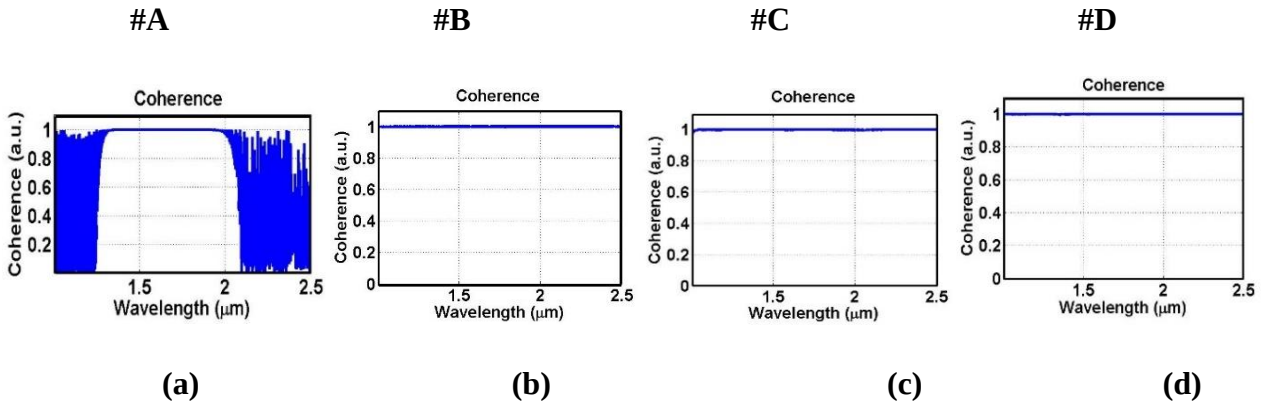

Figure 7.15. The coherence evolution using **(a)** pump power 800 W, 50 fs pulse width, 4 mm fiber length for (#A), **(b)** 800 W, 50 fs, 8 mm for (#B) , **(c)** 800W, 50 fs, 8 mm for (#C) and **(d)** 600W, 50 fs, 8 mm for (#D) at 1.55 µm .

Table 7.1. Table for comparison of numerous parameters among the proposed PCF and the previously published PCFs.

Author & Year	References	# PCF	Pump Wavelength (µm)	Fiber length	Pulse width (fs)	Peak power (kW)	SCG bandwidth (µm)
(Guo et al. 2016)	[19]	Cs_2	1.55	10cm	500	2.0	1.35-2.11
(Hoang et al. 2019)	[20]	CCl_4	1.03	20cm	400	62.5	0.85-1.25
(Van et al. 2019)	[21]	$CHCl_3$,#F_1	1.03	10cm	400	0.83	0.6-1.26
(Van et al. 2019)	[21]	$CHCl_3$,#F_2	1.03	10cm	400	4.16	0.6-1.40
(Van et al. 2020)	[22]	$C_6H_5NO_2$,#F_1	1.03	5cm	120	0.83	1.8 – 2.8
(Van et al. 2020)	[22]	$C_6H_5NO_2$,#F_2	1.56	5cm	90	5.55	0.8 – 2.1
(Van et al. 2020)	[22]	$C_6H_5NO_2$, #F_3	1.56	5cm	90	0.66	1.3-2.3
(Wen et al. 2022)	[23]	$C_6H_5NO_2$	1.81	5cm	50	1	1.3-2.8
(Wen et al. 2024)	[24]	$C_6H_5NO_2$	1.55	5cm	50	1	1.3-2.8
Proposed work	**-**	**Silica , #A**	**1.55**	**4mm**	**50**	**0.80**	**1.3-1.8**
Proposed work	**-**	**$C_6H_5NO_2$, #B**	**1.55**	**8mm**	**50**	**0.80**	**1.0-2.4**
Proposed work	**-**	**$C_6H_5NO_2$ - C_2H_5OH , #C**	**1.55**	**8mm**	**50**	**0.80**	**1.2-2.5**
Proposed work	**-**	**$C_6H_5NO_2$ - C_2H_5OH, #D**	**1.55**	**8mm**	**50**	**0.60**	**0.9-2.5**

On doing the comparative analysis of the proposed designs it has been found that design #A with only silica has minimum broadening, when liquid infiltration was performed it has resulted into broader spectra. For design #B when only one nonlinear organic liquid (nitrobenzene) was used it was able to lower down the dispersion values both in normal and anomalous region. On further infiltration with another nonlinear organic liquid (ethanol) in design #C the dispersion profile became all normal with lesser dispersion value. Also the broadening was further enhanced especially on the longer wavelength region.

Again, in design #D when ethanol was added along the alternative helical arms, the dispersion around pump wavelength was found to be minimum among all the designs and it also requires

minimum pump power for SCG among all the proposed designs (Since the power loss due to dispersion is minimum here). In this case also, the broadening was increased but symmetrically on shorter as well as longer wavelength region.

On comparing Design #A and #D we can observe that nonlinearity has been increased and dispersion has been reduced on adding a nonlinear liquid which is required for producing a coherent SCG. Introducing a nitrobenzene-filled core and ethanol in design (#D) substantially modifies its dispersion and nonlinear behavior due to the high refractive index and large Kerr nonlinearity of nitrobenzene. The increased index contrast enhances modal confinement and alters waveguide dispersion, leading to a shift in the zero-dispersion wavelength and modified phase-matching conditions. Simultaneously, the significantly larger nonlinear refractive index and reduced effective mode area result in a much higher nonlinear coefficient. These combined effects lower the supercontinuum generation threshold, enhance soliton dynamics, and enable broader spectral expansion compared to conventional silica-core PCFs.

Table 7.2. Table for comparison of various parameters among the proposed PCF designs

Design	Dispersion (ps/nm-km)	Nonlinearity ($W^{-1}km^{-1}$)	SCG Bandwidth (µm)
#A	52.25	1234.18	1.3-1.8
#B	20.81	5596.22	1.0-2.4
#C	-20.84	5569.71	1.2-2.5
#D	3.74	5584.28	0.9-2.5

The proposed designs show the capability of achieving a broad bandwidth for SCG using low input pump power and a small fiber length. Few of the previously documented results has been outlined in Table 1. Also at pump wavelength the proposed designs have very low attenuation. It can be seen, the SCG in reference [19] has been evaluated at -40 dB with higher peak power. For this fiber, the broadening is less than #B, #C & #D at -20 dB. Similarly, the designs mentioned in references [20-22] using higher peak power at -20 dB but have lesser broadening range than #B, #C & #D. The designs in references [23,24] operate at relatively high peak power levels and the broadening range has also been evaluated at -60 dB & -40 dB respectively.

7.4 Conclusion

On summarizing, the proposed designs demonstrate the competency to attain a broader bandwidth for SCG using low input peak power and short fiber length. Moreover, the difficulty of harmonizing SC broadening along with preserving coherence has been efficiently resolved. The center of this work

lies on a comparative study of proposed designs demonstrated as #A, #B, #C & #D for generation of NIR to MIR SCG. A coherent SC spectrum for #A spanning from 1.3 µm – 1.8 µm (at 4 mm, 800 W & 50 fs), for #B extending from 1.0 µm - 2.4 µm (at 8 mm, 800 W & 50 fs), for #C from 1.2 µm - 2.5 µm (at 8 mm, 800 W & 50 fs) and for #D extending from 0.90 µm - 2.5 µm (at 8 mm, 600 W & 50 fs) has been achieved. A broadband coherent SC source based on PCFs, extending from the NIR to MIR, offers notable advantages for advanced imaging, including improved resolution, enhanced contrast, and broader spectral accessibility.

Additionally, this technology supports the realization of stable optical frequency combs, which are fundamental for precision OCT and spectroscopic analysis. Furthermore, it plays a key role in biomedical detection, checking food quality, security applications, and sensing technologies.

REFERENCES

[1] P Jamatia, T S Saini, A Kumar and R K Sinha, "Design and analysis of a highly nonlinear composite photonic crystal fiber for supercontinuum generation: visible to mid-infrared", Applied Optics, 55(22), 6775-6781 (2016)

[2] T Sylvestre, E Genier, A N Ghosh, P Bowen, G Genty, J Troles, A Mussot, A C Peacock, M Klimczak, A M Heidt, and J C Travers, "Recent advances in supercontinuum generation in specialty optical fibers"; Journal of Optical Society of America B, 38 (12), F90-F103 (2021). https://doi.org/10.1364/JOSAB.439330

[3] J M Dudley, G Genty, G and S Coen, "Supercontinuum generation in photonic crystal fiber" Reviews of modern physics, 78(4),1135-1184(2006). https://doi.org/10.1103/RevModPhys.78.1135

[4] M Diouf, L M Mandeng, C Tchawoua and M Zghal, "Numerical Investigation of Supercontinuum Generation Through $AsSe_2/As_2S_5$ Chalcogenide Photonic Crystal Fibres and Rib Structures", Journal of Lightwave Technology, 37(22),5692-5698 (2019). http://dx.doi.org/10.1109/JLT.2019.2934034

[5] H Le, V Hoang, H T Nguyen et al. , "Supercontinuum generation in photonic crystal fibers infiltrated with tetrachloroethylene", Optical Quantum Electronics, 53,187(2021). https://doi.org/10.1007/s11082-021-02820-3

[6] C Heuteu, S K Boukar, L M Mandeng and C Tchawoua, "Supercontinuum generation of truncated Airy pulses in a cubic-quintic $AsSe_2/As_2S_5$ optical waveguide with rib-like structure"' Journal of Optics, 23(9),p.095503(2021).10.1088/20408986/ac0ff4

[7] S Kedenburg, A Steinmann, R Hegenbarth, T Steinle and H Giessen, "Nonlinear refractive indices of nonlinear liquids: wavelength dependence and influence of retarded response", Applied Physics B, 117,803-816 (2014). 10.1007/s00340-014-5833-y

[8] M Chemnitz, M Gebhardt, C Gaida, F Stutzki, J Kobelke, J Limpert, A Tünnermann, A and M A Schmidt, "Hybrid soliton dynamics in liquid-core fibres", Nature communications, 8(1), p.42 (2017). https://doi.org/10.1038/s41467-017-00033-5

[9] J Pniewski, T Stefaniuk, H L Van, V C Long, L C Van, R Kasztelanic, G Stępniewski, A Ramaniuk, M Trippenbach and R Buczyński, "Dispersion engineering in nonlinear soft glass photonic crystal fibers infiltrated with liquids", Applied optics, 55(19), 5033-5040 (2016) 10.1364/AO.55.005033.

[10] L C Van, A Anuszkiewicz, A Ramaniuk, R Kasztelanic, K D Xuan, M Trippenbach, and R Buczyński, "Supercontinuum generation in photonic crystal fibres with core filled with toluene", Journal of Optics, 19(12), 125604 (2017). https://doi.org/10.1007/s11082-021-02820-3

[11] B T Le Tran and L C Van, "Circular lattice benzene-core PCFs with flat near-zero dispersion for low-power broad-spectrum supercontinuum generation." Physica Scripta, 99(4),045527 (2024). https://doi.org/10.1088/1402-4896/ad347c

[12] M Vieweg, T Gissibl, S Pricking, B T Kuhlmey, D C Wu, B J Eggleton and H Giessen, "Ultrafast nonlinear optofluidics in selectively liquid-filled photonic crystal fibers" Optics express, 18(24), 25232-25240(2010). https://doi.org/10.1364/OE.18.025232

[13] S A Adnan, A W Abdulwahhab and S N Ismail, "Fusion splicing: the penalty of increasing the collapse length of the air holes in ESM-12B photonic crystal fibers", Optica Applicata, 46(2) (2016). http://dx.doi.org/10.5277/oa160211.

[14] X Lin, H Yan, Y Ma and Z Zhou, "A construction method of the quasi-monolithic compact interferometer based on UV-adhesive bonding", Review of Scientific Instruments, 94(7) (2023). http://dx.doi.org/10.1063/5.0155637

[15] P Fürjes, "Controlled focused ion beam milling of composite solid state nanopore arrays for molecule sensing",Micromachines, 10(11), (2019). https://doi.org/10.3390/mi10110774

[16] T S Saini, A Baili, A Kumar, R Cherif, M Zghal and R K Sinha, "Design and analysis of equiangular spiral photonic crystal fiber for mid-infrared supercontinuum generation", Journal of modern optics, 62(19),1570-1576 (2015). https://doi.org/10.1080/09500340.2015.1051600.

[17] G P Agrawal, "Nonlinear fiber optics", In Nonlinear Science at the Dawn of the 21st Century, 195-211. Berlin, Heidelberg: Springer Berlin Heidelberg, (2000). https://doi.org/10.1007/3-540-46629-0_9

[18] P Chauhan, A Kumar and . Kalra, “Numerical exploration of coherent supercontinuum generation in multicomponent $GeSe_2$-As_2Se_3-PbSe chalcogenide based photonic crystal fiber”, Optical Fiber Technology, 54,102100 (2020). https://doi.org/10.1016/j.yofte.2019.102100

[19] Z Guo, J Yuan, C Yu, X Sang, K Wang, B Yan, L Li, S Kang and X Kang, “Highly coherent supercontinuum generation in the normal dispersion liquid-core photonic crystal fiber”, Progress in Electromagnetics Research M, 48, 67-76 (2016).

[20] V T Hoang, R Kasztelanic, A Filipkowski, G Stępniewski, D Pysz, M Klimczak, S Ertman, V C Long, T R Woliński, M Trippenbach and K D Xuan, “Supercontinuum generation in an all-normal dispersion large core photonic crystal fiber infiltrated with carbon tetrachloride”, Optical materials express, 9(5), 2264-2278 (2019).

[21] C Van Lanh, K Borzycki, K D Xuan, V T Quoc, M Trippenbach, R Buczyński, and J Pniewski, “Optimization of optical properties of photonic crystal fibers infiltrated with chloroform for supercontinuum generation”, Laser Physics, 29(7),075107 (2019).

[22] L C Van, K Borzycki, K D Xuan, V T Quoc, M Trippenbach, R Buczyński and J Pniewski, “Supercontinuum generation in photonic crystal fibers infiltrated with nitrobenzene”, Laser Physics, 30(3),035105 (2020). https://doi.org/10.1007/s12648-023-02830-9

[23] J Wen, B Liang, W Qin, W Sun, C He, C and K Xiong, “High coherent supercontinuum generation in nitrobenzene liquid-core photonic crystal fiber with elliptical air-hole inner ring”, Optical and Quantum Electronics, 54(12), 817 (2022).

[24] J Wen, B Liang, W Sun, C He, K Xiong, H Yu, H Zhang, Z Wu and Q Wang, “Coherence analysis of supercontinuum generation in nitrobenzene liquid-core photonic crystal fiber based on adaptive step-size methods”, Optical and Quantum Electronics, 56(4), 619 (2024).

CHAPTER 8: CONCLUSION, FUTURE SCOPE AND SOCIAL IMPACT

In this chapter, we conclude our research work entitled "*Modeling and Design of Specialty Optical Fibers and Waveguides for Supercontinuum Generation*" and provide the future prospects of this work.

8.1 Conclusion

This section provides the concluding remarks of the research presented in this thesis and outlines prospective avenues for future investigation. The thesis has focused on detailed numerical simulations of ultra-broadband coherent SCG spanning the visible to mid-infrared spectral regions. The SCG was analyzed in both waveguide structures and highly nonlinear PCFs engineered from silica, chalcogenide glasses, and organic liquid-based materials. These platforms were evaluated for their potential in enabling key photonic applications, including broadband spectroscopy, trace gas detection, biomedical imaging, OCT, WDM, and free-space optical (FSO) communication systems.

A mid-IR supercontinuum spectrum using a parabolic-core waveguide pumped in the normal dispersion region, has been investigated. This design is crucial as the fabricated rectangular waveguide does not remain rectangular after laser post processing but becomes similar to the proposed parabolic design. The proposed design of the waveguide may substantially broaden the range of functions available in future for integrated photonics. The proposed waveguide design can be fabricated using plasma etching chemical vapour deposition technique already discussed in chapter 3.

Photonic crystal fiber which is a specialty optical fiber has been designed in such a way that it is suitable for the generation of an ultra-broadband supercontinuum spectrum from 1 µm to 11 µm in MIR domain when pumped with the peak power of 0.75 kW at 5 µm with 50 fs pulse width. Another silica based PCF infiltrated with ethanol for NIR to MIR supercontinuum generation has been analysed. A flat-top dispersion profile has been obtained with a low peak power of 0.55 kW at a pump wavelength of 1.55 µm. A dispersion value of +30.231ps/nm-km is obtained in the anomalous region. For the proposed structure nonlinear coefficient is as high as 281.4 $W^{-1}km^{-1}$ with effective mode area of 4.16 μm^2 at 1.55 µm.

PCF infiltrated with nitrobenzene for the purpose of generating supercontinuum light with low peak power in the near-infrared to mid-infrared ranges. With slight difference in geometries the PCF design has been labelled as circular (#C) and elliptical (#E). By utilizing a fiber length of 10 mm, a 50 fs

secant laser pulse source, and a pump power of 650 W, we achieved a broad supercontinuum spectrum ranging from 1.3 μm to 2.0 μm for the circular design (#C), from 0.9 μm to 2.3 μm for the elliptical *x*-polarised design (#EX) and from 1.0 μm to 2.4 μm for the elliptical *y*-polarised design (#EY).

As discussed in chapters 4-7, Photonic crystal fibers (PCFs) can be fabricated using the rod-in-tube fabrication technique, other available methods are stack and draw technique, drilling, sol-gel method. In contrast, infiltrated PCFs are produced using various infiltration methods, depending on the specific requirements. These techniques include photopolymerization, thermal collapse, the splicer process, UV adhesive bonding, and microchannel milling. On chip integration possibilities of these fibers include on-chip mechanical splicer, photonic wire bonding, micro-fluidic chips.

Another work consists of a comparative study of PCFs infiltrated with nonlinear organic liquids nitrobenzene and ethanol for NIR to MIR SCG. The suggested PCF design can be employed for various critical applications involving detection of explosives, various gases, cancers, ulcers and enhanced monitoring systems for food quality detection.

Nonlinear photonics carries both beneficial and challenging environmental impacts. On the positive side, nonlinear optical technologies contribute to energy-efficient optical communication, sophisticated environmental sensing, and compact laser systems that consume less power than traditional electronic counterparts. Techniques such as supercontinuum generation and frequency conversion further enhance capabilities in atmospheric analysis and pollutant detection. Nevertheless, the production of nonlinear materials and photonic components often requires energy-intensive procedures and may involve scarce or hazardous substances. Looking ahead, research in nonlinear photonics is directed toward sustainable material development, low-power all-optical processing, integrated photonic circuits, and eco-friendly fabrication methods. Prioritizing green manufacturing practices and scalable, economical production approaches will be essential to reduce environmental impact while continuing to advance high-performance photonic technologies.

8.2 Future scope

- To design and model photonic crystal fibers and waveguides to generate the supercontinuum at longer wavelengths.
- To study the high power supercontinuum generation in photonic crystal fibers for newly reported highly nonlinear materials such as silicon carbide (SiC), zinc-germanium diphosphide ($ZnGeP_2$) etc.
- To design PCF and waveguides using materials which are less toxic with low attenuation and are able to produce broader coherent SCG profile.

8.3 Social impact

In this thesis, different types of designs related to waveguide and specialty optical fibers have been discussed for various applications. This proposed work finds applications in security, biomedical diagnosis, spectroscopy, OCT and sensing technologies.

The proposed designs and their practical applications are not limited to the existing work and can be further expanded as follows:

- ***Atmospheric Gas Sensing***: *Detecting trace gases (like CO_2, CH_4, NO_2, SO_2) in the atmosphere*. SCG enables multi-species detection with high resolution using techniques like Differential Absorption Spectroscopy (DAS) or Cavity Ring-Down Spectroscopy (CRDS).
- ***Water Quality Monitoring***: *Identifying pollutants or contaminants in water bodies*. Broadband light allows for absorption spectroscopy to detect multiple organic and inorganic substances simultaneously
- ***Remote Sensing / LIDAR:*** *Mapping vegetation, aerosols, and terrain features*. Supercontinuum sources can enhance hyperspectral LIDAR, offering more data-rich analysis across different wavelengths for improved environmental modelling.
- ***Pollution Detection in Airborne or Portable Sensors***: *Mobile detection of industrial pollutants.* Compact supercontinuum sources can be integrated into portable spectrometers, enabling real-time environmental monitoring in remote or urban areas.

LIST OF PUBLICATIONS AND THEIR PROOFS

THESIS WORK

Received: 10 January 2024 | Revised: 21 February 2024 | Accepted: 25 February 2024

DOI: 10.1002/mop.34105

RESEARCH ARTICLE

WILEY

Design and numerical modeling of chalcogenide parabolic-core waveguide for on-chip supercontinuum generation extending from near-IR region to mid-IR region

Drishti Singh Tomer | **Ajeet Kumar**

Advanced Photonics Simulation Research Lab, Department of Applied Physics, Delhi Technological University, Delhi, India

Correspondence
Ajeet Kumar, Advanced Photonics Simulation Research Lab, Department of Applied Physics, Delhi Technological University, Delhi 110 042, India.
Email: ajeetdph@dtu.ac.in

Abstract

We present the design and computational examination of a waveguide structure with a parabolic core, implemented in $AsSe_2$ chalcogenide glass. This structure aims to generate a mid-infrared (mid-IR) supercontinuum (SC) spectrum, covering the wavelength range of 1.4−7.6 μm. It includes molecular fingerprint region as well as earth's atmospheric transparent window. A pulsed laser providing pulses of peak power of 250 W and pulse width of 200 fs at 2 μm was considered as the pump. The results illustrate that the broadband SC spectrum can be achieved in a short (~8 mm) waveguide pumped with commercially available fiber laser at 2 μm. The novelty of this work lies in the generation of a mid-IR SC spectrum using a parabolic-core waveguide pumped in the normal dispersion region, which has not been investigated earlier. This design is crucial as the fabricated rectangular waveguide does not remain rectangular after laser postprocessing but becomes similar to the proposed parabolic design.

KEYWORDS

integrated photonics, nonlinearity, parabolic-core waveguides, supercontinuum generation

1 | INTRODUCTION

Mid-infrared (mid-IR) supercontinuum generation (SCG) using integrated waveguides has been a stimulating and active research topic for the last two decades.[1,2] Mid-IR region offers two optical windows (i.e., 3−5 μm and 8−13 μm) which are optically transparent to the earth's atmosphere. Various sorts of Mid-IR light sources have been developed which are finding potential applications in diverse fields including optical communications, optical coherence tomography (OCT), medical endoscopy and gas sensing.[3–6] Ultrafast photonics plays a crucial role in SCG, as it involves the use of femtosecond or picosecond laser pulses.[7–11] Supercontinuum (SC) spectrum is generated when the large number of nonlinear effects such as stimulated Raman scattering (SRS), self-phase modulation (SPM), cross-phase modulation and four-wave mixing act all together on an intense pump beam to root the large spectral broadening of the original pump beam.[12] Microstructured Fibers, Photonic crystal fibers and waveguides have recently attracted significant research interest due to its high designing freedom.[13] Different materials like silica, tellurite and chalcogenide glasses have been used in waveguides, PCF and various step index fibers for employing SCG in mid-IR.[14–19] Silica based optical waveguides can be used to realize the strong modal confinement and dispersion profile. At the same time,

Journal of Optics
https://doi.org/10.1007/s12596-024-01954-3

RESEARCH ARTICLE

A Graded Index Hybrid Photonic Crystal Fiber for Supercontinuum Generation using $AsSe_2$- As_2S_5

Drishti Singh Tomer[1] · Ajeet Kumar[1]

Received: 24 April 2024 / Accepted: 30 May 2024

Abstract
We design and simulate an especially engineered photonic crystal structure. $AsSe_2$ as the solid core and As_2S_5 in graded-index hybrid cladding. Hybrid cladding region with inner cladding as a graded helical structure and outer cladding is a hexagonal structure. We have tailored the structural parameters to obtain nearly zero flat-top dispersion profile with all normal dispersion profile. The dispersion at 5 μm is -53.13 ps/nm-km with effective mode area of the fundamental mode as 4.18 μm^2. Proposed PCF is suitable for the generation of an ultra-broadband supercontinuum spectrum from 1 μm to 11 μm in MIR domain when pumped with the peak power of 0.75 KW at 5 μm with 50 fs pulse width. Proposed PCF design holds potentiality for applications like early cancer diagnostics, gas sensing and food quality check.

Keywords Photonic crystal fibers · Supercontinuum generation · Nonlinear optics · Photonic integrated circuits

Introduction

In recent years, research in mid-infrared (MIR) supercontinuum has gathered significant attention [1, 2]. Supercconntinuum generation (SCG) is the process where amalgamation of various nonlinear phenomena including stimulated Raman scattering, self-phase modulation (SPM), cross-phase modulation (XPM), and four-wave mixing takes place (FWM). They work together on an intense pump beam, leading to a significant amount of spectral broadening compared to the original pump beam in an optical fiber. This concept of SCG was first introduced in 1970 [3]. It involves interplay between Raman effect, Kerr effect and dispersion properties of the fiber. Among fibers we have a special class of fibers called holey fibres (HFs) or the microstructured fibers (MOFs) or photonic crystal fibers (PCFs) due to their exclusive linear and nonlinear properties they have been a good choice among researchers [4]. The reason for such fascination is their properties such as dispersion management, large mode area with endlessly single-mode operation, higher birefringence, SCG and high power delivery. When compared to traditional optical fibers, PCF requires lesser initial peak power of the input laser pulses. It results in a huge spectral broadening at a very mimimal peak power this fact can be utilized in applications like frequency metrology [5].

The fiber of choice has traditionally been the silica PCF because it can be made endlessly single-mode, its dispersion can be tailored and its zero-dispersion wavelength (ZDW) can move down into the visible region [6]. Chalcogenide glasses have wider transmission range and a greater nonlinear coefficient in a MIR waveband when compared to silica (non-transparent beyond 2.5 μm), sulfur, fluoride and telluride glasses (long wavelength spectrum is limited at 5 μm) [7].The chalcogenide materials are preferred for broadband SCG because of the lower peak power requirement and high nonlinearity. Compared to single glass chalcogenide fibers, step-index fibers with hybrid-glasses offer several benefits. Firstly, they exhibit a higher refractive-index (RI) difference between the fiber core and cladding, enhancing the effectiveness of light confinement in the core and reducing loss. Secondly, the fiber's numerical aperture is increased due to the higher RI difference, facilitating the collection of light into the core during coupling. Lastly, effective controlling over the chromatic dispersion can be achieved by using

✉ Ajeet Kumar
ajeetdph@dtu.ac.in

Drishti Singh Tomer
drishti.tomer@gmail.com

[1] Advanced Photonics Simulation Research Lab, Department of Applied Physics, Delhi Technological University, Delhi 110042, India

Published online: 15 June 2024

Journal of Optics
https://doi.org/10.1007/s12596-024-02152-x

RESEARCH ARTICLE

Ethanol-infiltrated circular photonic crystal fiber for low peak power supercontinuum generation from near-infrared to mid-infrared region

Drishti Singh Tomer[1] · Ajeet Kumar[1]

Received: 27 June 2024 / Accepted: 5 August 2024

Abstract
We report computational modeling of a silica based Photonic Crystal Fiber (PCF) infiltrated with ethanol for NIR to MIR supercontinuum generation. Full vectorial finite element method (FEM) has been used to analyse the impact of infiltration. A flat-top dispersion profile has been obtained with a low peak power of 0.55 kW at a pump wavelength of 1.55 µm. A dispersion value of +30.231ps/nm/km is obtained in the anomalous region. For the proposed structure nonlinear coefficient is as high as 281.4 $W^{-1}km^{-1}$ with effective mode area of 4.16 μm^2 at 1.55 µm. A broadband supercontinuum spanning, from 1.25 µm to 3.0 µm is achieved by using a fiber length of 20 cm with 60 fs secant laser pulse source. The suggested PCF design assure several critical applications such as biomedical diagnostics, explosives detection, enhanced gas sensing capabilities and improvised food quality monitoring systems.

Keywords Nonlinear optics · Supercontinuum generation · Photonic crystal fibers · Photonic integrated circuits

Introduction

In recent times, supercontinuum generation (SCG) has become a focal point of extensive research interest [1–4]. In 1970, the concept of SCG was introduced for the first time [5]. Stimulated Raman scattering (SRS), self-phase modulation (SPM), cross-phase modulation (XPM), and four-wave mixing (FWM), assimilation of these nonlinear phenomena results in the process of SCG. When a high-intensity pump beam propagates through an optical fiber, these effects collectively interact with incident beam, causing substantial spectral broadening beyond the initial spectrum of the pump beam. This phenomenon arises from the interaction between the Raman effect, the Kerr effect, and the fiber's dispersion characteristics. Within the category of fibers, there exists a unique class known as holey fibers (HFs), photonic crystal fibers (PCFs) or microstructured fibers (MOFs). Their incredible linear and nonlinear properties of these fibers, make them a popular choice among researchers [6–10].

All normal dispersion (ANDi) profile of PCFs offer several advantages, including the preservation of ultrashort pulses, characterized by a uniform power spectral density and temporal profile. The absence of modulation instability (MI) due to soliton dynamics minimizes noise effects, facilitating the generation of coherent flat spectra. This characteristic is advantageous for applications in spectroscopy, metrology, and optical tomography systems including optical coherence tomography (OCT) [11, 12]. But the disadvantage with them they require high input power which can lead to photo thermal effect which can damage the fiber.

However, if we use anomalous dispersion regime with lesser input power broad spectra can be achieved, but coherency will be compromised. In order to balance out this soft glasses like chalcogenide was used [13–15]. However, they exhibit steep normal dispersion and a long zero-dispersion wavelength (ZDW) in the near-infrared (NIR), which restricts the flatness of the dispersion curve and the spectral bandwidth of supercontinuum generation.

To overcome these shortcomings recently liquid infiltrated PCFs are designed which have high nonlinear refractive index like CS_2 where $n_2 = 2.2 \times 10^{-18}$ m^2 W^{-1} at 1032 nm [16] which is quite large in comparision to silica. The advantages of using liquids in the air holes enables

✉ Ajeet Kumar
ajeetdph@dtu.ac.in

Drishti Singh Tomer
drishti.tomer@gmail.com

[1] Department of Applied Physics, Advanced Photonics Simulation Research Lab, Delhi Technological University, Delhi 110042, India

Published online: 30 August 2024

JOURNAL OF MODERN OPTICS
https://doi.org/10.1080/09500340.2025.2478641

Taylor & Francis
Taylor & Francis Group

Photonic crystal fibres infiltrated with nitrobenzene for low peak power supercontinuum generation in NIR to MIR region

Drishti Singh Tomer and Ajeet Kumar

Advanced Photonics Simulation Research Lab, Department of Applied Physics, Delhi Technological University, Delhi, India

ABSTRACT

We present a comparative study of silica-based Photonic Crystal Fibres infiltrated with nitrobenzene to generate supercontinuum light with low peak power in the near-infrared to mid-infrared ranges. Using a full vectorial finite element method, we analyzed three designs: symmetrical circular (#C) and asymmetrical elliptical X-polarised (#EX) and Y-polarised (#EY). The circular design showed a dispersion of + 30.211 ps/nm/km, effective mode area of 4.13 μm^2, and nonlinear coefficient of 1962.0 W^{-1} km^{-1} at 1.55 µm. The elliptical designs had dispersions of −10.852 ps/nm/km (#EX) and −8.356 ps/nm/km (#EY), with effective mode areas of 4.55 and 4.60 μm^2, and nonlinear coefficients of 1780.9 and 1761.5 W^{-1} km^{-1}. Using a 10 mm fiber, 50 fs laser pulse, and 650 W pump power, we achieved supercontinuum spectra ranging from 1.3–2.0 µm (#C), 0.9–2.3 µm (#EX), and 1.0–2.4 µm (#EY). These designs are promising for biomedical and sensing applications.

ARTICLE HISTORY
Received 10 November 2024
Accepted 7 March 2025

KEYWORDS
Photonic integrated circuits; supercontinuum generation; nonlinear optics; photonic crystal fibres

1. Introduction

SCG is a complex phenomenon where new frequency in the pulse spectrum is generated by the interaction between various non-linear effects in the fibre, leading to the expansion of a narrow spectrum by several multiples into a continuous broad spectrum. In recent times, SCG has become a focal point of extensive research interest [1–6]. For the first time in 1970, the concept of SCG was introduced [7]. SC is characterized by a continuous broadband spectrum, good coherence and stability. The performance of SCG depends on the pump wavelength, fibre nonlinearity, input pulse energy, fibre length and pulse duration. In addition, important PCF properties such as attenuation, effective mode area, and dispersion also affect the performance of SCG [8]. Preferably, a flat curve with near zero dispersion value, minimum attenuation constant and, an effective mode area are required. These parameters can be controlled by changing the geometrical parameters of the Photonic crystal Fibre (PCF). However, subject to the choice of pump wavelength within the dispersion range, corresponding effects occur in SCG [9]. The performance of the SC is measured by three leading indicators: bandwidth, coherence, and flatness. Nonlinear effects like self-phase modulation (SPM) and optical wave breaking (OWB) contribute to spectral broadening in the all-normal dispersion regime (ANDi). Maintenance of ultrashort pulses without distortion, a consistent and stable power spectral density and a uniform and even temporal profile are a few of the advantages associated with using the ANDi profile of PCFs. The generation of a coherent flat spectrum is made possible by the absence of modulation instability (MI), which is typically detrimental to spectral quality. In this context, the dynamics of solitons play a crucial role by effectively minimizing the impact of noise. These characteristics are advantageous for applications in spectroscopy, metrology, and optical tomography systems including optical coherence tomography (OCT) [10,11]. However, the associated shortcoming with ANDi is the onset of a photo-thermal effect, causing damage to the fibre on the application of high input power.

Conversely, on utilizing anomalous dispersion regime a broad SC spectra can be achieved with low input peak power. SC generation through pumping in the anomalous dispersion regime arises from the combined effects of various soliton dynamics. Key contributing factors include interactions with dispersive waves, the process of soliton splitting, shifts in the soliton's natural frequency,

CONTACT Ajeet Kumar ajeetdph@dtu.ac.in Advanced Photonics Simulation Research Lab, Department of Applied Physics, Delhi Technological University, Delhi 110042, India

Journal of Nonlinear Optical Physics & Materials
(2025) 2550050 (22 pages)

DOI: 10.1142/S021886352550050X

A comparative study of photonic crystal fibers filled with organic liquids for low peak power supercontinuum generation

Drishti Singh Tomer* and Ajeet Kumar†

Advanced Photonics Simulation Research Laboratory,
Department of Applied Physics, Delhi Technological University,
Bawana Road, Delhi 110042, India
*drishti.tomer@gmail.com
†ajeetdph@dtu.ac.in*

Received 9 June 2025
Accepted 17 October 2025
Published 14 November 2025

This study presents a comparative study of Photonic Crystal Fibers (PCFs) infiltrated with nonlinear organic liquids nitrobenzene and ethanol for near infrared to mid-infrared (MIR) supercontinuum generation (SCG). The liquids in the air holes enable high nonlinear and tunable properties. The enhancement of nonlinear properties results in a broader SC spectrum with low pump power and low attenuation. To analyze the impact of infiltration, a full vectorial finite element method (FEM) has been employed. For silica-based PCF (#A), dispersion around +52.25 ps/nm/km, effective mode area as 6.57 μm^2 and nonlinear coefficient as 1234.18 $W^{-1}km^{-1}$ is obtained at 1.55 μm. For other infiltrated designs (#B), (#C) and (#D) at 1.55 μm dispersion around +20.81 ps/nm/km, −20.84 ps/nm/km, +3.74 ps/nm/km, effective mode area as 1.45 μm^2 and nonlinear coefficient as 5596.22 $W^{-1}km^{-1}$, 5569.71 $W^{-1}km^{-1}$ and 5584.28 $W^{-1}km^{-1}$ are obtained, respectively. A broadband supercontinuum spanning from 1.3–1.8 μm for #A, 1.0–2.4 μm for #B, 1.2–2.5 μm for #C and 0.9–2.5 μm for #D is obtained by using a fiber length of 4 mm to 8 mm with 50 fs secant laser pulse source and a pump power of 600 W to 800 W. The suggested PCF design can be employed for various critical applications involving the detection of explosives, various gases, cancers, ulcers and enhanced monitoring systems for food quality detection.

Keywords: Photonic crystal fiber; photonic integrated circuits; supercontinuum generation; nonlinear optics.

1. Introduction

Supercontinuum generation (SCG) is a complex process in which interactions among various nonlinear effects within an optical fiber produce new frequency components, transforming a narrow input spectrum into a significantly broader and continuous one. It has recently emerged as a prominent area of research interest.[1,4,45–47]

†Corresponding author.

DELHI TECHNOLOGICAL UNIVERSITY

(Formerly Delhi College of Engineering)

Shahbad Daulatpur, Main Bawana Road, Delhi-42

PLAGIARISM VERIFICATION

Title of the Thesis **Modeling and Design of Specialty Optical Fibers and Waveguides for Supercontinuum Generation.**

Total Pages **121** Name of the Scholar **Drishti Singh Tomer .**

Supervisor **Dr. Ajeet Kumar .**

Department of **Applied Physics .**

This is to report that the above thesis was scanned for similarity detection. Process and outcome is given below:

Software used: **TURNITIN** Similarity Index: **4%**,

Total Word Count: **32,403**.

Date: 26-08-2025

Candidate's Signature **Signature of Supervisor**

CURRICULUM VITAE

Drishti Singh Tomer

Date of Birth: 23rd January, 1995

Designation: Research Scholar
Department of Applied Physics

Delhi Technological University (DTU), India

CONTACT INFORMATION

Advanced Photonics Simulation Research Laboratory

Department of Applied Physics

Delhi Technological University
Delhi – 110 042, India

Email – drishti.tomer@gmail.com, drishti_2k19phdap501@dtu.ac.in

Phone - +91 9467787014

EDUCATION

Ph.D. (January 2020 to Present)

Thesis Title: Modeling and Design of Specialty Optical Fibers and Waveguides for Supercontinuum Generation

Department of Applied Physics,

Delhi Technological University, Delhi, India
CGPA: 8.33/10 **(Coursework)**

M.Sc in Physics (2015-17)
Department of Physics,
Deenbandhu Chhotu Ram University of Science and
Technology, Haryana, India
Percentage: 74.95/100

B.Sc with Physics, Chemistry and Mathematics (2011-14)
Maitreyi College, University of Delhi, New Delhi
Percentage: 70.52/100

Senior Secondary Examination (12th) with Physics, Chemistry, Mathematics, English and Physical Education (2011)
Central Board of Secondary Education, Delhi, India
Percentage: 76/100

Secondary Examination (10th) with Science, Mathematics, Social Sciences, English, Sanskrit and Hindi (2012)
Central Board of Secondary Education, Delhi, India
Percentage: 87.40/10

RESEARCH INTERESTS: Fiber Optics, Integrated Photonics, Nonlinear Optics

ACHIEVEMENTS

GATE Qualified (2019)

Research Excellence Award in 2025 (awarded by DTU)

SKILLS

Operating systems: Microsoft Windows

Programming skills: Matlab Programming Language, FORTRAN 90

Software Packages: COMSOL, MATLAB

Experience of working on High-Performance computers (HPC)

Graphical software: Origin

PEER-REVIEWED PUBLICATIONS

1. D.S. Tomer and A. Kumar, "Design and numerical modeling of chalcogenide parabolic-core waveguide for on-chip supercontinuum generation extending from near-IR region to mid-IR region", Microwave and Optical Technology Letters, 66(3), e34105 (2024). https://doi.org/10.1002/mop.34105
2. D.S. Tomer and A. Kumar, "A graded index hybrid photonic crystal fiber for supercontinuum generation using $AsSe_2$-As_2S_5", Journal of Optics, 54, (3268-3277) (2025). https://doi.org/10.1007/s12596-024-01954-3
3. D.S. Tomer and A. Kumar, "Ethanol-infiltrated circular photonic crystal fiber for low peak power supercontinuum generation from near-infrared to mid-infrared region", Journal of Optics 1-9 (2024). https://doi.org/10.1007/s12596-024-02152-x
4. D.S. Tomer and A. Kumar, "Photonic crystal fibres infiltrated with nitrobenzene for low peak power supercontinuum generation in NIR to MIR region", Journal of Modern Optics, 72(4–6), 175–187 (2025). https://doi.org/10.1080/09500340.2025.2478641
5. D.S. Tomer and A. Kumar, "A comparative study of photonic crystal fibers filled with organic liquids for low peak power supercontinuum generation", Journal of Nonlinear Optical Physics and Materials. https://doi.org/10.1142/S021886352550050X

WORK PRESENTED IN CONFERENCES/ WORKSHOPS

1. D.S. Tomer and A. Kumar , "Photonic crystal fiber infiltrated with nitrobenzene for nonlinear applications", 2nd International Conference on Recent trends in Applied Physics and Material Science (RAM 2024), 15-16 Nov 2024, Bikaner Technological University (BTU), Bikaner, Rajasthan, India.

2. D.S. Tomer and A. Kumar, “A highly nonlinear photonic crystal fiber with two zero dispersion wavelengths for nonlinear applications”, International Conference on Atomic, Molecular, Material, Nano, and Optical Physics with Applications (ICAMNOP 2023) , 20-22 Dec 2023 , Department of Applied Physics, Delhi Technological University, Delhi, India.
3. D.S. Tomer and A. Kumar, “Nonlinear applications of photonic crystal fiber with organic solvent toluene using computational analysis”, 9th National Conference on Nanoscience and Instrumentation Technology (NCNIT-2021) 20-21 Nov 2021, Department of Physics, NIT, Kurukshetra, India.
4. D.S. Tomer and A. Kumar, “Computational analysis of toluene infiltrated photonic crystal fibers for nonlinear applications”, 44th Annual Symposium of the Optical Society of India: Frontiers in Optics and Photonics (FOP21), 24-27 Sep 2021, IIT Delhi, India.
5. A. Khamaru, K. Sharma, D.S. Tomer, & A. Kumar, “Mid-IR supercontinuum generation in dispersion flattened $As_{38}Se_{62}$ chalcogenide photonic crystal fiber”, Journal of Physics: Conference Series, 2426(1), 012002 (2023)